2013

Characterizing Crown Struture of Three Interior Northwest Conifer Species Using Terrestrial Laser Scanning

Jena Ferrarese
The University of Montana

CHARACTERIZING CROWN STRUCTURE OF THREE INTERIOR NORTHWEST CONIFER SPECIES USING TERRESTRIAL LASER SCANNING

By

JENA ALISSA FERRARESE

B.S., Cornell University, Ithaca, NY, 1999

Thesis

presented in partial fulfillment of the requirements
for the degree of

Master of Science
in Forestry

The University of Montana
Missoula, MT

May 2013

Approved by:

Sandy Ross, Associate Dean of The Graduate School
Graduate School

Dr. Carl Seielstad, Chair
Department of Forest Management, College of Forestry and Conservation

Dr. David Affleck
Department of Forest Management, College of Forestry and Conservation

Dr. Ragan Callaway
Department of Biological Sciences, College of Arts and Sciences

(this page intentionally left blank)

Ferrarese, Jena, M.S., Spring 2013 Forestry

Characterizing Crown Structure of Three Interior Northwest Conifer Species Using Terrestrial Laser Scanning

Chairperson: Dr. Carl Seielstad

Emerging interests in wildland fire behavior and risk, bioenergy utilization, carbon sequestration, and wildlife conservation increasingly rely on accurate assessments of the amount and location of biomass within the dominant plants on the landscape, often at finer scales than traditional methods have provided. At the tree scale, current studies often distribute biomass uniformly through simple volumes (e.g., cones and cylinders). However, biomass is heterogeneous at a variety of scales from needle clusters to groups of trees. This thesis presents techniques for using terrestrial laser scanning data to define crown profiles and describe within-crown heterogeneity in *Pseudotusga menziesii, Pinus ponderosa,* and *Abies lasiocarpa* of the Interior Northwest. Crown profiles were modeled using parametric curves applied to crown-length normalized laser point clouds, dimensioned by height above ground and distance from bole-centroids. A crown-base metric was derived from the laser data and compared to conventional field measurements. For all species, a modified Weibull curve fit crown points with significantly smaller error than a beta curve, cone, or cylinder; crown profile Weibull curves were species-specific and not interchangeable without producing signifcantly greater error. Within-crown patterning was described using a 3-D form of the Ripley's K function. Ripley's K analysis detected maximum clustering occuring at scales of 1.25 – 2.50 percent of crown length (e.g., 25-50 cm radius clusters in a 20 meter crown). *P. ponderosa* demonstrated clustering over the largest range of scales and to the greatest degree, while *A. lasiocarpa* exhibited clustering over the smallest range of scales. The scale of clustering did not change when points roughly corresponding to branchwood were excluded from the analysis. This study provides groundwork for predicting the spatial distribution of biomass with tree crowns. Limitations of the work include uncertainty regarding the impacts of occlusion of inner crowns and the relationships between laser points and foliage-branch elements, and the lack of spatial explicitness inherent to Ripley's K. Future work should examine these issues with an eye toward refinement of predictive models linking traditional biomass allometry with spatial arrangement of canopy material.

(this page intentionally left blank)

TABLE OF CONTENTS

Chapter 1. Introduction

Overview

Understanding the distribution of the above-ground biomass of the dominant plants on a lanscape is of critical and growing importance in forest conservation and management. Emerging interests in wildland fire behavior and risk (Ottmar et al. 2012, Parsons et al. 2011, Hiers et al. 2009), bioenergy utilization (Dassot et al. 2012, Fernandez-Sarria et al. 2013), carbon sequestration (Clark et al. 2011), and wildlife conservation (Lesak et al. 2011, Palminteri et al. 2012) among others, increasingly rely on accurate assessments of the amount and location of biomass, often at finer scales than traditional methods have provided. As field measurements are not always a viable option for every application, many scientists and managers employ models to infer biomass from tree lists, stand tables, and maps of vegetation composition and structure. The conventional approach to assess tree biomass is to measure tree diameters by species and then to estimate biomass from allometric relationships derived from destructive sampling studies. Studies that rely on destructive sampling can be limited by small sample sizes and restricted geographic distributions, and there is renewed interest in revisiting tree allometries to improve prediction effectiveness and remove bias.

For example, in the northern Rocky Mountains, Affleck and Turnquist (2012) are re-calibrating many of Brown's (1978) equations for estimating standing crown biomass using randomized branch sampling (RBS). RBS overcomes the sample size limitation by measuring only small parts of individual trees. It uses the correlation between foliar/branch mass and branch basal diameter to select a subsample of branches within each crown to be weighed and measured. Because of the limited sampling of each tree, RBS allows sampling of larger number of trees in the same amount of time as previous methods that processed entire trees; this permits more extensive sampling over wider geographic and size class distributions. These revised allometric

relationships are expected to produce more robust estimates of crown biomass and provide enhanced utility for the interests mentioned above.

In addition to knowing the amount of biomass in a forest, stand, or tree, there is growing interest in understanding how that biomass is distributed within individual tree crowns. The within-crown arrangement of vegetation is becoming particularly important to wildland fire modelers and managers who wish to understand fire behavior and effects at finer scales than have been studied in the past (Hoffman 2012, Parsons et al. 2011). A suite of new fire models and a growing appreciation for the complexities of fire behavior are stimulating interest in linking traditional allometric approaches with information about where tree biomass is found in space. The denouement of this approach is to develop predictive models that will take a tree list, populate it with reasonable estimates of biomass, and provide spatially explicit parameters for that biomass.

The RBS approach described previously addresses estimation of biomass by species, and this thesis considers where that biomass occurs within tree crowns. In order to understand the spatial distribution of crown biomass, a first step is to quantify the space that the crown occupies, then describe the internal heterogeneity of material, and, finally, to allocate biomass in a spatially-explicit, realistic manner, based on our understanding of heterogeneity. Here, I consider the initial two steps – crown volume and internal heterogeneity for three conifer species of the Northern Rocky Mountains. I do so by utilizing an emerging technology (terrestrial laser scanning) to collect detailed 3-dimensional data for many tree specimens, integrating the data to produce species-specific crown shapes, and characterizing internal crown structure by species.

Background

The focus of this study (characterizing tree crown architecture using laser scanning for wildland fire simulation) demands an understanding of several bodies of work. Modeling crown architecture encompasses describing both the bounding volume of the crown (as delineated by a

crown profile) and the internal structure, and past approaches to each are described below. Additionally, an introduction to terrestrial laser scanning and some of its applications to tree crown and canopy work is given. Lastly, implications of canopy structure assumptions to fire behavior modeling are considered, as well as how this study may impact implementation of the newest fire behavior models.

Most approaches to modeling crown profiles can be classed as either direct or indirect methods. Indirect methods begin by first predicting branch attributes (e.g. length and angle) and then computing the crown envelope from the resulting trigonometric relationships (Roeh and Maguire 1997, Deleuze et al. 1996, Cluzeau et al. 1994). Direct methods utilize regression analysis to calculate crown width as a function of other, more easily measurable tree attributes such as total tree height, crown ratio or crown length, relative height within the crown or largest crown width (Crecente-Campo et al. 2009, Marshall et al. 2003, Hann 1999, Baldwin and Peterson 1996, Biging and Wensel 1990). In either case, detailed field measurements are needed, but can only be obtained through costly and time-consuming destructive sampling.

Using a different approach, and one more similar to terrestrial laser scanning (TLS) than the destructive sampling described above, Gill and Biging (2002) modeled crown profiles derived from photographs taken from a single perspective. In stands that had been thinned within three years or clearcut in the past year, they targeted stands across a range of densities (basal areas from $\leq$29.8 m^2/ha – $\geq$57.4 m^2/ha), and selected trees across a span of height classes ($\leq$18.3m – $\geq$36.6m). Each image was scanned, and the crown profile digitized from the scan. Gill and Biging acknowledge that in most cases only one side, left or right, of the profile was visible (the other being blocked by vegetation between the camera and the tree of interest), that in some cases the tree crown edge was difficult to distinguish due to shadowing, and that the images as scanned were distorted by an average of 3% (with a high of 14%) which was deemed an acceptable level. The protocols used in this work are well-suited to address those limitations. First, an unobstructed line-of-sight was

created between every sample tree and the laser. Second, due to the 3-dimensional nature of TLS, information can be captured about the entire canopy, not just a single profile slice. Thus while Gill and Biging had at most two profiles per tree (left and right) to inform their models, TLS provides an essentially unlimited number of potential profiles to incorporate. Third, because laser scanning is an active remote sensing technology, problematic shadowing is minimal. Because contiguous vegetation was removed before scanning, the points comprising the tree of interest were clearly separate from neighboring trees and surrounding vegetation. Lastly, photographic distortion is not an issue with laser scanning. Although utilizing TLS to capture crown profiles *in situ* address many limitations associated with photography, it does introduce other potential sources of error. For example, although sampling was not conducted in strong winds that visibly moved the crown, light breezes could stir individual needle clusters or branch tips, resulting in their being scanned multiple times, potentially affecting the resultant profile. Additionally, although there was a clear line of sight between the laser and the sample tree, because scanning was conducted roughly 2m above ground (the height of the support tripod for the laser), lower portions of the tree itself can partially or fully obscure the upper portions of the tallest trees

Although crown profiles can be used to estimate overall crown volume, they do not inform distribution or arrangement of material within the volume. Internal canopy structure refers to the spatial arrangement of tree components, and is reflected in many ecological measures such as leaf area index (LAI), gap fraction, radiative transfer modeling and bulk density. Most of the work involving non-random groupings of crown vegetation has focused on implications for within-crown light regimes using simulated canopies (e.g. Oker-blom and Kellomaki 1983, Da Silva et al. 2008, Parveaud et al. 2008, Duursma 2007). There has been some work to capture the structure of actual plants, and early attempts to use 3D digital imaging were moderately successful, but were limited by available technology (Sinoquet and Rivet 1997). Sonohat et al. (2006) considered "exhaustive" 3D digitizing the most accurate way to describe plant architecture, but acknowledged its limitations

at the time when applied to larger plants and trees. Utilizing more recent technological advances, terrestrial laser scanning has been shown to capture the vertical and horizontal patchiness within a crown and is capable of characterizing the deviation from uniformity (Takeda et al. 2008). In agricultural systems, laser scanning was determined to be one of the most promising techniques for capturing the geometry of tree crops (Rosell and Sanz 2012), and should be equally useful when applied to non-agricultural trees.

Time-of-flight terrestrial laser scanning (TLS) works by emitting pulses of light that are intercepted by objects and returned to the scanner. Knowing the angle of the scanner and the timing between emittance and reception allows calculation of where the pulse was intercepted (relative to the scanner). With a sufficient number and density of pulses, the 3-D structural characteristics of a solid-with-interstices object (such as vegetation) can be captured. TLS has been applied to studies of leaf area (Beland et al. 2011, Sanz-Cortiella et al. 2011, Delagrange and Rochon 2011, Henning and Radtke 2006, Lovell et al. 2003), gap fraction (Danson et al. 2007, Moorthy et al. 2011), radiative transfer modeling (Cote et al. 2009), and bulk density (Skowronski et al. 2011). Although these studies were not explicitly developing models of the within-crown heterogeneity, they demonstrate a potential for that application.

Important to fire modeling, canopy bulk density has shown to be non-homogeneous at the stand and plot level, and has been successfully modeled using terrestrial, airborne and satellite laser scanning data (Riano 2003, Riano 2004, Erdody and Moskal 2010, Garcia et al. 2012). However, very few studies have examined crown bulk density at the individual tree scale. Riano's (2004) use of airborne laser scanning to characterize individual tree crown bulk density was unsuccessful due to the difficulty of assigning laser pulses to specific trees and low data density.

Current wildfire simulation models such as FARSITE (Finney 1998) or the Fire and Fuels Extension (FFE; Reinhardt and Crookston 2003) of the Forest Vegetation Simulator (FVS; Dixon 2002a, Crookston and Dixon 2005), assume a uniform distribution of crown biomass over an

estimated crown length (a uniform CBD). In order to parameterize CBD, vegetation is field sampled at discrete locations in the crown and those results are applied over the entire canopy. Reconciling total biomass, bulk density and fire behavior is difficult within the limitiation of the current modeling systems. CBD is known to vary within a stand (Reinhardt et al. 2006, Keane et al. 2005) but a single CBD value representing vegetation that is packed tightly enough to burn is needed to produce modeled fire behavior that is reasonable. This uniform application of CBD to a given canopy volume overpredicts total biomass. Conversely, if the actual total biomass was distributed uniformly throughout the crown volume, calculated CBD would be uncharacteristically low and the modeled fire behavior would be unrealistic. Newer, physics-based models (e.g. FIRETEC [Linn 2002] or WFDS [Mell 2006, Mell 2009]) can accept non-uniform (spatially heterogeneous) canopy fuels as model inputs – thus reconciling observed CBDs with actual biomass, and improving fire behavior modeling. Parsons et al. (2011) demonstrated the impact of using non-uniform fuel models on modeled fire behavior, although there is little detailed vegetation data to act as inputs. Ultimately, the work of this thesis will be part of improving those inputs – better estimates of crown biomass, more realistic crown shapes and volumes, and characterization of where that biomass is located within the crown.

Goals and Objectives

The overarching goal of this work is to provide species-specific information about crown architecture that could lead to predictive models for distributing biomass realistically within tree crowns. Many TLS studies focus on detailed characterization of a limited number of trees or small plots (e.g. Beland et al. 2011, Henning and Radke 2006, Hosoi and Omasa 2006). Because this study intended to make some generalized statements about species crown shape and structure, a larger sample was needed. This drove the sampling technique, in which many trees were scanned from one angle instead of one or a few trees being scanned from many angles. Although limiting the

information collected for any one tree, the approach provides data well suited to making generalized observations about universal characteristics.

The goals and objectives are outlined below, as is a short discussion of what is not addressed in this study.

Goal 1. ***To develop an objective measure of crown base height derived solely from TLS data.***

In order to reduce the reliance on field data collection and increase objectivity, a crown base metric was derived directly from the TLS data. Field measures of crown base metrics are commony done using a handheld laser rangefinder and are subject to field crew judgement and precision. Results were compared to two different field-measured crown base metrics and the reasons for variation among measures were considered.

- Objective 1.1 *Define an objective, repeatable metric.*
- Objective 1.2 *Assess differences in LiDAR-derived versus conventional field-measured crown base metrics: crown base height (CBH) and height to live crown (HLC).*

Goal 2. ***To develop species-specific crown profile curves.***

Defining the crown profile is important because, when rotated about its central axis, it defines the crown volume. In the context of this study, crown volume is the initial parameter of spatial organization for predicted biomass. As noted previously, crown profiles have been modeled using several methods, each with their own limitations. TLS is able to capture the crown extent in three dimensions, without destructive sampling, overcoming many of those limitations. By folding 3-dimensional data into two dimensions, information about the extent of the entire sampled crown (not just one slice) is retained. For each tree within a species, width percentiles of the laser returns were calculated at a series of height increments and aggregated into one composite, species-specific profile. Parametric curves were fit to the collection of points and assessed for accuracy. The implications of using different width percentiles, simplified geometries and other species' curves were considered.

- Objective 2.1 *Compare differences in crown profile shapes and volumes using different crown width percentiles.*
- Objective 2.2 *Determine, through goodness-of-fit comparison, the best-fitting modeled curve for each species.*
- Objective 2.3 *Assess the accuracy of the modeled curves relative to those resulting from simple geometric shapes (e.g. a cone or cylinder).*
- Objective 2.4 *Examine species-specificity by exploring permutations of pairings between modeled curves of one species and crown profile points of another.*

Goal 3. ***To characterize patterns of within-crown laser return spatial heterogeneity.***

Describing within-crown spatial patterning is the second step of predicting where biomass is located within a crown. An initial characterization of patterning is simply to identify if a deviation from spatial randomness is observed, and if so, what type of pattern exists. This deviation could be clustering or regularity; in this study, due to the known framework of branches that vegetation is organized around, I expected to see clustering. Another characterization of patterning is determining the scale at which it occurs (i.e. at what size clusters tend to occur). Using a 3D distance matrix, Ripley's K and L functions were calculated to provide a measure of 3D clustering using the point clouds for each tree. Ripley's K uses a count of all the events within some radius of the event in question, iterated over all events (for this study, an event is a laser return from the crown of interest). For a given radial increment, when the event count is higher than what would be expected under complete spatial randomness, this indicates clustering at that scale. The comparison to randomness is made at multiple radii, developing the shape of the function. Differences in clustering patterns were compared among species and within different parts of the crowns.

- Objective 3.1 *Identify the occurrence of within-crown clustering by comparing laser point patterns to spatial randomness.*

- Objective 3.2 *Explore differences in clustering due to canopy position (upper versus lower canopy) and vegetative type (e.g. fine foliage versus branchwood).*
- Objective 3.2 *Determine the scales at which clustering occurs.*

Study Bounds

This work provides species-specific crown profile models for three Northern Rocky Mountain conifers and considers the accuracy of each. It also describes the scale and extent of clumping of laser points by species. An important limitation of the latter effort is that TLS does not directly characterize biomass in terms of amount, size, or type. Rather, it identifies the locations of reflective materials whose other properties are unknown. Although some inference about the type and size of materials is possible using laser intensity data, this thesis does not explicitly address biomass prediction. More significantly, the internal crown structures described in this study are not inherently spatially explicit. Therefore, this research does not yet provide logic for rational allocation of crown biomass in space and additional work is needed to enable full parameterization of tree lists.

Organization

This thesis is organized in four chapters. Following this introduction (Chapter 1), the study methods comprise Chapter 2, the results make up Chapter 3, and a discussion of the findings and limitations of this work, as well as possible future directions, are contained in Chapter 4. Following the body of the thesis are appendices containing detailed, supplemental information. In this work, I show how crown profile models vary among and within species, as well as the implications for choosing a particular model on calculated crown volume and profile accuracy. I show the differences in clustering functions associated with different species and different partitions of the crown volume. I also consider the potential applications and necessary limitations of this work in

allometric and fire behavior modeling contexts. Lastly, I propose directions for future work that build on and enhance this study's findings.

Chapter 2. Methods

Study Sites

During the summers of 2011 and 2012, three northern Rocky Mountain conifer species (*Pseudotsuga menziesii* [Douglas fir – DF], *Pinus ponderosa* [ponderosa pine – PIPO] and *Abies lasiocarpa* [subalpine fir – SAF]) were sampled on 15 study sites in eastern Washington, northern Idaho and western Montana that coincided with the biomass allometry study of Affleck and Turnquist (2012) (Figure 1 and Table 1). Stands were chosen to represent a variety of elevations, tree densities and site conditions; stand selection was constrained by landowner permission to fell trees.

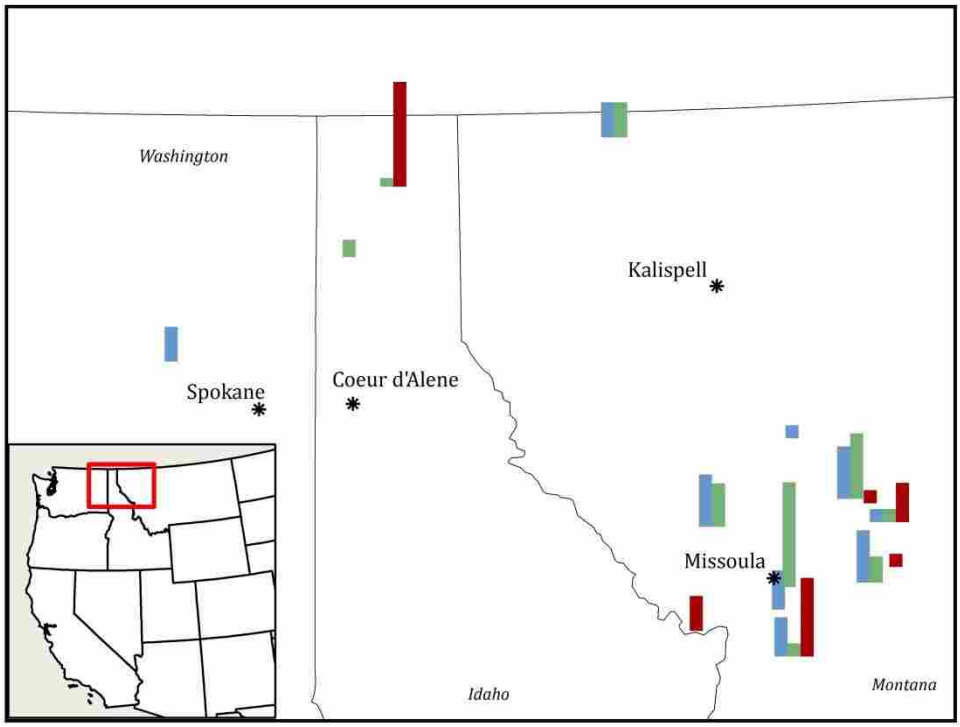

Figure 1. Sample site locations across WA, ID and MT showing relative counts of trees at each site. *Pseudotsuga menziesii* is shown in blue, *Pinus ponderosa* in green and *Abies lasiocarpa* in red.

Multiple trees were sampled at each site; thus, the UTM coordinates given in Table 1 should be considered the general area in which sampling occurred. DF and PIPO were most often sampled

from mixed conifer stands comprised of varying balances of *Pseudotsuga menziesii, Pinus ponderosa, Pinus contorta, Larix occidentalis* and others. SAF was sampled from stands comprised primarily of *Abies lasiocarpa, Picea engelmannii, Abies grandis*, and others. Sites ranged in elevation from 700 – 1900 meters (Table 1): DF was sampled at sites between 700 – 1850m, PIPO at sites between 950 – 1850m, and SAF at sites between 1350 – 1900m. Again, because multiple trees were sampled at each site, elevations as given in Table 1 are approximate elevations for the general sample area.

Table 1. Study site information: name, sampled species, location and elevation.

Site	Species Sampled	UTM Zone	Easting	Northing	Elevation (m)
Ambrose Saddle	DF, PIPO, SAF	12	277750	5154750	1800
Bandy	DF, PIPO, SAF	12	330650	5218450	1350
Bonner's Ferry	PIPO, SAF	11	532930	5391612	1500
Deer Creek	PIPO	12	277950	5189800	1300
Granite Pass	SAF	11	682250	5168250	1900
Kootenai	DF, PIPO	11	650650	5416450	1000
Lubrecht Garnet	DF, PIPO	12	321779	5188647	1850
Lubrecht Section 1	SAF	12	325599	5196356	1900
Lubrecht Stinkwater	SAF	12	316750	5192250	1550
Morrell Creek	DF, PIPO	11	315109	5231482	1350
Nine Mile	DF, PIPO	11	699970	5220532	1400
Plant Creek	DF	11	278151	5178450	1300
Priest River	PIPO	11	514050	5356150	950
Swan-hemlock	DF	12	291614	5263745	1200
Wellpinint - Tomine	DF	11	431013	5303639	700

Stands ranged in basal area (measured around each sample tree) from 20 – 300 ft^2/acre (Figure 2): DF sample sites ranged between 4.6 – 34.4 m^2/ha, PIPO sample sites ranged between 2.3 – 36.7 m^2/ha, and SAF sample sites ranged between 9.2 – 68.9 m^2/ha. "Typical" basal area ranges for a forest type are dependent on many factors (site quality, age, treatment history, etc...). Nevertheless, the stand basal areas measured in this study are consistent with those found in other studies, albeit weighted toward lower values due to sampling constraints (as discussed below). Cochran et al. (1994) model stocking level curves for *Pseudotsuga menziesii* over a basal area range from 11.5 – 55.1 m^2/ha, and for *Pinus ponderosa* over a basal area range from 3.4 – 41.3 m^2/ha.

Studies done in a variety of mixed conifer forests of the Inland Northwest with a significant proportion of *Pseudotsuga menziesii* and/or *Pinus ponderosa* reported basal areas of 9.6 and 12.6 m^2/ha (Reinhardt and Ryan 1998), 11.0 – 62.4 m^2/ha (Moore et al. 1991), 14.0 – 17.2 m^2/ha (VanderSchaaf 2008) and 30.5 – 37.7 m^2/ha (Reinhardt et al. 2006). Stage et al. (1988) present yield tables for natural stands that include *Abies lasiocarpa*: given a site index of 21.3m (which they present as being the plurality for Inland Northwest forests), the stand basal area is expected to range from 0.2 – 60.6 m^2/ha, depending on site age. Edminster (1987) found basal areas of *Picea engelmannii – Abies lasiocarpa – Pinus contorta* stands in the central Rocky Mountains with the highest stand density indices ranged from 55.1 – 97.6 m^2/ha, which can thus be considered an upper limit of expected values. Although most of the trees sampled in this study were located in areas with basal areas toward the lower end of other observed and predicted values, this study did include trees from mid-range and higher basal area sites as well.

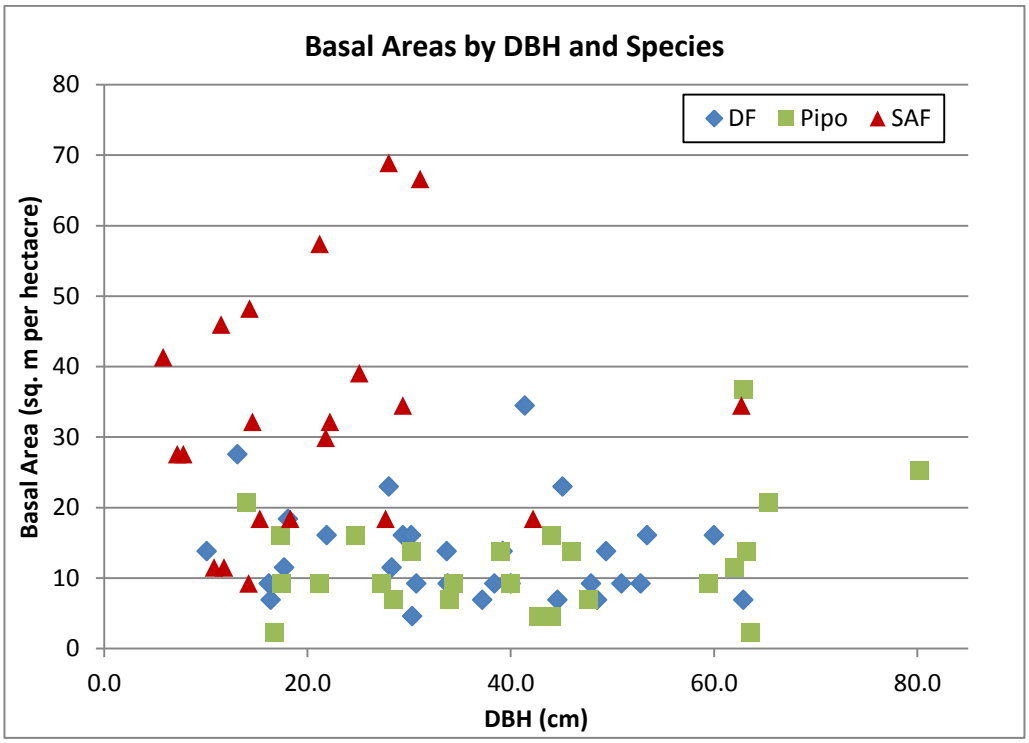

Figure 2. Stand basal area (BA) distribution by DBH and species of trees sampled in 2012. BA was calculated using a 10ft/acre factor angle gauge, and included the sampled tree.

Field Data Collection

Tree Selection

Although the stands chosen were also those sampled by Affleck and Turnquist (2012), the individual trees sampled had incomplete overlap. Some of the trees selected for RBS were also sampled by TLS for this study, but at each site additional trees were also scanned (i.e. not all scanned trees have corresponding biomass measures). The trees that were sampled using both methods can be used in further work to link laser return data to biomass measures. Laser scanning was completed both temporally coincident with biomass sampling and during recurring visits. In order to sample a large number of trees across many species, trees were scanned from one perspective only. Although this provides limited information about any one tree, together, many tree scans are able to capture species variability across size classes and geographic distributions.

Selected trees were required to be:

1. live, with an intact top and no noticeable forks
2. larger than 4cm DBH
3. free from noticeable mistletoe brooms, conks or marked defoliation
4. free from signs of successful beetle attack or root rot disease
5. free from noticeable human alteration (e.g. sawn branches)
6. in stands that had not been treated (harvested, burned, etc…) within five years of data collection

Field measurements taken in 2012 for each sample tree included DBH (to nearest 0.1 cm), basal area before clearing adjacent vegetation (using a 10 ft/acre factor angle gauge), tree height, height to live crown (HLC: height of the lowest branch with live foliage) and crown base height (CBH: the height at which two live branches are separated by at least 90 degrees and are continuous with the crown [USDA Forest Service 2009]). All height measurements were taken using a TruPulse 360 hand-held laser range finder. During field data collection in 2011, no

supplement field measurements were collected. Photographs were taken using the digital camera integrated with the scanner. Because photographic quality was variable (often poor), photographs were used only for reference, not analysis.

Trees were selected to represent varying diameter at breast height (DBH) classes within each species (Figure 3). DBH ranged from 10.1 – 62.9 cm in *Pseudotsuga menziesii,* 14.0 – 80.2 cm in *Pinus ponderosa*, and 5.8 – 62.7 cm in *Abies lasiocarpa*.

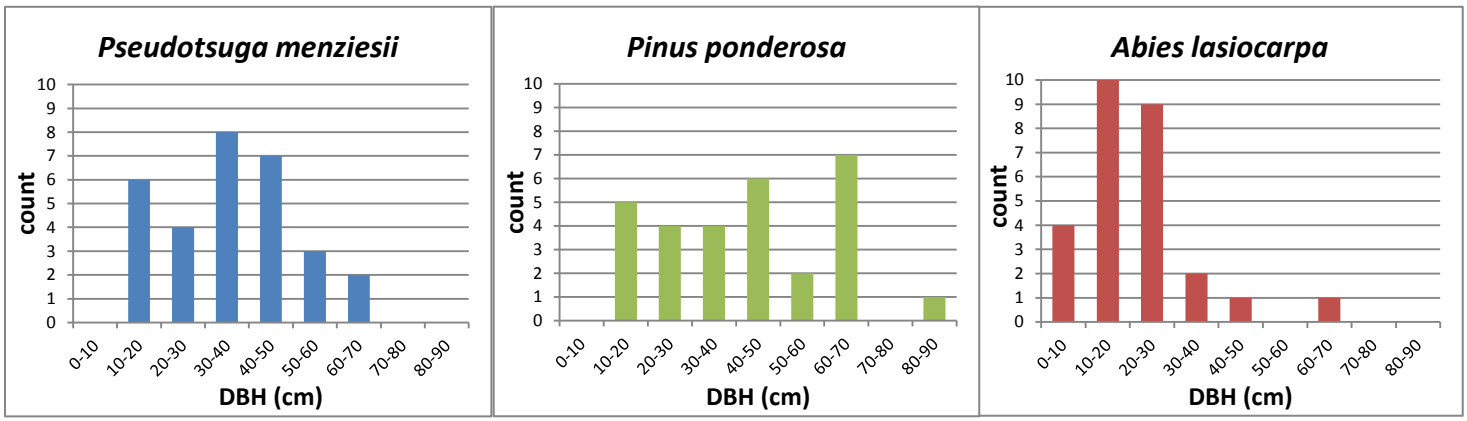

Figure 3. DBH size class distribution.

Crown visibility also played a role in tree selection. A clear line of sight between the laser and at least half of the sample tree is required, and because of this, trees in semi-open conditions (gaps, stand edges, etc…) were disproportionately selected. However, there was no strong association between basal area (as an indicator of stand density) and tree size (Figure 2). Furthermore, although not purposely selected for, the sample trees did span a range of crown base heights and crown lengths (Figures 4 and 5). Of the trees sampled in 2012 that had supplemental field measurement taken, CBH ranged from 0.9 – 14.1 m in *Pseudotsuga menziesii,* 1.0 – 21.9 m in *Pinus ponderosa*, and 0.0-8.4m in *Abies lasiocarpa*. The crown length (tree height – CBH) ranged from 5.6 – 20.9 m in *Pseudotsuga menziesii,* 2.4 – 19.9 m in *Pinus ponderosa*, and 3.8 – 35.5 m in *Abies lasiocarpa*.

Although visibility did influence tree selection, in almost every case, some removal of adjacent vegetation (herbaceous and/or woody, including neighboring trees) was required. Because this study utilized stands associated with an allometry study (Affleck and Turnquist 2012), full tree removal was permitted, although often with some limitations. This allowed sampling in stands that required neighbor trees to be felled to create a line of sight between the sample tree and the laser. Once a sample tree was identified, any vegetation that obstructed the view between the laser and the tree was removed using chainsaws, loppers and/or clippers (from grasses and shrubs at the base of the bole, to entire neighboring trees that impinged upon the sample tree's crown). From the perspective of the laser, the base of bole to top of crown, and the entire width of the crown were required to be isolated from other vegetation. Equal sampling of the range of all possible stand densities was both time prohibitive and hindered by limited landowner permission (e.g. restrictions on the number or species of trees that could be felled to create line of sight). Most of the true closed growth samples in this study were trees co-acquired with Affleck and Turnquist's (2012) study. Because of the limits of the sampled basal area range, results of this work may not apply to closed growth trees.

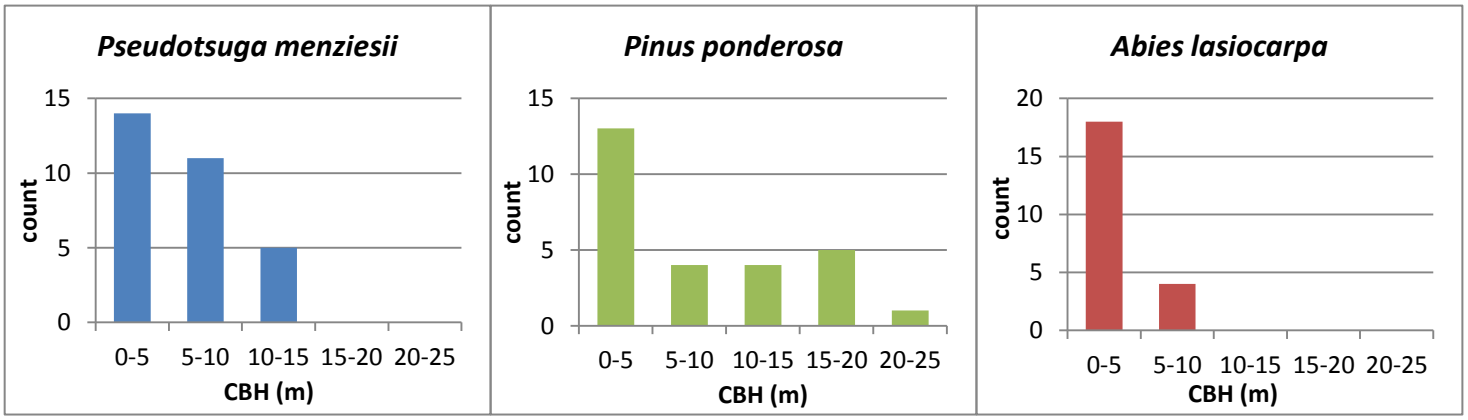

Figure 4. CBH distribution. Note that information is only presented here for trees sampled in 2012 (30 *Pseudotsuga menziesii*, 27 *Pinus ponderosa*, and 22 *Abies lasiocarpa*).

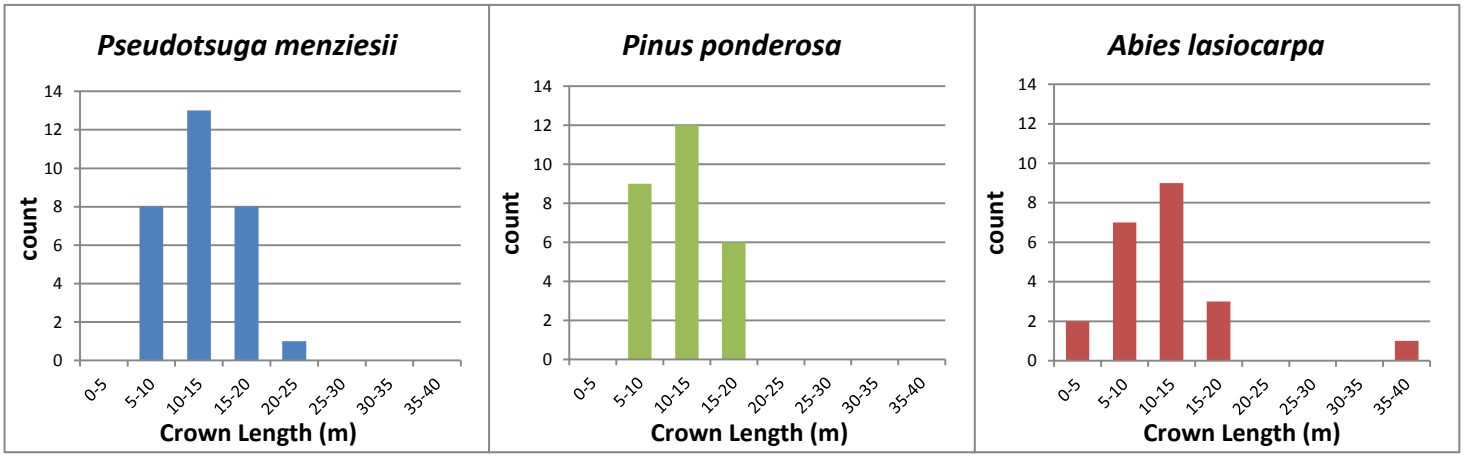

Figure 5. Crown length distribution. Note that information is only presented here for trees sampled in 2012 (30 Pseudotsuga menziesii, 27 *Pinus ponderosa*, and 22 *Abies lasiocarpa*).

Scans

Trees were scanned using an Optech ILRIS 3_6D HD discrete return, time-of-flight terrestrial laser scanner. The laser was mounted on a pan-tilt unit (allowing for bi-directional rotation), atop a level tripod (Figure 6). The laser emits a beam of energy at 1535 nm wavelength (near infrared) with a 0.008594^{o} divergence, resulting in a beam diameter of 19mm at 100 meters (7.75mm at 25m). Sampling was done at 10,000Hz in a zigzag pattern from bottom to top. The laser records position and intensity information (x, y, z, i) for each return. The ILRIS 3_6D HD uses two gain settings for intensity, separating bright and dim returns. Bright returns (low gain) are scaled between 0-255; dim returns (high gain) are scaled between 300-25,500 and binned by increments of 100. Essentially, this results in two 8-bit datasets that are of limited usefulness for reflectance-based classification decisions without substantial signal processing.

Scan parameters were set such that the tree of interest was scanned with a spot-spacing of approximately 4 mm (3.6 to 5.6, median 3.9, Figure 7). The scanner was located at distances ranging from 8.2m to 54.9m, with a median distance of 23.28m (Figure 8). As a function of tree size and distance, individual scan times ranged from just a few minutes to over 30 minutes. Many trees were fully captured in a single scan, but due to limitations of distance and tilt angle, some trees

required separate scans of the lower and upper portions of the tree. In those cases, the scans were designed to include an area of overlap to allow subsequent merging of the scans. Scan parameters for each tree are given in Appendix A.

Figure 6. The Optech ILRIS 3_6D HD terrestrial laser scanner. The laser and scan head (yellow) are mounted on a pan-tilt unit that permits bi-directional rotation, and sit atop a level tripod. The laser is powered by a battery pack and scanning is controlled remotely through a hand-held device. Data is written to a USB that connects at the rear panel of the scan head.

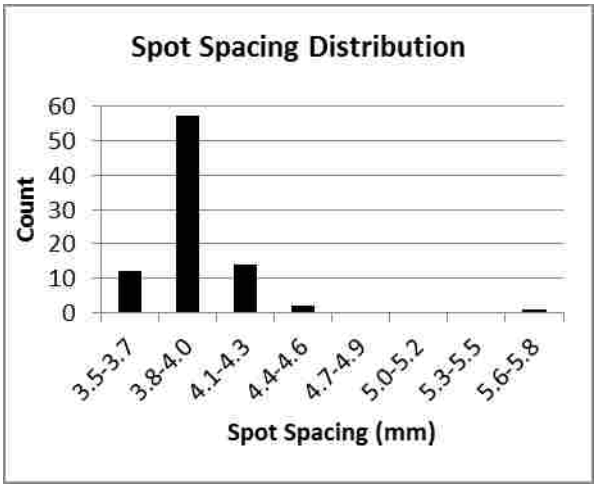

Figure 7. Spot spacing distribution for all scans. Instrument settings allowed specification to the 0.1mm.

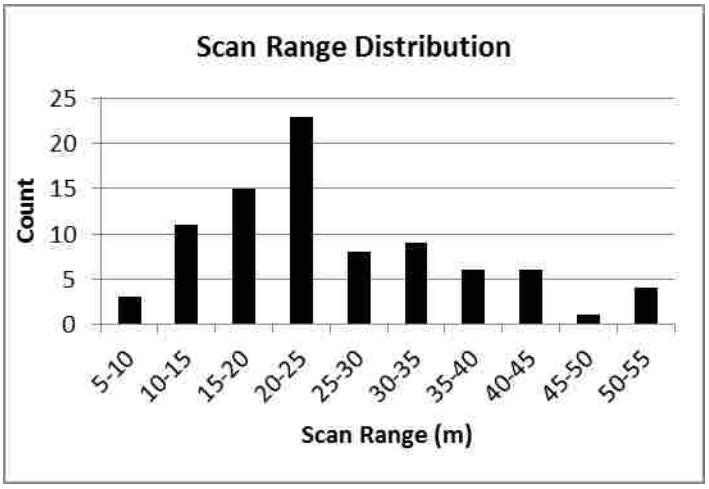

Figure 8. Range distribution for all scans.

Data Pre-Processing

Raw scan data (.i3d) were initially parsed using Optech software into .pf (pif; binary) and .xyz (text) files. When multiple scans had been required to capture the entire tree, the scans were aligned and merged into a single scan for further processing. Overlapping bottom and top scans (as pif files) were aligned in Innovmetric's Polyworks V11.0.1 IMAlign. Using the automated best-fit alignment and comparison tools, matching point patterns between scans were identified and a global shift was applied to the upper image coordinate system to align the point patterns. The maximum search distance iteratively decreased from 1.0 to 0.001 m; each iteration reached a convergence threshold of 0.000016 m. After alignment, the rotation matrix describing the coordinate shift was output. Using code executed in Excelis IDL 8.2.0 (Excelis Visual Information System 2007), the rotation matrix was applied to the upper .xyz file. The (unaltered) lower and (coordinate-shifted) upper scans were merged in a process that eliminated overlap between the scans. Single scans that captured the entire tree in one scan did not require alignment or merging (Figure 9).

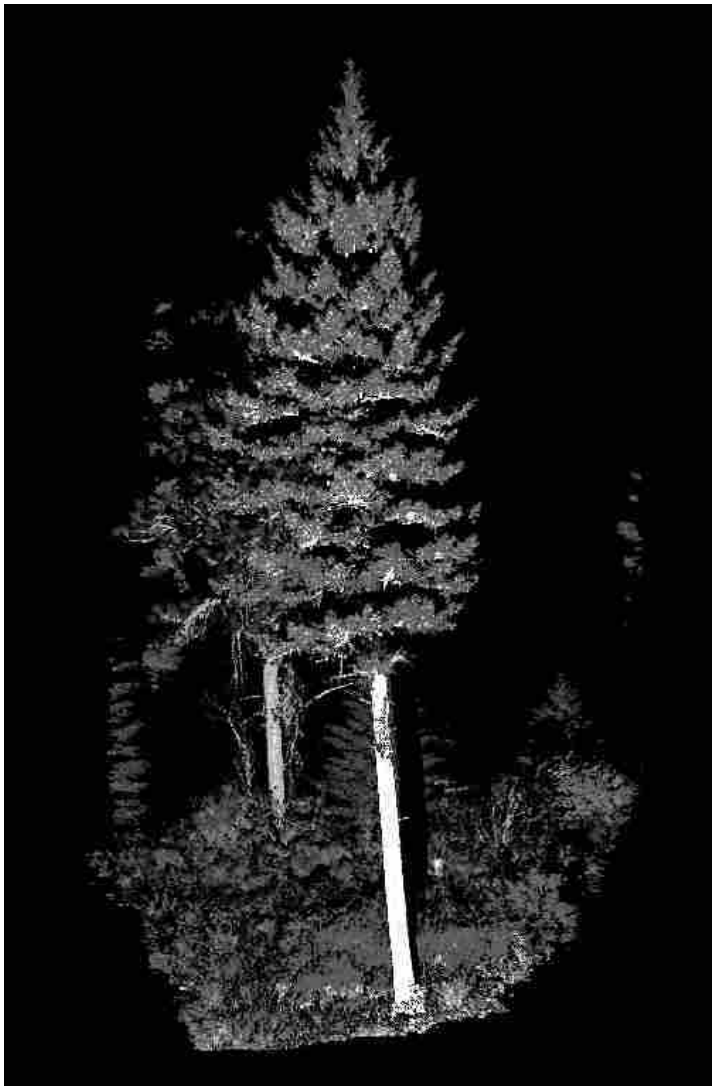

Figure 9. An original single (unmerged) tree scan as initially viewed in Polyworks. Note that the sample tree in the foreground needs to be isolated by removing other vegetation in the scene.

The tree of interest was isolated from each point cloud (derived from either the originally single or newly merged scans), using a semi-automated process. IDL code written in-house identified a proposed tree location, which the user could accept or visually modify by moving within the scan (Figure 10).

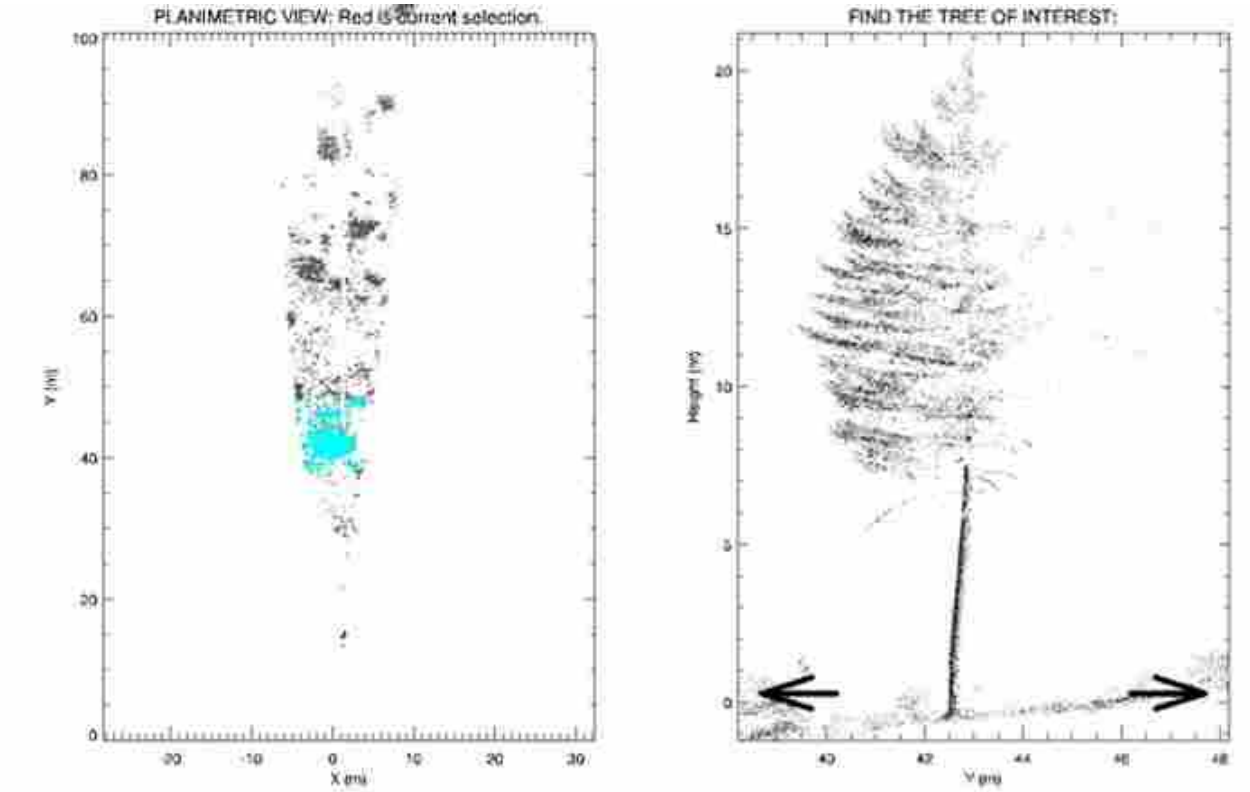

Figure 10. Identifying the tree location (base of bole). On the left is a top-down view that shows in blue the view seen on the right On the right is a side view in which the user identified the center of the bole at ground level. The process is repeated in the other horizontal plane, providing a final location in XYZ space for the bottom of the bole.

When the base of the tree was correctly identified in XYZ space, the remainder of the bole was delineated using a similar process of modifying/correcting a series of ascending bole centroids (Figure 11). Based on proximity to the corrected bole, a line of demarcation in XZ and YZ spaces (i.e. front view and side view) was created to separate points associated with the tree of interest from the surrounding point cloud. Again, user correction to a suggested delineation was allowed (Figure 12). In the YZ (side) view, laser returns behind the bole (away from the laser) were excluded from the remainder of the point cloud. After isolation, the point cloud consisted of just the points from the half of the tree of interest that was closest to the scanner (Figure 13).

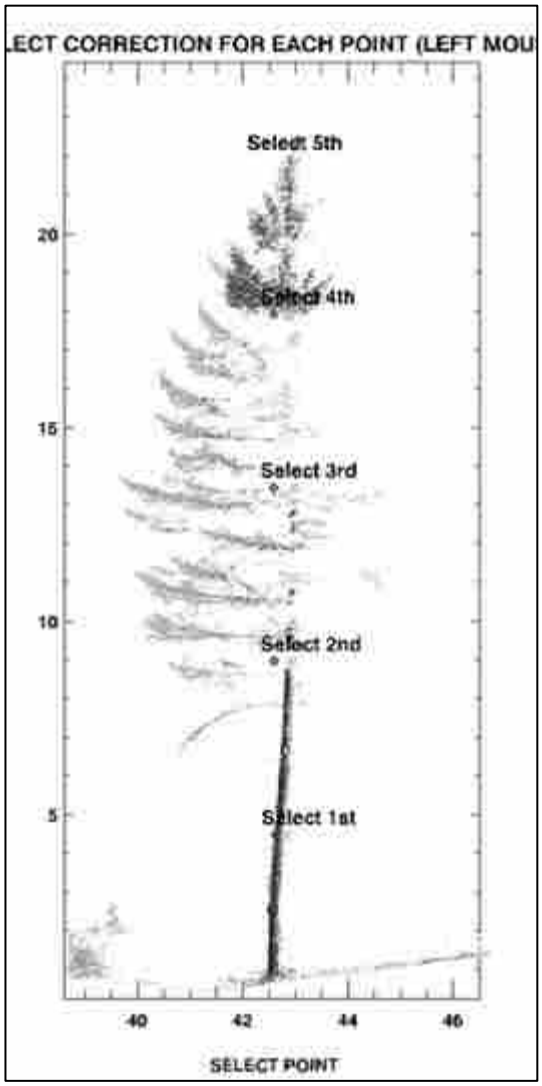

Figure 11. When defining the bole, centroids are proposed (dark grey diamonds), but can be modified by the user to correct their locations (light grey squares).

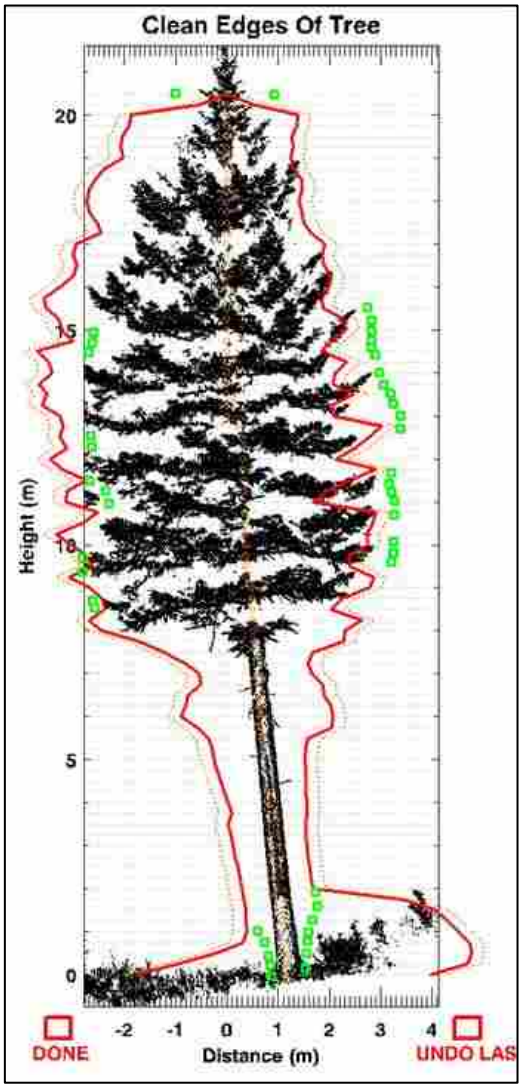

Figure 12. The canopy is delineated, and the user is allowed to expand or contract (green squares) the suggested boundary (red line). The process is repeated in both horizontal planes.

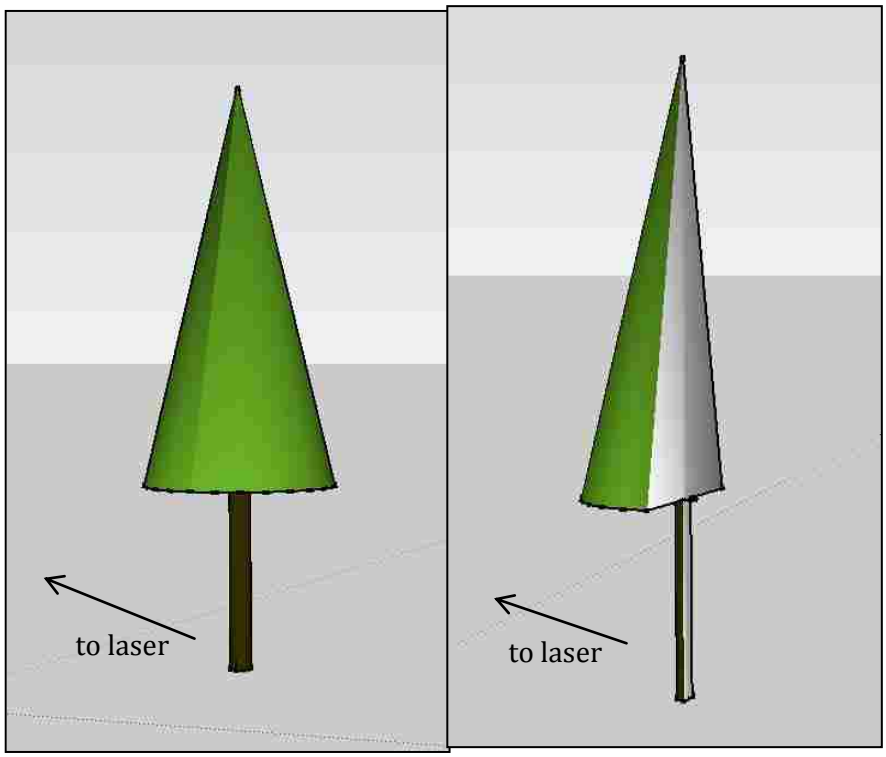

Figure 13. Illustrations showing the extent of the original point cloud (left) and hemisphere of the tree closest to the scanner, after isolation.

Crown Profile Generation

Width Percentiles

Crown profiles were generated from 2D simplifications of the 3D point cloud. The Z coordinate of each return in the preprocessed point cloud was retained. However, the X and Y coordinates of each return were combined into one value that described the horizontal Euclidean distance between that return and the bole centroid. This essentially "folded" the point cloud through a vertical rotation using the center of the bole as the axis, resulting in a 2D point distribution. In the new XY space, the center of the bole was the origin: the x-axis measured horizontal distance from the bole and the y-axis measured height above ground.

In 0.25m height increments, the distribution of returns in X space was used to calculate cumulative width distribution percentiles for each height bin. Following the points delineating a given percentile (e.g. the 50^{th}, 95^{th}, etc…) vertically through each height increment yielded a profile

for that percentile (Figure 14). Width percentiles were generated using code executed in IDL; all other crown profile analysis was completed in R (R Development Core Team 2008).

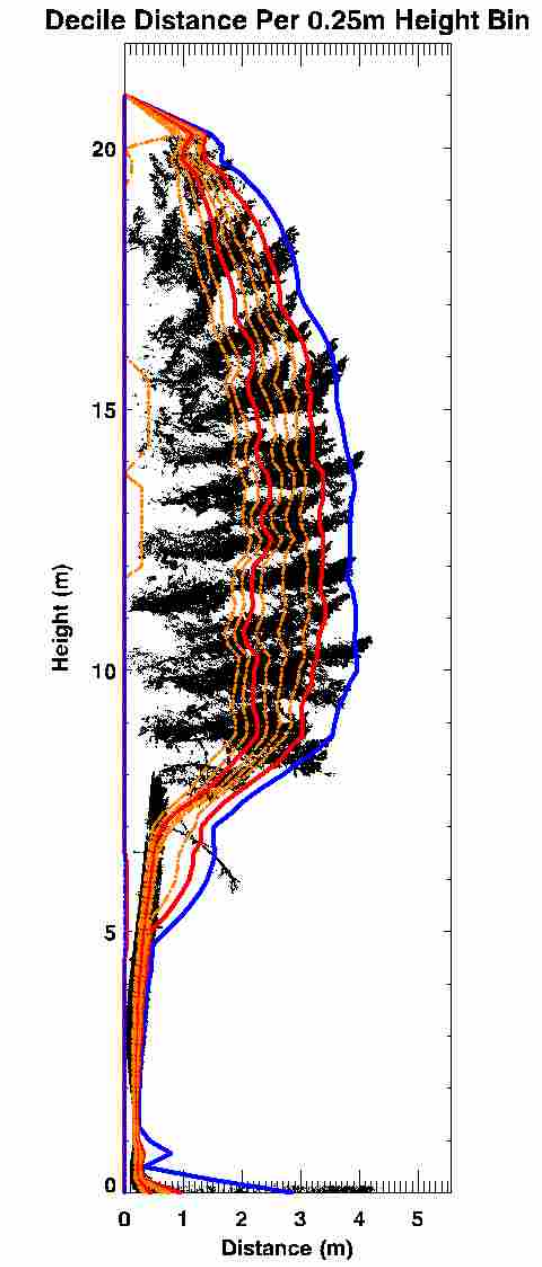

Figure 14 (left). The 2D point configuration, with width percentiles overlaid as colored lines. The solid red lines mark the 50th and 90th percentiles, the orange dashed lines mark 10th percentile increments between, and the solid blue line marks the 100th percentile. Note that the *displayed* percentiles have been smoothed (e.g. the 100th percentile falls inside some material), but the actual data used henceforth was not.

Crown Delineation and Rescaling

The LiDAR crown base height (LBH) was defined as the lowest height at which one-half the maximum width of the 95th width percentile was reached. Thus, if the maximum width of the 95th width percentile was 4.2m, the height where the 95th width percentile was 2.1m was used as the

crown base. The calculated metric was evaluated relative to the field measures of crown base height (CBH) and height to live crown (HLC) (USDA Forest Service 2009).

The LBH was used to separate the percentile points into crown and below-crown, and the lower subset (the branchless bole) was discarded. For every tree, the retained crown 95th width percentile points were vertically rescaled between zero and one to allow comparisons between trees of different crown lengths. First, the minimum height attributed to "crown" points (minimum y) was subtracted from all values, and then those values were divided by the total crown length (the maximum y minus the minimum y). Longer crowns had a greater number of points than shorter crowns due to different numbers of height bins within the original crown. The width values were rescaled proportionate to original crown length for each tree by dividing each x coordinate (representing the crown width as the distance from bole) by the crown length as calculated above. Thus, the crown percentiles were both scalable (because width was tied to height) and comparable between trees of different original sizes.

Crown Profile Modeling

After rescaling, the 95th width percentile points for all trees were aggregated into one composite representation of the 95th width percentile. Past studies have used a variety of mathematical models to predict crown width, including parabolic forms (Biging and Wensel 1990) and polynomials (Baldwin and Peterson 1997, Hann 1999), with little consensus and few ties to other canopy parameter models. Conversely, beta and Weibull curves (Equations 1 and 2, respectively) have been used to model foliage distribution at the tree and branch level (Saito et al. 2004, Mori and Hagihara 1991, Kershaw and Maguire 1996, and Maguire and Bennett 1996), a characteristic that can reasonably expected to be tied to the ultimate extent of the foliage (i.e. the profile).

$$\text{beta: } y = \frac{(x^{a-1})*((1-x)^{b-1})}{\beta(a,b)} \quad \text{(Equation 1)}$$

$$\text{Weibull: } y = \left(\frac{b}{a}\right) * \left(\left(\frac{x}{a}\right)^{b-1}\right) * \left(e^{\left(-\left(\frac{x}{a}\right)^{b}\right)}\right) \quad \text{(Equation 2)}$$

In this study, beta and Weibull curves were fit to these aggregated points to produce an aggregate crown shape for each species. Additionally, modeled beta and Weibull curves fit to each individual tree were averaged to produce a mean crown shape for each species. These two methods were evaluated for consistency by comparing the aggregate curve to the mean-curve-plus-one-standard-deviation envelope.

Because using the 95th width percentile to define the crown envelope was arbitrary, aggregate crown profile curves were also fit to the 91st and 99th width percentile point sets and compared. Lastly, typical simple shapes used by modelers (cones and cylinders) were also used to represent tree profiles. Various approaches have been used to fit simple geometries to tree crowns. Canham et al. (1999) used cylinders whose radius was the average of the two longest perpendicular radii of the outermost crown projection to model nine species (both coniferous and deciduous). Mell et al. (2009) used cones whose diameter was based on the furthest extent of branch tips at the bottom of the crown (not necessarily the absolute lowest branches) to model tree-farm grown *Pseudotsuga menziesii*. Mawson et al. (1976) used cones base on the radius at the bottom of the crown, but noted that along the vertical extent of the crown, the widths of the actual trees exceeded the extent of the model. In this study, cones were shaped so that the radius of the cone at half the max height (0.5 after rescaling) was the median value of the aggregate 95th width percentile points between heights of 0.45 and 0.55. The radius of the cylinders was set using the same criteria. Those values were: DF – 0.160, PIPO - 0.178, SAF - 0.782.

Crown Volumes

The calculated average crown profile curves were used to generate volumes representing species-specific modeled tree crowns. These volumes were compared to volumes derived from the simple geometries (cones and cylinders). Volumes from the 91st and 99th percentile point sets were also generated, and compared to those from the 95th width percentile points to assess variability due to width percentile selection. Lastly, crown volumes were calculated using the curves modeled on the 95th width percentile points, but plus or minus the error for that species' curve. This indicated the maximum potential volumetric variability due to curve fit issues.

Goodness of Fit Analysis

A leave-one-out cross validation was used within each species to assess curve fit using mean absolute error (MAE). Each tree's points were iteratively removed from the aggregated 95th width percentile point set, beta and Weibull curves fit to the remaining tree points, and the position of the reserved tree points were predicted from those fitted curves. MAE was calculated by subtracting the predicted width value for each reserved 95th width percentile point from the actual width value, and taking the absolute value of the result. The errors for all width percentile points were considered collectively for each species (not calculated on a per-tree basis) to determine the MAE. Thus N was $\geq$1400 (depending on the species), not 27 (SAF), 29 (PIPO) or 30 (DF).

The MAE was used for two reasons. First, using the absolute error allows a simple interpretation of the error statistic, in the same dimension as the data. The error metric is the potential crown width error; because crown width is rescaled relative to crown length (i.e. proportionate to crown length), the error is also proportionate to crown length. Second, it is less sensitive to outliers than the root mean squared error (RMSE) that is also dimensioned relative to the original data.

In addition to the cross validation analysis, the fit of each species' modeled curve (generated using all the data) against the aggregated 95th width percentile points for that species was also assessed. Although the resultant error would be artificially low (due to being modeled from the data it is being assessed against), I was interested in exploring the result from using the actual, final equation for that species, not a series of very-similar-but-not-identical curves produced through cross-validation. The 95th width percentile points for each species were also compared to the predictions from the aggregate curves from the other species (e.g. Douglas fir 95th width percentile points as predicted by the Pinus ponderosa aggregate curve) and from the simple geometries (cones and cylinders). In all cases, the MAE statistic was used to assess goodness-of-fit. Two-tailed Student's T-tests were used to evaluate the differences in MAEs between combinations.

Cluster Analysis

The first step in characterizing the internal heterogeneity of crowns was to determine if the distribution of material departed from spatial randomness (i.e. is there clustering or dispersion). Then, more detailed properties of the clusters could be described. For cluster analysis, the 3D point cloud (after pre-processing) of each tree was used – i.e. the points from the half of the tree that that was closest to the scanner. Clustering within a volume necessarily considers the native 3D point cloud (retaining the X, Y, Z, and I values), not the 2D folded data used previously for deriving crown profiles. Cluster analysis was conducted in IDL (Excelis Visual Information Solutions 2007).

Crown Delineation and Rescaling

All laser returns above each tree's LBH were considered crown returns, and those lower than the crown base metric were discarded. Within the "crown" returns, no differentiation was made between points that may have come from needles, branches or the bole. The Z value of each crown return was rescaled between zero and one by first subtracting the smallest crown Z value

from all crown Z values and then dividing each result by the crown length (max Z minus min Z). The X and Y values rescaled relative to the original crown length by dividing each coordinate by the crown length as calculated above. Similar to the rescaling employed for crown profile generation, this has two primary advantages. First, only one value (crown length) is needed to recreate the original crown proportions, and second, after rescaling, the crowns are comparable across many original sizes.

Global Clustering

Ripley's L (a variant of Ripley's K) was implemented in three dimensions to assess the overall scale of clustering within each crown. Ripley's K is an index that describes departure from random patterning (Ripley 1977). For a series of radii (representing areas in 2D or volumes in 3D) around each point in a dataset, the number of other points that fall within that area/volume is counted. The average count per area/volume is compared to the average that would be expected under complete spatial randomness (CSR) (λ). Ripley's L is a version of Ripley's K where the CSR value is used for normalization (Besag, discussion in Ripley 1977 and Graham 2012); CSR becomes zero and values above zero represent spatial clustering whereas values below zero represent spatial dispersion. Due to computational limitation, every 15^{th} data point was used for analysis. The impacts of varying subsampling methodologies is explored in the *post facto* section. Ripley's K and L were calculated for each tree individually. Lambda (λ) was calculated by dividing the number of each tree's selected sample points by the volume calculated from rotation of that tree's Weibull curve through 180^{o}.

Calculation of Ripley's Khat (the estimate of the Ripley's K function) began with creation of a 3D distance matrix between all remaining points ($1/15^{th}$ of the original dataset). As Khat is the average count of events that are within some radius divided by the expected count for that area under CSR (Equation 1), the total count of distance matrix values less than the radius in question

was divided by the total number of events and then multiplied by λ^{-1}. Dixon (2002b) recommends utilizing search radii less than one-half the shortest dimension of the study area. Here, Khat was calculated for radii between 0-0.1 in 0.0125 increments. In 2D, the expected number of events is the area of the circle with some radius; in 3D, the expected number of events is the volume of the sphere with that radius. As most applications of Ripley's K and L have been in 2D, examples of implementation in 3D are uncommon, but available (e.g. da Silva et al. 2008, Jafari-Mamaghani 2010, Beil et al. 2005).

$$Khat(r) = \frac{1}{\lambda N} \sum_{i=1}^{N} \sum_{j \neq i} I(d_{ij} \leq r) \qquad \text{(Equation 1)}$$

where λ= expected average number of events per unit area/volume under CSR

N=number of events within distance r of any event

i,j=the i^{th} and j^{th} points ("events")

$d_{i,j}$ = distance between the i^{th} and j^{th} points

r=radius of interest

$$I(d_{i,j} \leq r) = \begin{cases} 1 \; if \; d_{ij} \leq r \\ 0 \; if \; d_{ij} > r \end{cases}$$

The same series of radii (0-0.1, by 0.0125) were used to construct the theoretical Ripley's K curve under an assumption of CSR, using a simplified form (Equation 2).

$$K(r) = \frac{4}{3}\pi r^3 \qquad \text{(Equation 2)}$$

where *r*=radius of interest

Ripley's L is based on the same premise in 3D as 2D – normalizing the K value. Similar to above, calculating this in 3D means employing a volume relationship instead of one based on area. The empirical Lhat was calculated for all values of Khat (using radii from 0-0.1in 0.0125

increments) using Equation 3. Ripley's L under CSR was calculated the same way but used the values of K from Equation 2, which normalized the function to zero.

$$\text{Lhat(r)} = \sqrt[3]{\frac{3Khat(r)}{4\pi}} - r \qquad \text{(Equation 3)}$$

where *r*=radius of interest

In most applications of spatial statistics, an edge effect correction term is needed, because the sampled events lie within some boundary arbitrarily delineating the study area from the larger event population (Dixon, P. 2002). In these cases, events that are adjacent to, but outside of, the study area are not counted, even if they would have fallen within the search radius for a point inside the study bounds. Without compensation, this leads to an underestimation of the clustering. Although multiple edge effect corrections are available for point pattern analysis in 2D, none is directly extendable and applicable to 3D, although some solutions have been proposed (Jafari-Mamaghani et al. 2010). However, an important question is the suitability of edge correction, regardless of dimension. Lancaster and Downes (2004) state that application of edge corrections "depends on the underlying assumption that the region surrounding the study plot has a point density and distribution pattern similar to areas within the plot. … Many habitats have hard, 'real' edges, e.g., aquatic-terrestrial boundaries, and the point pattern cannot possibly extend beyond the plot boundary." In this work, the study area (a tree scan) is defined as the full extent of all points on the tree (laser returns); the space around the tree is empty, and no correction for edge effects was applied, although the potential consequences of these real edges are examined in the *post facto* section of this thesis.

Clustering by Height Partition (Upper versus Lower Crown)

The original approach to analyzing clustering within the crown was to consider the entire crown as one unit. However, visual observations of tree crowns suggested that perhaps material

was arranged differently in different parts of the crown. Bulk density (biomass per volume) has been shown to vary vertically within the canopy of an entire stand (Reinhardt et al. 2006, Keane et al. 2005), and I was interested to find out how the patterning of material varied vertically within a single crown. This possibility of differences in the upper and lower portions of a tree crown was first tested on a subsample of six *Pseudotsuga menziesii*. The rescaled crowns of those trees were vertically divided evenly into two sections (rescaled heights of 0 – 0.5 and >0.5 – 1.0), and Ripley's K and L were calculated separately for the upper and lower halves. The vertical partitioning produced consistently different clustering results across all sample trees, and was subsequently applied to all trees. It is worth noting that dividing the crown in half did create an arbitrary study boundary that, because no edge correction was applied, could result in underestimation of the clustering. The impacts of this upper-lower boundary (the edge effect) is explored in greater detail as a *post facto* analysis.

Within each height-partitioned portion of the crown, the Ripley's L values at each radius increment (i.e. distances representing the scale of clustering) were averaged across all trees to produce an average function per species. Due to dataset errors incurred during the last stage of pre-processing (a failure to write the data completely to a file), not all trees had point clouds suitable for cluster analysis. The width percentiles generated earlier in the data processing for those trees were correct, but the final 3D data exported incompletely. The number of trees used for these analyses are *Pseudotsuga menziesii* = 23, *Pinus ponderosa* = 17, and *Abies lasiocarpa* = 26.

Clustering by Material Size Stratification (Fine Fuels versus Branchwood)

Fine fuels (< 0.635 cm) are the most important fuel size class to understanding fire behavior, as their high surface area to volume ratio results in high flammability. Unfortunately, the laser only records the location of material; it does not classify returns as possessing any particular attributes other than location and intensity (e.g. fuel size class or tree species). However, the work

of Seielstad et al. (2011) showed the potential to used return intensity to discriminate fine from coarse fuels, as the return brightness is related to the target properties: large, solid targets produce brighter returns while small, diffuse targets produce dimmer returns. The same subsample of six *Pseudotsuga menziesii* were used to investigate possible differences in clustering functions from intensity-stratified point clouds (representing fine fuels and branchwood). Because intensity is known to decay with distance (Seielstad et al. 2011 and Beland et al. 2011) all points were first intensity normalized to 15m using an empirically derived decay function, Equation 4 from Seielstad et al. 2011, where *x*, *y* and *z* are the linear distances in each plane from the point to the scanner, d_{ref} is the reference distance (15m), i_{raw} is the raw intensity, and i_{rc} is the range corrected intensity.

$$\frac{e^{0.04*\sqrt{x^2+y^2+z^2}}}{e^{0.04*d_{ref}}} * \ i_{raw} = i_{rc} \qquad \text{(Equation 4)}$$

The normalized intensity was systematically thresholded to separate returns from solid and diffuse material (essentially branchwood and foliage/fine fuel) and the crown was displayed under that classification scheme. Through visual inspection of the results, a breakpoint was chosen that appeared to best separate fine fuels from branchwood. Apparent branching structure and coincident photographs were used to support the evaluation process, but no true ground truth data was available for a quantitative accuracy assessment. For the subset trees, Ripley's L functions calculated for both the entire set of crown points and just those points falling below the breakpoint (returns considered diffuse material/fine fuels) were compared. Because the results of this stratification indicated little/no difference in clustering between point sets, this separation was not applied in the final analysis.

Post Facto Exploratory Analysis

After the main analyses were completed, several issues were examined in detail to understand their impact on the original findings. The reasoning behind each consideration and a descriptions of how it was addressed are outlined in this chapter, with the results and discussion of each in *post facto* sections of those respective chapters. The considerations include: effects of rescaling the data relative to crown length; effects of the subsample method employed in calculation of Ripley's K and L; and edge effect on the calculated Ripley's K and L functions.

Rescaling

Because all crowns were rescaled relative to crown length, the observed scale of clustering can be interpreted as a proportion of crown length. Thus, one premise of the methods employed here was that actual cluster size (in unscaled space) was tied to crown length (i.e. the size of clusters as measured in real space increases with crown length). In order to investigate that assumption, a Ripley's L function was calculated for the *Pseudotsuga menziesii* with the longest and shortest crowns as determined using the LBH (26.38 and 6.32 m, respectively), using the unscaled, native point locations. The observed scales of maximum clustering were compared with the predicted scales from the average clustering function for the species to confirm agreement between the datasets.

Because the tree crowns were rescaled prior to analysis, the search increments used in calculating the Ripley's K and L values are proportionate to the crown length. Thus, as crowns increase in length, although the relative increment remains constant, the absolute search radius also increases. The unrescaled point clouds of the same trees described above, representing the extremes of crown length in *Pseudotsuga menziesii*, were analyzed using 36 increments, invariant with crown length (0-0.1 by step 0.01; 0.12-0.4 by step 0.02; and 0.45-0.9 by step 0.05 – meters). Clustering differences between the large and small trees across all scales were compared both to

each other and to the original, coarser Ripley's functions for each tree to examine the influence of the original cluster increments on clustering results.

Subsample methodology

The cluster analysis done in this study used a subsample of every 15th laser return. To explore the effects of different subsampling choices, repeated calculation of Ripley's L was done for one *Pseudotsuga menziesii* (22.5m ht, 37.2cm dbh, 16.5m crown length) and one *Abies* lasiocarpa (4.5m ht, 5.8cm dbh, 4.5m crown length) using the following datasets: a random selection of 1/15th of all crown returns; every 6th laser return (representing a spot spacing of ~24mm where the footprint of any one return should not overlap with that of a neighboring return); sampling at every 15th return, but at each sample point, counting neighbors using all crown returns; sampling a random selection of 1/15th of the crown returns, but at each sample point, counting neighbors using all crown returns. An attempt was made to calculate Ripley's L for the entire crown dataset (no subsampling), but was computationally prohibitive for the larger tree; this was completed for the smaller *Abies lasiocarpa*. The resulting Ripley's L functions were compared to the original method used in this study to determine the influence of subsample method. When the minimum search radius is larger than the minimum spacing, the subsampling method should not greatly influence the resulting K and L values, because the predicted counts will be subject to the same manipulation of what constitutes the "total" sample size. A crown would need to be shorter than 4.8m to have a relative search radius smaller than the spacing at 1/15th of the data points; only one tree in this study (the *Abies lasiocarpa* sampled here) met this criterion.

Edge Effects

Calculation of Ripley's K and L rely on a comparison between the actual number of points within a series of search radii and the predicted number found under complete spatial randomness

(CSR). CSR assumes that the random distribution of points within the study area is part of a continuous field of a random distribution. When a sample point is located near the study area edge, the predicted count of neighbors under CSR will reflect this assumption of a continuous field, while the actual count will only consider the points within the study area. This leads to an underestimation of the Ripley's K and L values for that radius, an underestimation that is expected to increase with the search radius as more of the search area/volume lies outside the study area. In this study, two types of edges were present: the artificial edges created by removing the back half of the tree and separating the upper from lower crown, and the actual edge at the extent of the crown.

Artificial edges:

One *Pseudotsuga menziesii* (22.5m ht, 37.2cm dbh, 16.5m crown length) was used to investigate the effects of the artificial edges in three scenarios. First, in order to isolate the effect of the upper-lower crown boundary, Ripley's L was calculated using the original sample points from each vertical section (every 15th point from the front half of the tree), but including the entire front-hemisphere as a "searchable" volume. Thus, search volumes for points near the upper-lower boundary that extended beyond the boundary had neighboring points to count (as if, similar to CSR, the point distribution was inside the study area was part of a continuous field with that distribution). Second, in order to isolate the effect of the front-back boundary, Ripley's L was calculated using the original sample points from each upper or lower section and the entire front half, but with that section mirrored around the y-axis to create a "whole" tree. Lastly, Ripley's L for each of the upper, lower and entire front-hemisphere sections was calculated using the original set of sample points for that section, but searching the entire mirrored crown to eliminate both the upper-lower and front-back boundaries.

Actual edges:

Although the *post facto* investigation described above corrected for the artificially introduced edges, the clustering results may still be influenced by the effect of the actual edge of the

canopy extent. Although this is actual boundary, the amount of canopy edge varies between upper and lower crown sections, as well as between trees of different crown shapes and sizes (related to the height:width ratio). Thus, the consistent pattern of clustering in the lower crown occurring across larger scales and to a greater degree than that of the upper crown may have been an artifact of the amount of crown edge, and not a reflection of actual pattern differences within the crown. To determine if the differences in the Ripley's L functions between upper and lower crown sections was due to a greater edge effect or to actual morphological differences, a series of Ripley's L calculations were done in which the surface area/volume ratio of the test segments was held constant. In these trials, the actual effect of the edge is not known, but because the relative amount of edge is consistent, differences in the Ripley's L function should be attritutable to actual differences in the point pattern. The unrescaled crown of one *Abies lasiocarpa* (20.1m ht, 29.4cm dbh, 19.4m crown length) was first mirrored to eliminate the artificial front-back edge, and then partitioned into seven slices that maintained a consistent surface area to volume ratio. The increments of these slices, as height in m above the LBH, were 2.211-3.0, 5.0-5.801, 8.0-8.883, 10.005-11.0, 13.0-14.42, 14.0-15.81, and 15.0-19.0. For each slice, the volume and surface area were calculated for the frustum formed by the radii predicted by the Weibull curve at those heights and the interval between the heights.

Additionally, Ripley's L was calculated for the slice of an unrescaled small *Abies lasiocarpa* (5.5m ht, 7.2cm dbh, 5.5m crown length) that met the same surface area to volume ratio as the segments described above. The segment from the small tree was 0.5-5.25, as height in m above the LBH. The resulting Ripley's function was compared to those of the larger tree to assess the prediction that clustering in smaller trees is similar to that occurring in the upper portions of larger trees. For all calculations (large and small trees), the search radii used were 0.0-0.1, by 0.01; 0.12-0.4, by 0.02; and 0.45 and 0.5. As the tree crowns used were not rescaled, these search radii are absolute measures, in meters.

(this page intentionally left blank)

Chapter 3. Results

Crown Base Delineation

The crown base heights (both those measured in the field and calculated from the TLS data) showed different trends among species. Both *Pinus ponderosa* and *Pseudotsuga menziesii* showed field-measured CBHs distributed quasi-uniformly between the minimum and maximum values for each species (0.9 – 14.1 and 1.0 – 21.9 m, respectively). *Abies lasiocarpa* however, had a lower maximum field-measured CBH (8.4m), and over 80% of trees (18 of 22) had a CBH below 3.8m.

The relationships between the LiDAR derived crown base metric (LiDAR base height - LBH) and the field measured CBH and HLC are shown in Figure 15. In all species, LBH consistently underestimated CBH. The field-measured HLC was underestimated in trees with low crown bases and overestimated in trees with high crown bases, although this trend is weak in *Pinus ponderosa*. *Pseudotsuga menziesii* and *Abies lasiocarpa* showed moderate correlation between calculated and field-measured crown base measures; the correlation in *Pinus ponderosa* was strong. The disparity between field-measured and laser-derived crown base metric was largely due to the presence of dead branches below the live crown that were considered in the LBH, but not in the CBH or HLC. This was most common in *Pseudotsuga menziesii,* and was also seen in some trees of *Abies lasiocarpa.*

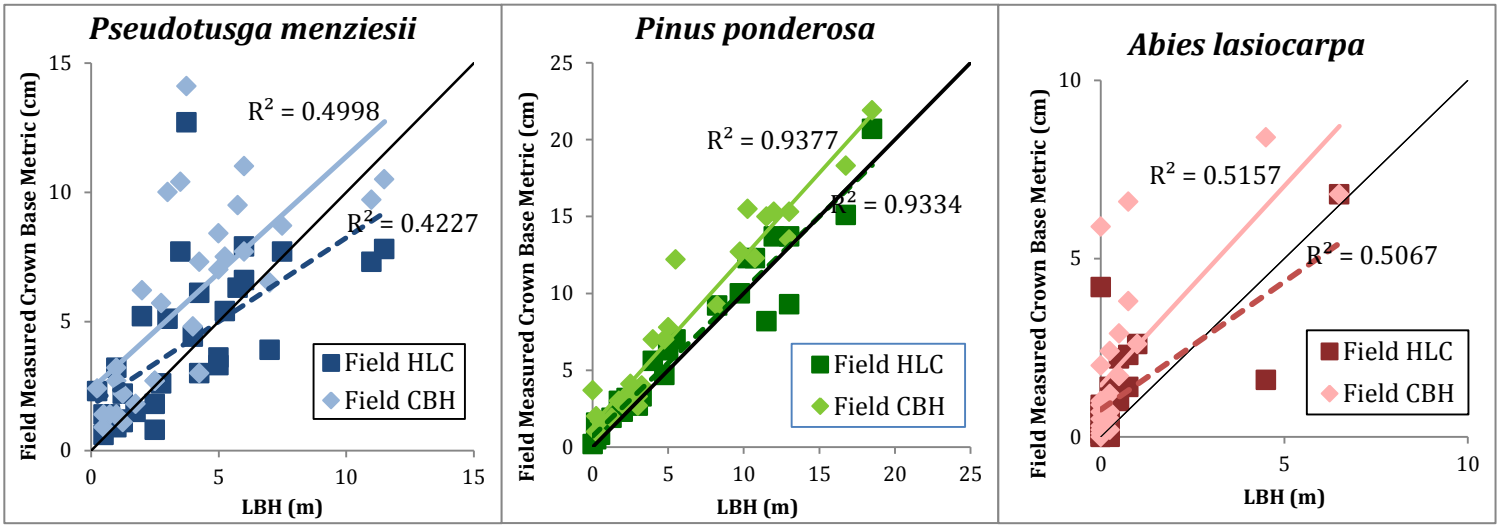

Figure 15. Crown base comparisons for each species. In each case, the light, solid line is the trendline for the crown base height, the dark, dashed line is the trendline for the height to live crown, and the black line is a 1:1 relationship. Field measures of crown base metrics were only available for trees scanned in 2012: 30 *Pseudotsuga menziesii*, 27 *Pinus ponderosa* and 22 *Abies lasiocarpa*. Note the difference in scales among graphs.

Crown Profiles

Aggregate Percentiles

After determining the LBH for each tree, the points comprising the 95th width percentile of each crown were combined into one aggregate outer crown per species. The aggregated outer crowns for each species are shown in Figure 16.

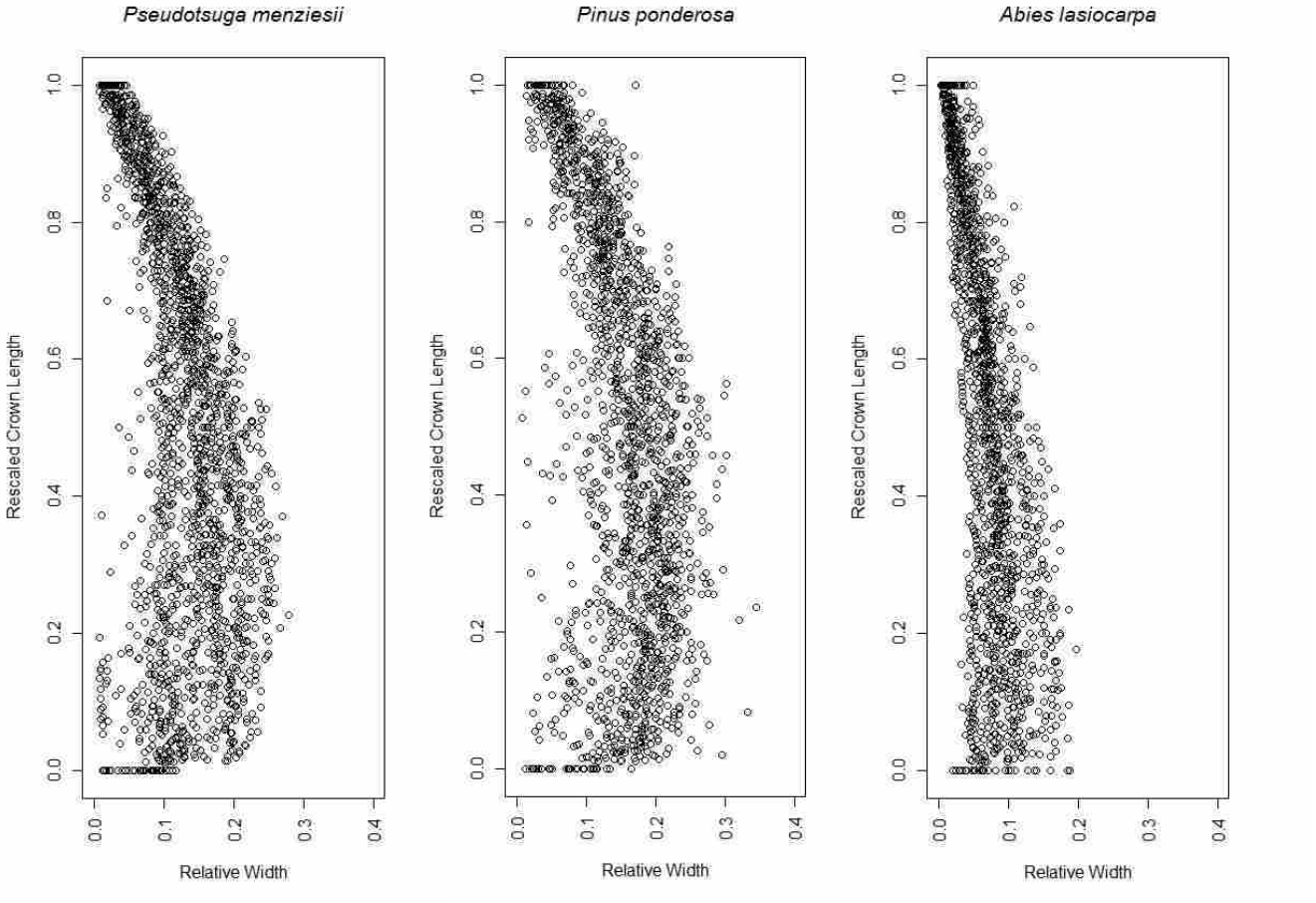

Figure 16. Aggregate 95th width percentile points for each species, after rescaling the crown length 0-1 and the crown width relative to the crown length.

Crown Profile Modeling

Average beta and Weibull curves (Equations 5 and 6) were fit to the 91st, 95th and 99th percentile width points (at each height bin) for each species. The Weibull equation required modification to compress the scale over which it decayed. The general shape is reasonable but an additional scaling term ("c") was required to fit the curve to the y-values of the points. The beta curve was used unaltered. The parameters for each case are given in Tables 2 and 3. To display the variability in parameters within each species, Figure 17 shows the parameters for each individual tree's curve as related to crown length; there was no strong trend of parameter variation with crown length.

$$\text{beta: } y = \frac{(x^{a-1})*((1-x)^{b-1})}{\beta(a,b)} \qquad \text{(Equation 5)}$$

$$\text{Weibull (modified): } y = \left(\left(\frac{b}{a}\right) * \left(\left(\frac{x}{a}\right)^{b-1}\right) * \left(e^{\left(-\left(\frac{x}{a}\right)^{b}\right)}\right)\right) * c \qquad \text{(Equation 6)}$$

Table 2. Beta parameter values for varying percentiles of each species.

Beta Parameters			
Species	91st	95th	99th
Pseudotsuga menziesii	a = 1.97446 b = 2.54670	a = 1.94204 b = 2.53031	a = 1.94615 b = 2.45278
Pinus ponderosa	a = 1.85215 b = 2.42685	a = 1.85512 b = 2.39775	a = 1.82688 b = 2.35153
Abies lasiocarpa	a = 2.04210 b = 3.56608	a = 2.01894 b = 3.50605	a = 1.99874 b = 3.39807

Table 3. Weibull parameter values for varying percentiles of each species.

Weibull (modified) Parameters			
Species	91st	95th	99th
Pseudotsuga menziesii	a = 0.65115 b = 1.43478 c = 0.14562	a = 0.66098 b = 1.40262 c = 0.15398	a = 0.665333 b = 1.438891 c = 0.160203
Pinus ponderosa	a = 0.708733 b = 1.335055 c =0.188839	a = 0.72410 b = 1.32662 c = 0.194334	a = 0.720075 b = 1.336466 c = 0.204142
Abies lasiocarpa	a = 0.573449 b = 1.270374 c = 0.078580	a = 0.577955 b = 1.267652 c = 0.083247	a = 0.573449 b = 1.270374 c = 0.078580

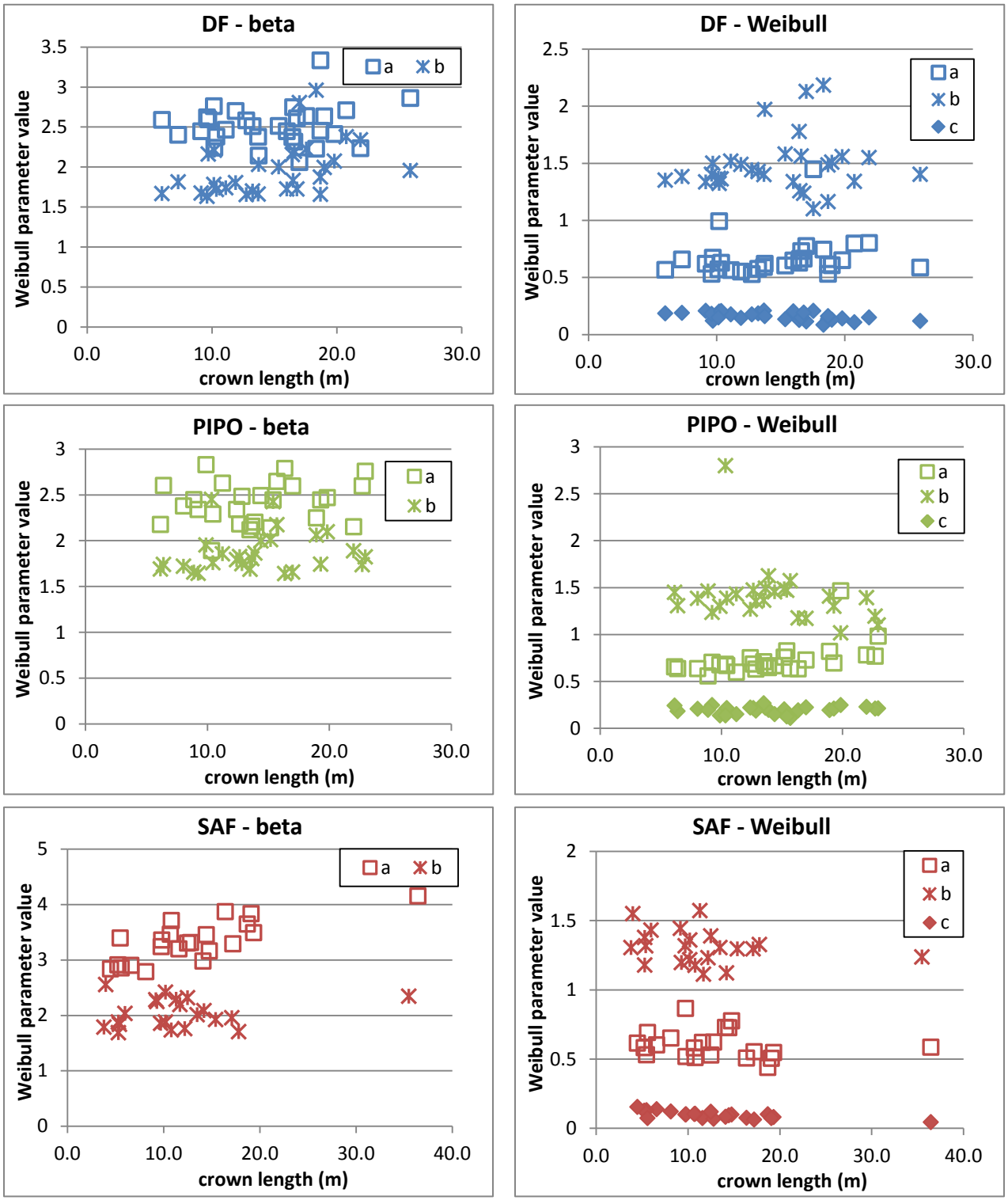

Figure 17. Parameters for Weibull and beta curves of individual trees as related to crown length. Note the variation in y-axis among plots.

Figures 18 and 19 show the resultant beta and Weibull curves for each species under each potential "outer" profile. Use of the 95th percentile width did not produce a noticeably different aggregate beta or Weibull curve shape than use of either the 91st or 99th percentiles. The resultant volumes from rotation of each profile (as relative to the volume produced using the 95th width percentile) are presented in Figure 20 and 20a. Consistent across species, there was a slightly greater difference in volume between the 95th and 99th percentile curves and the 91st and 95th. In most cases, the volumetric effects due to percentile choice were minor compared to the volumetric differences between modeled curves and simple geometries. The exception to this pattern was the volume of *Abies lasiocarpa* as modeled by a cylinder; volumetrically, it fell between the values from the 95th and 99th percentile curves. As crowns are scaled up from a crown length of one unit, the relative crown volumes will remain consistent, although the absolute differences between modeled shapes will increase.

The beta curves (Figure 18) have a rounder "belly" and a more tapered base than do the Weibull curves. Without comparing to the points, they appear (to my eye) closer to a stylized tree crown shape than the Weibull curves. However, when the beta curves derived from the 95th width percentile points are overlaid on the points (Figure 21), those curve characteristics are not necessarily seen in the aggregate width percentile points. The belly of the beta curve appears to fit *Pseudotsuga menziesii* well, somewhat overestimate the extent of *Pinus ponderosa*, and add a curve to *Abies lasiocarpa* that the points do not indicate. The base of the beta curve also appears to fit *Pseudotsuga menziesii* the best (although with some underestimation), *Pinus ponderosa* with greater underestimation, and add a strong taper to *Abies lasiocarpa* that is not indicated by the aggregate points. The upper portion of the curve underestimates all species to an apparently similar degree.

The Weibull curves (Figure 19) have a much gentler "belly", and flatter base and a top that does not return to an x-axis value of zero (an inherent property of the Weibull). When overlaid

onto the 95th width percentile points (Figure 22), the middles and bases of the curves fit all species well, although there is still a base curve attributed to *Abies lasiocarpa* not indicated by the points. In many cases, the *Abies lasiocarpa* crown base was at ground level (or very nearly so), resulting in a continual decrease in width from the lowest (which in those cases is also the widest) portion of the crown upward. In all species, the upper portion of the Weibull curve overestimates the profile extent.

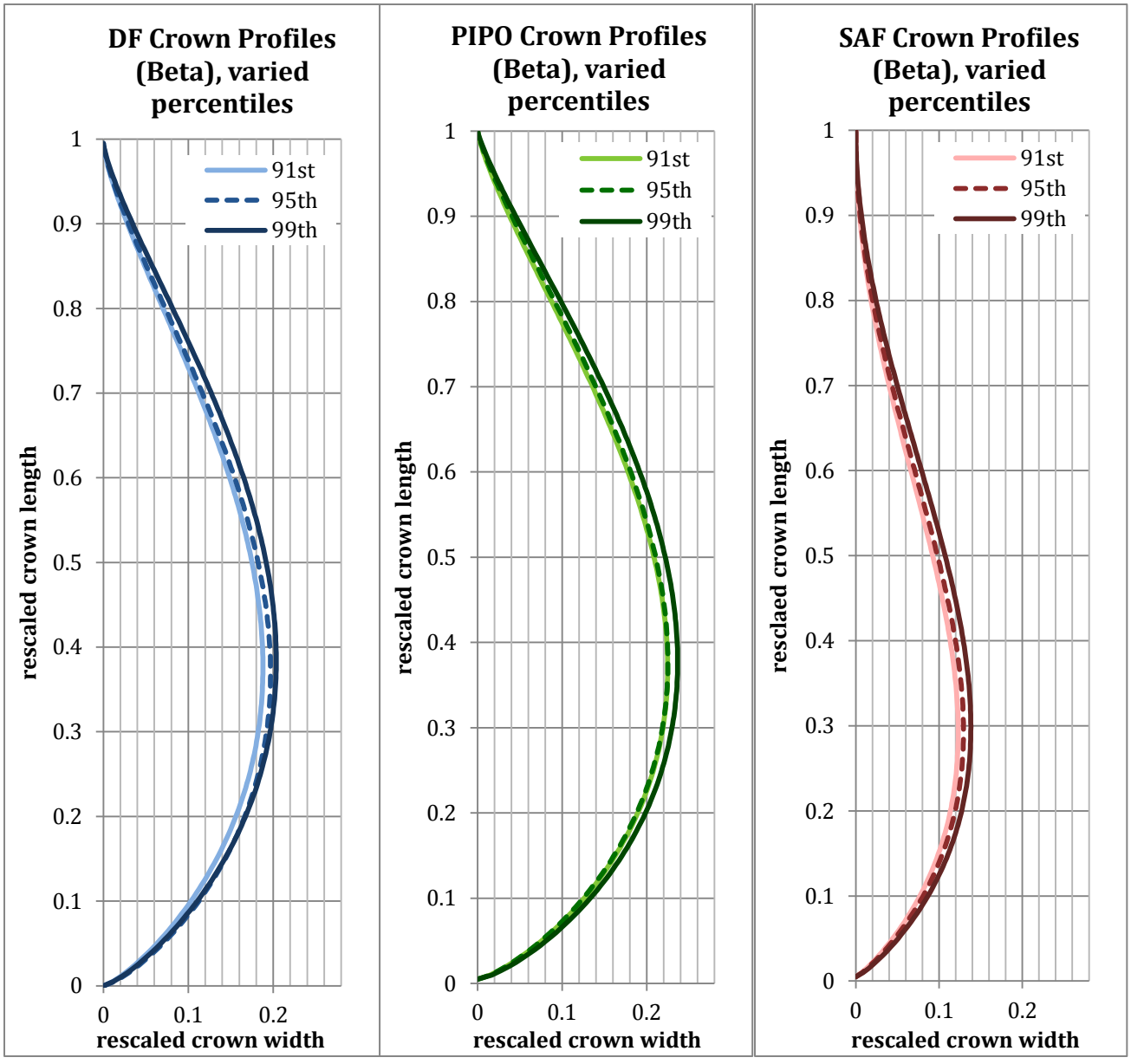

Figure 18. Beta curves modeled on the 91st, 95th or 99th width percentile points for each species.

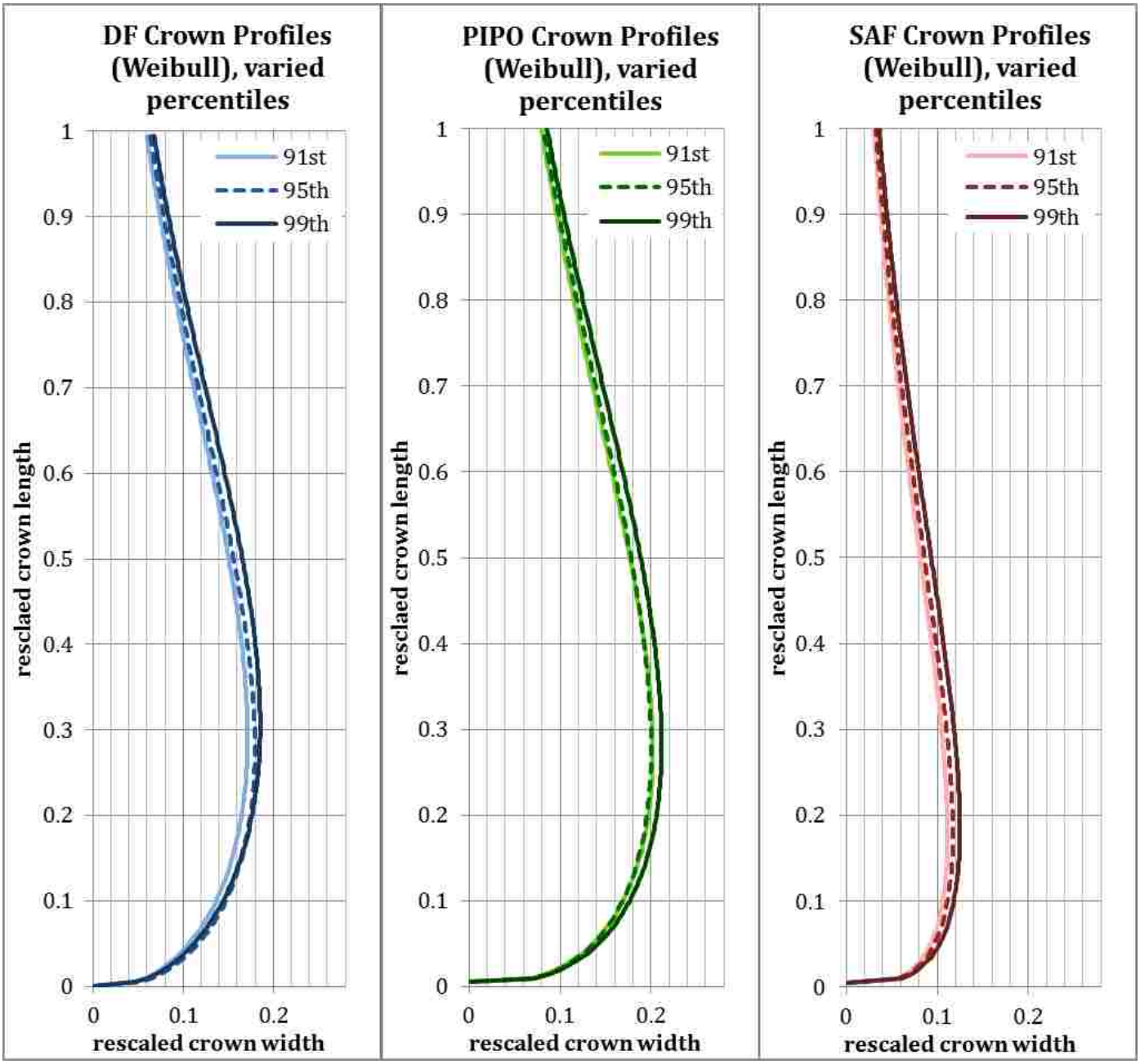

Figure 19. Weibull (modified) curves modeled on the 91st, 95th or 99th width percentile points for each species.

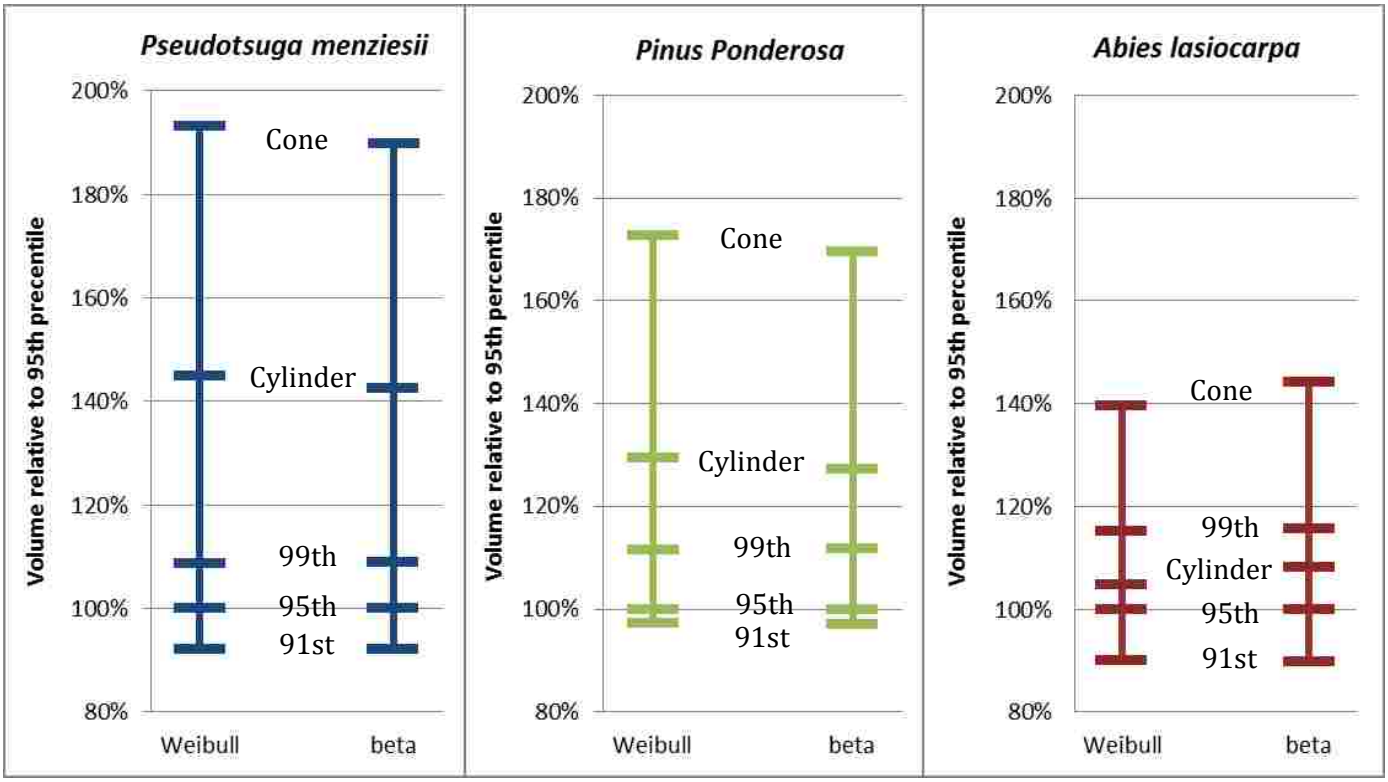

Figure 20. For each species, the beta or Weibull curve modeled on the 95th width percentile was used to calculate a "base case" volume. Then, volumes calculated from the 91st and 99th width percentile profile curves, and the modeled cone and cylinder for each species were compared to the base case.

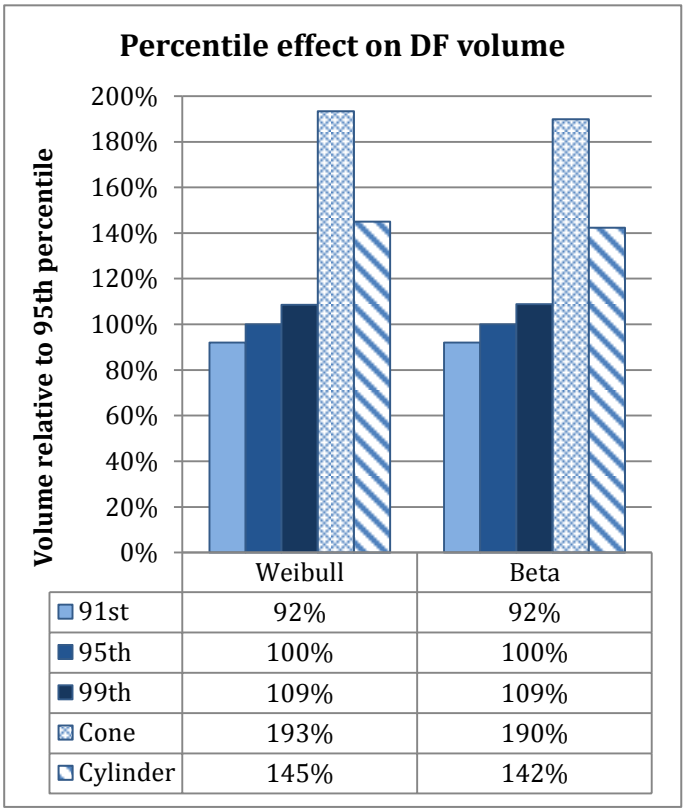

	Weibull	Beta
91st	92%	92%
95th	100%	100%
99th	109%	109%
Cone	193%	190%
Cylinder	145%	142%

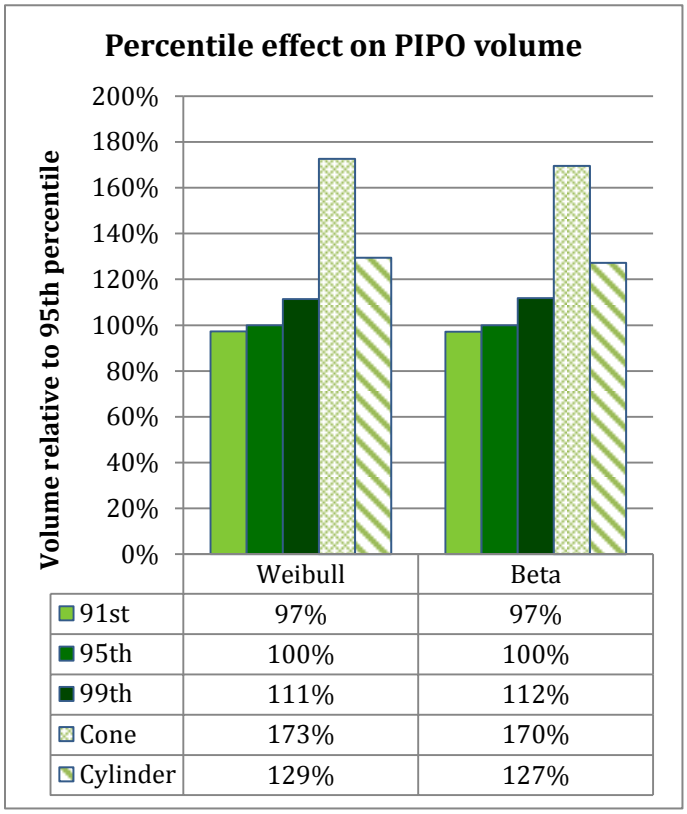

	Weibull	Beta
91st	97%	97%
95th	100%	100%
99th	111%	112%
Cone	173%	170%
Cylinder	129%	127%

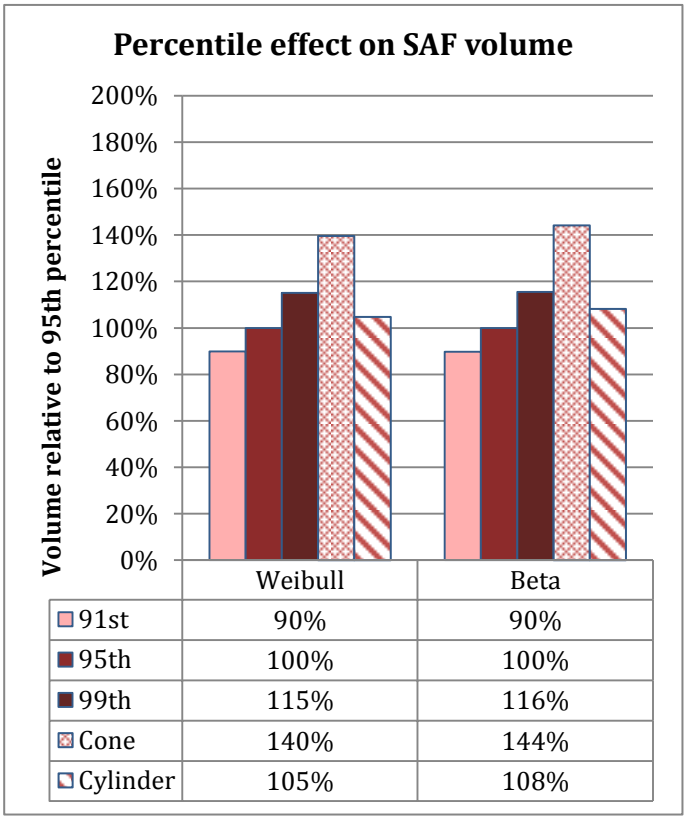

	Weibull	Beta
91st	90%	90%
95th	100%	100%
99th	115%	116%
Cone	140%	144%
Cylinder	105%	108%

Figure 20a (another depiction of the data in Figure 20, with additional numeric detail). For each species, the beta or Weibull curve modeled on the 95th width percentile was used to calculate a "base case" volume. Then, volumes calculated from the 91st and 99th width percentile profile curves, and the modeled cone and cylinder for each species were compared to the base case.

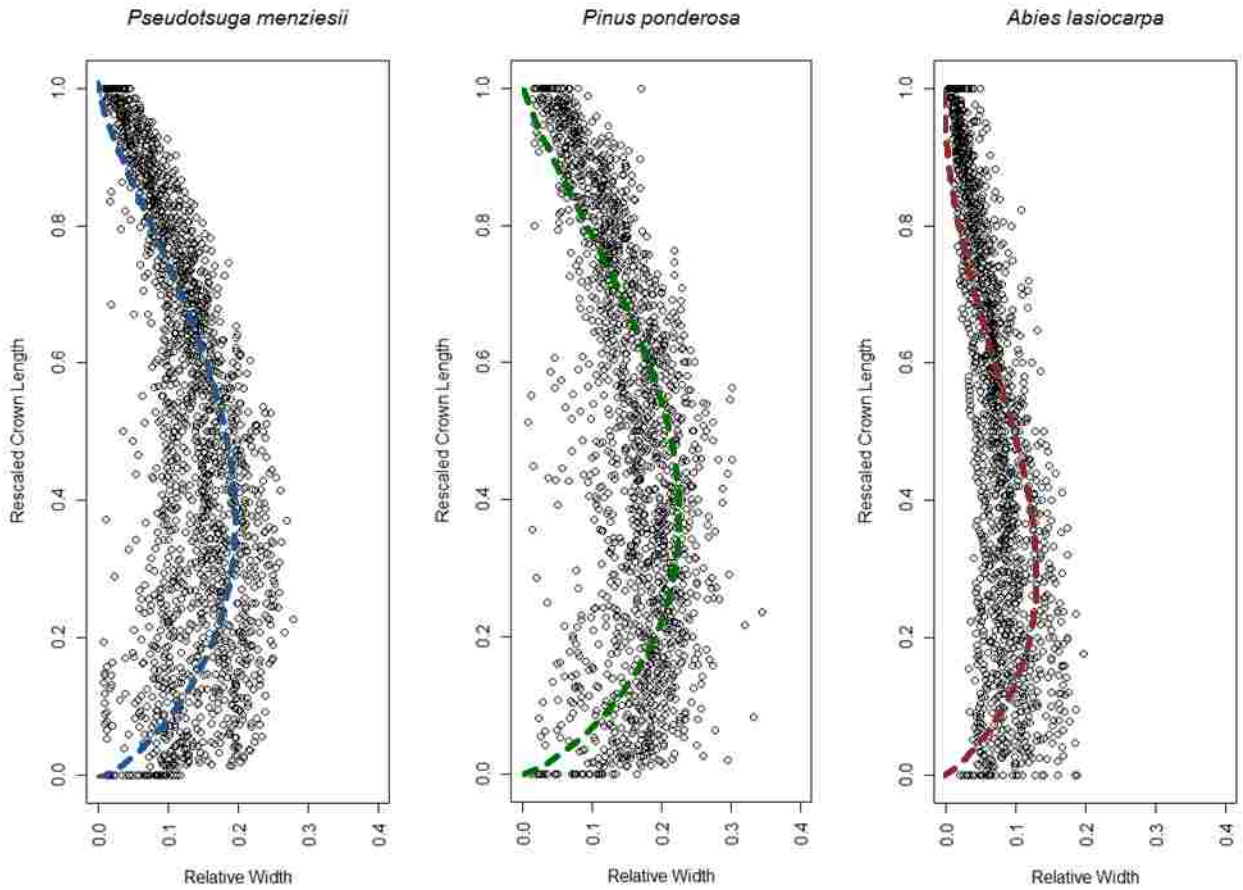

Figure 21. Beta curves overlaid on aggregate 95th width percentile points for each species, after rescaling the crown length 0-1 and the crown width relative to the crown length.

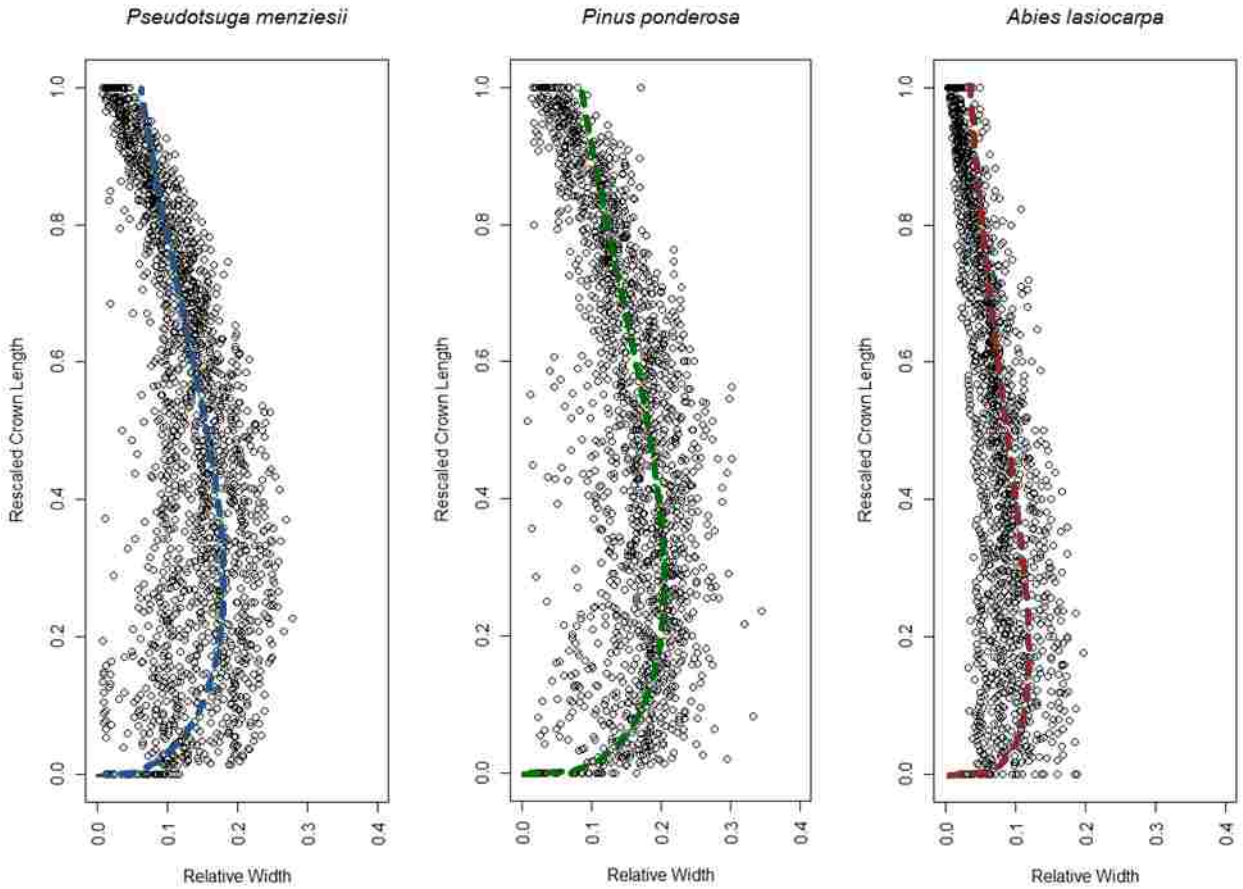

Figure 22. Weibull curves overlaid on aggregate 95th width percentile points for each species, after rescaling the crown length 0-1 and the crown width relative to the crown length.

Goodness of Fit Analysis

The mean absolute error (MAE) and corresponding variance from differencing each species' 95th width percentile points from the modeled curve predictions are reported in Tables 4 and 5. The error reported for the tree's own modeled curve is that from the cross-validation analysis. The errors produced by cross-validation were (as expected) larger than those from predictions made using the curve derived from the entire dataset. However, the differences between the two methods were not statistically significant for any species, although use of one error metric over the other did affect the statistical significance of error differences between a species and other prediction curves/shapes.

MAE values and variances are presented in Table 4 for beta curves and Table 5 for Weibull curves. Personal observations from fieldwork noted distinctive crown shapes associated with each species, and the findings support those observations. In every case, the individual points of a species were best predicted by the curve for that species. For example, the curve calculated by *Pseudotsuga menziesii* was better at predicting the 95th width percentile points than any other shape, either curves modeled on other species or simple geometries. Student's T-tests were used to determine the significance of the difference between the amounts of error generated by predictions from the same species as the tree compared to predictions by the other species. Results are noted Tables 4 and 5.

The results generally argue for use of a fitted curve instead of a simple geometry. In all cases, the beta or Weibull curve for each species produced a significantly better fit to those species' 95th width percentile points than the corresponding beta or Weibull curve for the other species. In other words, there are statistically different shapes to the profile curves of different species. However, although all Weibull curve comparisons resulted in highly significant differences, the beta curves produced more mixed results. *Abies lasiocarpa* was shown to be highly different from either *Pseudotsuga menziesii* or *Pinus ponderosa*, with the *Abies lasiocarpa* curve fitting those species poorly and those species fitting *Abies lasiocarpa* poorly. The *Pseudotsuga menziesii* beta curve fit to the *Pinus ponderosa* points did produce significantly more error than the *Pinus ponderosa* curve fit to the same dataset. The *Pinus ponderosa* beta curve fit to *Pseudotsuga menziesii* produced errors that were significantly different than those from the cross-validated *Pseudotsuga menziesii* beta curve at a=0.1. See Table 4 for error values and significance levels.

Use of the cone or cylinder produced less error in *Pinus ponderosa* and *Pseudotsuga menziesii* than the *Abies lasiocarpa* Beta or Weibull curve. The cone and cylinder produced significantly more error for *Abies lasiocarpa* 95th width percentile points than did the *Abies lasiocarpa* Weibull curve; the cylinder produced statistically no different error than *Abies*

lasiocarpa's own beta curve, and the cone actually had less error than the *Abies lasiocarpa* beta curve. See Table 5 for error values and significance levels. Again, this reinforces the better fit of the Weibull curve than the beta.

Table 4. Mean absolute error (variance in parentheses) for predictions made by the average curve of a species for the 95th width percentile points of each tree. Significance levels (indicated as 0.1*, 0.01**, 0.001***) relate to differences in the MAEs in each row between the species of interest and the alternate models (curves or geometries).

Beta MAE	**Modeled Curve Predictor Species/Shape**				
Reference Species 95th Width Percentile Points	**DF**	**PIPO**	**SAF**	**Cone**	**Cylinder**
DF	0.043 (0.0011)	0.046* (0.0014)	0.071*** (0.0015)	0.066*** (0.0041)	0.054*** (0.0014)
PIPO	0.053** (0.0014)	0.048 (0.0014)	0.093*** (0.0019)	0.075*** (0.0041)	0.052** (0.0016)
SAF	0.059*** (0.040)	0.078*** (0.049)	0.030 (0.023)	0.027*** (0.001)	0.031 (0.001)

Table 5. Mean absolute error (variance in parentheses) for predictions made by the average curve of a species for the 95th width percentile points of each tree. Significance levels (indicated as 0.1*, 0.01**, 0.001***) relate to differences in the MAEs in each row between the species of interest and the alternate models (curves or geometries).

Weibull MAE	**Modeled Curve Predictor Species/Shape**				
Reference Species 95th Width Percentile Points	**DF**	**PIPO**	**SAF**	**Cone**	**Cylinder**
DF	0.036 (0.0008)	0.040*** (0.0010)	0.062*** (0.0016)	0.066*** (0.0041)	0.054*** (0.0014)
PIPO	0.043*** (0.0010)	0.037 (0.0009)	0.083*** (0.0019)	0.075*** (0.0041)	0.052*** (0.0016)
SAF	0.059*** (0.0008)	0.082*** (0.0009)	0.022 (0.0004)	0.027*** (0.001)	0.031*** (0.001)

Cluster Analysis

Global Clustering

As previously described, the initial question of internal structure is its departure (or lack thereof) from spatial randomness toward clustering. Then, additional information about the clusters (e.g. size/scale, location, etc…) can be used to model crown internal heterogeneity. Past work at the stand level had suggested the potential for vertical variance within a single crown (Reinhardt et al. 2006, Keane et al. 2005) and work done on individual branches demonstrated that fine foliage can be separated from branchwood based on laser return intensity values (Seielstad et al. 2011), which are important distinctions for fire behavior modeling. Results from a small subsample of trees used to explore the effects of height (by crown partition) and intensity are presented below, followed by the results from the entire dataset.

The Ripley's L function is shown in the figures below. Because it is normalized to an expectation of complete spatial randomness (CSR), when the function is at zero, there is no pattern exhibited (the data set exhibits randomness). Ripley's L values greater than zero indicate clustering and values below zero indicate dispersion. The x-axis is the series of search radii over which patterning is examined; the x-axis values correspondent with non-zero Ripley's L values indicates the scale at which that patterning is observed. The magnitude of the deviation from zero on the y-axis indicates the strength of patterning.

Height Stratified Sample Trees

Six sample *Pseudotsuga menziesii* were used to investigate changes to the clustering functions when the upper and lower crown portions were analyzed separately. These results, shown in Figure 23, show a greater magnitude of clustering in the lower portion of the tree crowns than in the upper (larger y-axis values). Additionally, the scale of patterning in the lower crowns tends to be larger (the function crosses the x-axis further from zero). The differences exhibited

here were consistent enough among trees that I felt application of the vertical partitioning to the entire dataset was warranted (see *Entire dataset* and Figure 26 below).

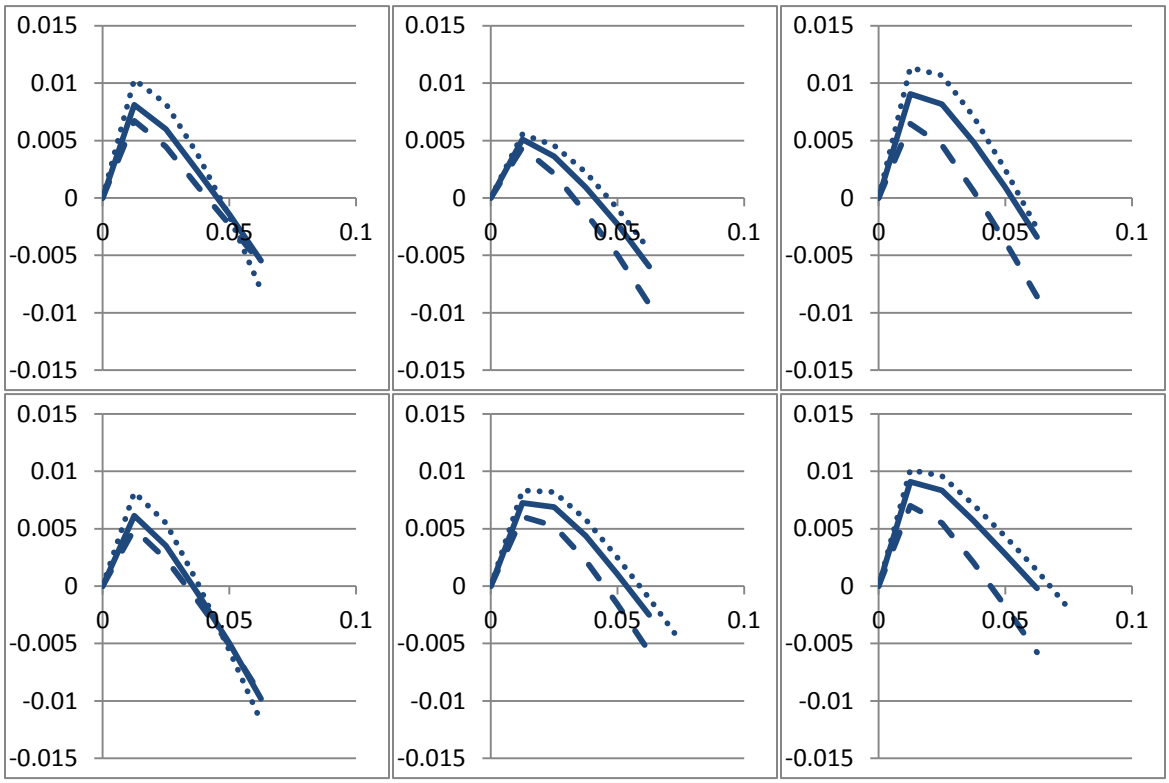

Figure 23. Clustering of upper (dashed) and lower (dotted) halves of the crowns for six *Pseudotsuga menziesii*. Clustering for the entire crown is shown as a solid line, and in all cases, falls between the stratified partitions. In all cases, the y-axis is the Ripley's Lhat value and the x-axis is the search radius on the scale of the original data (here, the unitless, rescaled 0-1 crown length). In this case, the x-axis can be interpreted as the proportion of crown length (e.g. 0.05 is 5% of a 1 unit long crown).

Intensity Stratified Sample Trees

Although height stratification produced noticeably different clustering functions, the effect on the clustering functions of the six sample *Pseudotsuga menziesii* from intensity stratification was weak. The stratification here was somewhat different from that of the vertical partitioning. I was interested in if there was a difference in patterning exhibited between all of the crown points (the unthresholded point cloud) and just the points identified as likely belonging to fine foliage

The intensity partitioning was conducted manually, supported by visual inspection of the resultant branching structure in the classified point cloud and comparisons with photographs from the field. One example of an intensity-classified crown is shown below in Figure 24. Although the point classification appears reasonable, there was no suitable data for an accuracy assessment.

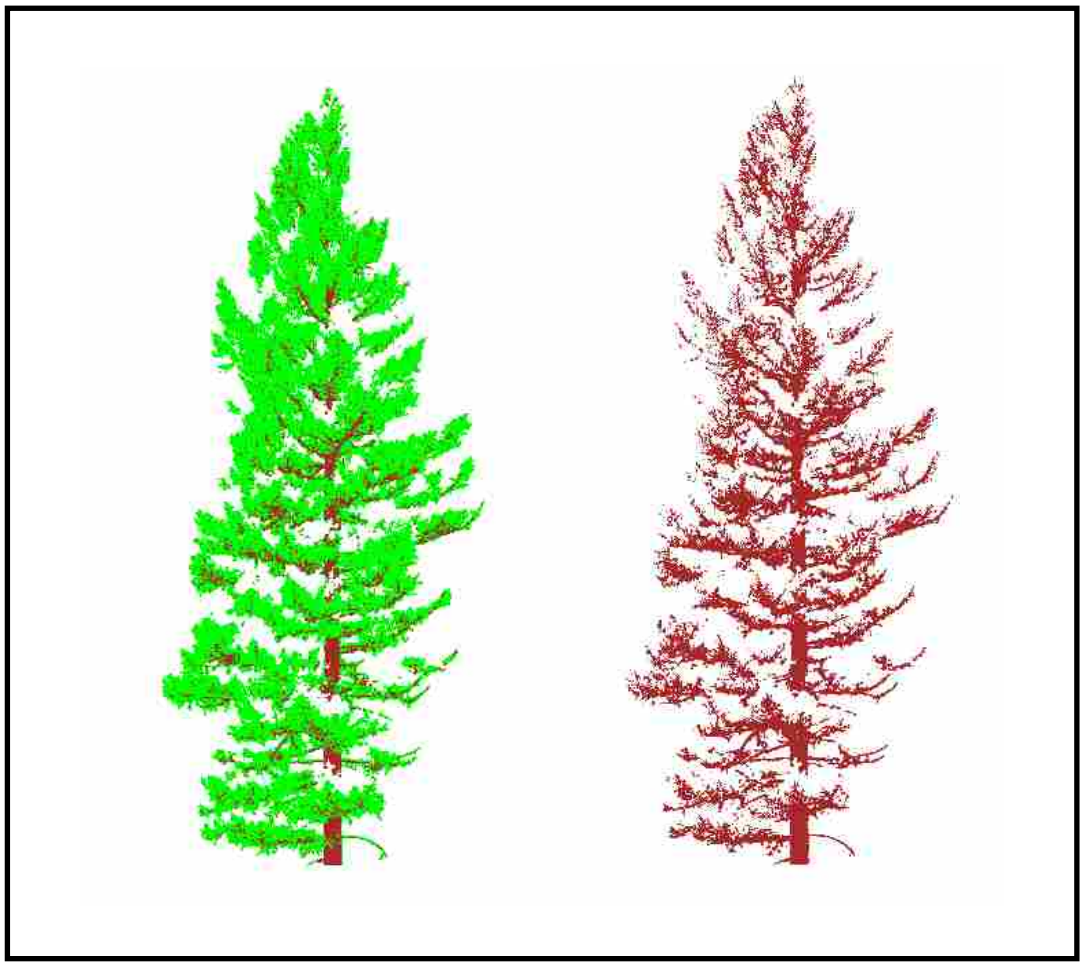

Figure 24. The entire classified crown point cloud (left) and classified branchwood points (right) of one *Pseudotsuga menziesii* crown showing the results of intensity stratification. Although the branching structure appears reasonable, there was no true ground truth data to assess the classification.

As shown in Figure 25, although there are clustering magnitude and scale differences among trees, there was little difference within each tree between point sets (all crown points or

only fine fuel returns). The similarity within each tree, in conjunction with the lack of true ground truth data, supported the decision not to intensity threshold the entire dataset.

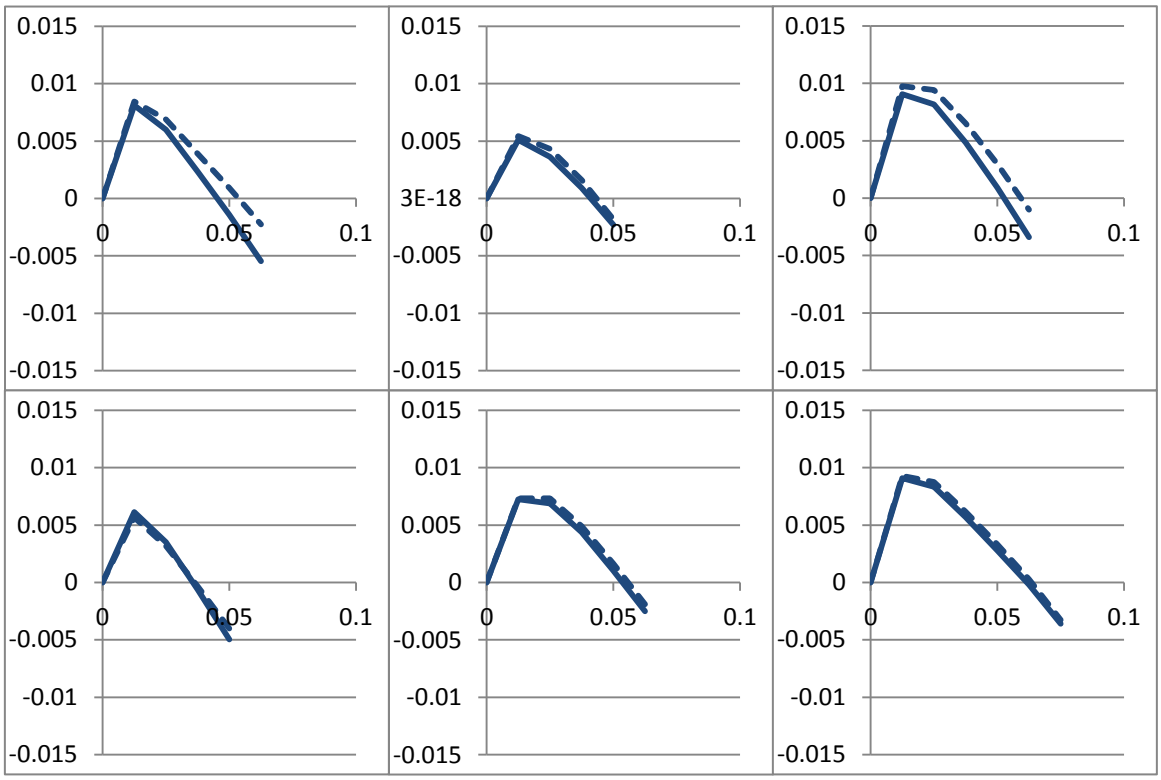

Figure 25. Clustering of all crown points (solid line) and just diffuse/fine fuel returns (dashed line) for six *Pseudotsuga menziesii*. Each tree was individually intensity thresholded to separate diffuse/fine fuel returns from larger fuel returns. In all cases, the y-axis is the Ripley's Lhat value and the x-axis is the search radius on the scale of the original data (here, the unitless, rescaled 0-1 crown length). In this case, the x-axis can be interpreted as the proportion of crown length (e.g. 0.05 is 5% of a 1 unit long crown).

Entire dataset

Height stratified cluster analysis was performed on all trees, and the results averaged by species. Figure 26 shows the average clustering by the upper and lower crown portions of each species (Ripley's L functions for individual trees are given in Appendix B). All species showed clustering occurring across larger scales (x-axis) and of greater magnitude (y-axis) in the lower portion of the crowns than the upper, consistent with the trial sample set. The strongest clustering

in *Pseudotsuga menziesii* and *Pinus ponderosa* was observed at search radii of 0.0125 and 0.025, and at a radius of 0.0125 for *Abies lasiocarpa*. Recall that the search radii can be interpreted as the proportion of crown length. Thus, extrapolating values of 0.0125and 0.025 to a theoretical 20m crown produces radii of 0.25 and 0.5m at which clustering is predicted. Therefore, clusters in a 20m crown would be expected to be most prevalently sized at 0.5 – 1.0m (twice the radii) in P*seudotsuga menziesii* and *Pinus ponderosa*, and at 0.25m in *Abies lasiocarpa*, which suggests it is describing clustering at roughly branch scale. Because 0.0125 was the smallest radii used, branching at the individual shoot level would not be detected, except perhaps in the smallest trees.

Among species, *Pinus ponderosa* showed clustering occurring over the largest scales and *Abies lasiocarpa* over the smallest. *Pinus ponderosa* and *Pseudotsuga menziesii* had similar magnitude of clustering, while the observed clustering in *Abies lasiocarpa* was weaker (smaller Ripley's L values on the y-axis). Within each species, observed clustering properties between upper and lower crowns diverged as the scale of clustering increased. The average clustering in the lower crown was close to one standard deviation above the upper crown average; the average clustering in the upper crown was close to one standard deviation below the lower crown average. Worth noting is the implicit link between crown length and cluster size, where larger clusters are predicted for longer crowns. The x-axis of the Ripley's L plot represents the scale at which patterning occurs, and is in the same units as the data. Here, the data are expressed as a unitless proportion of crown length, and value of one denotes the entire crown length. If the data were rescaled to their original dimensions, peak clustering is predicted to occur at larger cluster sizes in longer crowns.

Although the Ripley's K and L functions describe the scale at which material is patterned, they do not provide explicit spatial information. Thus, no information was obtained about where in 3D space (e.g. horizontally relative to the bole or vertically in the crown) clusters were located.

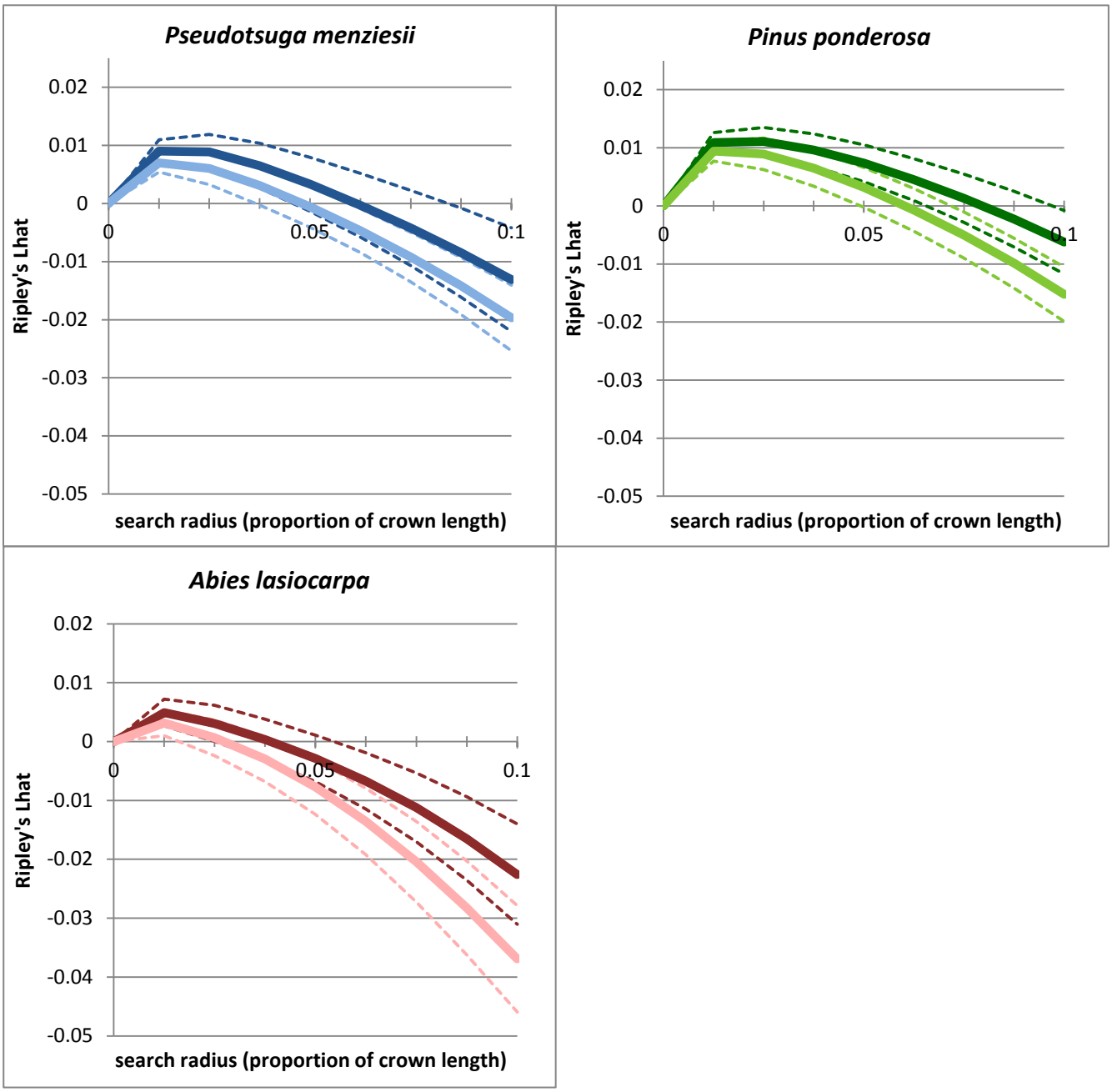

Figure 26. Average clustering by species. Solid lines represent the means, and dashed lines are one standard deviation above and below the mean. In each graph, the darker color represents the lower portion of the canopy and the lighter color represents the upper canopy. Because the return coordinates were rescaled relative to crown length, the x-axis of search radius distance can be interpreted as the percentage of crown length. In all cases, the y-axis is the Ripley's Lhat value and the x-axis is the search radius on the scale of the original data (here, the unitless, rescaled 0-1 crown length). Because of the rescaling of the data, the x-axis can be interpreted as the proportion of crown length (e.g. 0.05 is 5% of a 1 unit long crown).

Post Facto Exploratory Analysis

Rescaling

Two *Pseudotsuga menziesii*, those with the longest and shortest crowns, were used to investigate in more detail two of the predictions and limitations of the clustering analysis as described above: one, the assumption that actual cluster size (in unscaled measures) increases with crown length; and two, the implications for detectable cluster size due to the search increment increasing with crown length. To address both inquiries, clustering analysis was performed on unrescaled crown points, using invariant search radii on an absolute scale of meters (the same as the original scan points).

Actual cluster size relative to crown length:

As presented above in Figure 26, the average Ripley's L function for each species was originally calculated using rescaled crown point locations (rescaled relative to crown length). Under this condition, the search radii can be interpreted as a proportion of crown length. If the crown is of length one (any units), the search radii will also be the actual distances (in real, unscaled space) at which clustering is assessed. In longer crowns, the search radii need to be scaled up by the crown length to determine the actual (not proportional) distances over which clustering is assessed. The radii are easily scalable using crown length, but this relationship inherently predicts that the actual sizes at which the greatest clustering occurs will increase with crown length. For example, if peak clustering occurs at a search radius of 1.25% of crown length, this would translate to a cluster radius of 12.5cm in a 10m crown, 25cm in a 20m crown, etc… Figure 27 shows the Ripley's L functions for the upper and lower portions of the longest and shortest crowns of *Pseudotsuga menziesii*. Note that the strongest clustering in the long crown peaks between 0.18 – 0.4 m (with some offset between the upper and lower portions), whereas clustering in the short

crown peaks between 0.1 – 0.2 m, with a less pronounced offset. This supports the results predicting that larger clusters will be found in longer crowns, but requires further exploration.

Cluster detection limits:

Another effect of the search radii being scalable to the crown length was that as crowns increased in length, the absolute scale of detection became coarser (i.e. the "smallest" search radius became larger, as did the increments between radii). The Ripley's L functions shown in Figure 27 were calculated using search radii particularly targeted at assessing clustering at a finer grain. The points in black show where the original Ripley's L values fall if they are inverted to reflect the actual crown length in metric units. In the longer crown, the first search increment is at or near the peak clustering. This is the minimum detection limit in the scale of clustering using proportional search radii. This limited analysis suggests that small-scale clustering in long crowns does occur, and warrants further analysis. The original data for the shorter crown demonstrate the finer resolution of the original analysis, as compared to that of the longer crown. Although the original data do not allow conclusions to be drawn regarding what is happening in longer crowns at fine scales, it is reasonable to conclude that coarse-scale clumping does not occur in shorter crowns. This result would benefit from assessment of additional trees across an array of crown lengths.

<u>Subsample methodology</u>

Multiple subsampling methods were used to explore the sensitivity of the Ripley's K and L functions to subsample choice. For the larger tree (*Pseudotsuga menziesii)*, the resulting Ripley's L functions are too similar for a graph to be useful, as all the points lie (visually) directly atop one another. The calculated Ripley's L values for each sample radius under each scenario are presented in Table 6. The results from the small tree (*Abies lasiocarpa)* are presented in Figure 28 and Table 7.

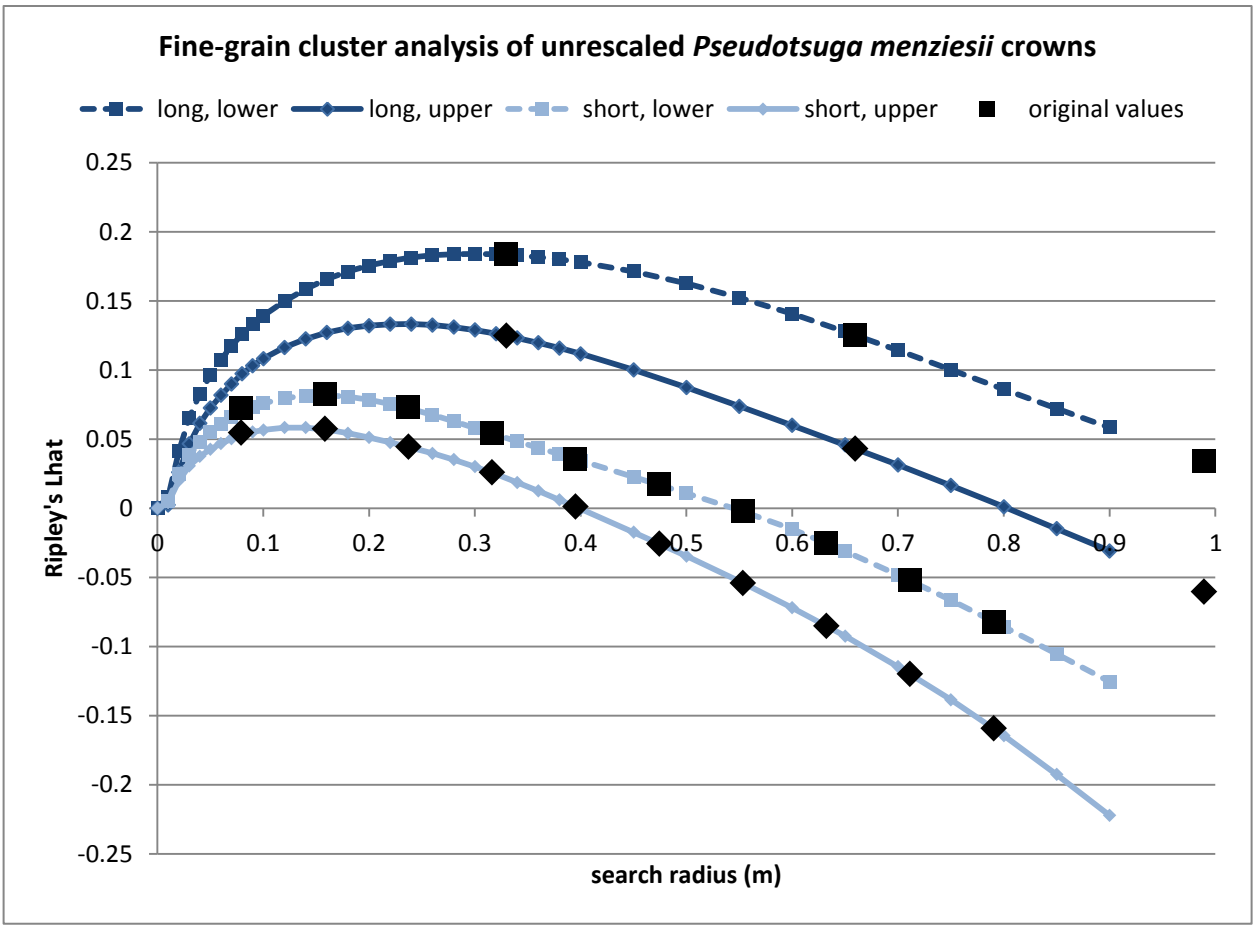

Figure 27. Ripley's L functions for two unrescaled crowns of *Pseudotsuga menziesii*, the longest (26.38m) and shortest (6.32m) of the sampled trees. The dark blue lines are the lower and upper portions of the long crown; the light blue lines are the lower and upper portions of the short crown. Calculation of Ripley's L occurred at 36 search radii, specifically incremented to capture clustering at short distances. Black points represent the original Ripley's L values for those trees, scaled up to the actual crown lengths.

Table 6. Ripley's L values for a *Pseudotsuga* menziesii with a 16.5m crown length, calculated under different subsampling scenarios.

Search Radius	Every 15th pt, as done for thesis	Random 1/15th	Every 6th pt	Every 15th pt, count all	Random 1/15th, count all
0	0.00000	0.00000	0.00000	0.00000	0.00000
0.0125	0.00907	0.00909	0.00907	0.00910	0.00911
0.025	0.00834	0.00836	0.00835	0.00836	0.00837
0.0375	0.00567	0.00566	0.00567	0.00568	0.00567
0.05	0.00279	0.00274	0.00278	0.00279	0.00277
0.0625	-0.00018	-0.00025	-0.00020	-0.00019	-0.00022
0.075	-0.00360	-0.00367	-0.00361	-0.00360	-0.00364
0.0875	-0.00758	-0.00766	-0.00759	-0.00758	-0.00762
0.1	-0.01198	-0.01206	-0.01198	-0.01198	-0.01202

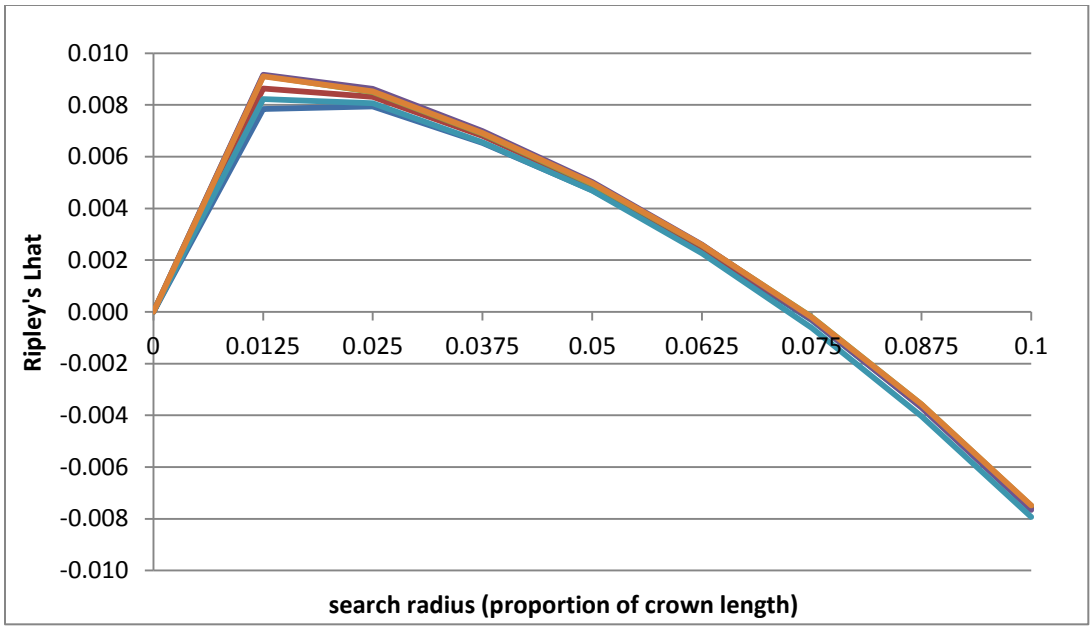

Figure 28. Ripley's L functions for an *Abies lasiocarpa* with a 4.5m crown length, calculated under different subsampling scenarios (all points, every 15th laser return, a random 1/15th sample, every 6th return, sampling at every 15th return but counting all, and sampling at a random 1/15th but counting all).

Table 7. Ripley's L values for an *Abies lasiocarpa* with a 4.5m crown length, calculated under different subsampling scenarios.

Search Radius	Every 15th pt, as done for thesis	Random 1/15th	Every 6th pt	Every 15th pt, count all	Random 1/15th, count all	All points
0	0.00000	0.00000	0.00000	0.00000	0.00000	0.00000
0.0125	0.00784	0.00823	0.00864	0.00913	0.00917	0.00910
0.025	0.00794	0.00807	0.00831	0.00850	0.00862	0.00852
0.0375	0.00654	0.00656	0.00681	0.00689	0.00699	0.00692
0.05	0.00470	0.00469	0.00489	0.00494	0.00502	0.00497
0.0625	0.00240	0.00226	0.00251	0.00257	0.00259	0.00258
0.075	-0.00031	-0.00061	-0.00027	-0.00020	-0.00027	-0.00020
0.0875	-0.00367	-0.00403	-0.00364	-0.00358	-0.00370	-0.00358
0.1	-0.00757	-0.00793	-0.00755	-0.00749	-0.00765	-0.00749

Edge Effects

Artificial edges:

Ripley's L functions were calculated for one *Pseudotsuga menziesii* under three scenarios that removed one or more of the artificial edges introduced in this study (the upper-lower boundary between vertical crown sections and the front-back boundary created from originally selecting only the front hemisphere of points). Figure 29 displays the Ripley's L functions for the entire front half (not separated into upper and lower sections) as originally done in this study, and using the mirrored point set to eliminate the front-back boundary. Figure 30 displays the Ripley's L functions for the upper portion of the crown under 4 scenarios: as originally done in this study; sampling only the front-hemisphere, upper points but including the lower crown points as searchable to eliminate the upper-lower boundary; sampling only the front-hemisphere, upper crown points, but including the mirrored upper points as searchable to eliminate the front-back boundary; sampling only the front-hemisphere, upper crown points but including the entire set of mirrored points as searchable to eliminate all artificial boundaries. Figure 31 displays the Ripley's L functions for the lower portion of the crown under the same, respective scenarios. In Figure 28, there was no upper-lower edge, and thus eliminating the front-back edge was the same as eliminating all edges. Figures 30 and 31 show that the front-back edge had a greater effect on the Ripley's L function than did the upper-lower edge, and that eliminating all artificial edges produced the greatest change in the Ripley's L values. In all scenarios, as expected, the degree of change in the Ripley's L value (the edge effect) increased with an increasing search radius, as the search volume for more points intercepted one or more edges. After removing the effect of the artificial edges, the lower crown portion showed the greatest degree of clustering (largest Ripley's L values) and clustering across the largest range of sizes (positive Ripley's L values for larger search radii) than either the whole crown or the upper portion. The edge-compensated upper portion showed

clustering across smaller scales and to a lesser extent. These results are consistent with the non-artificial-edge-corrected findings.

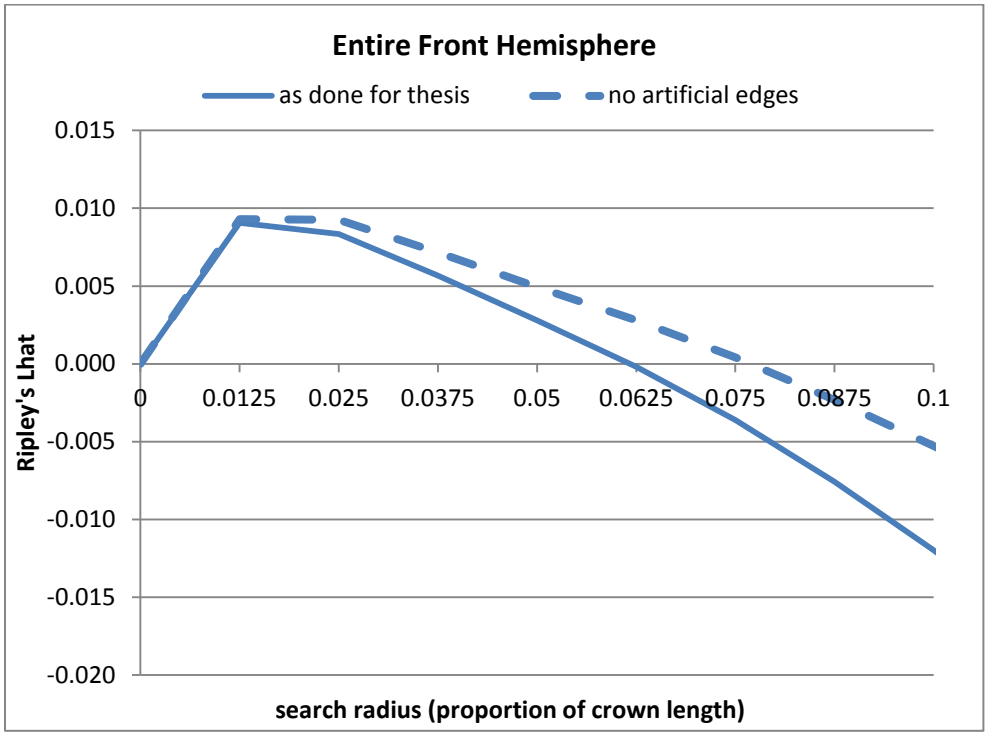

Figure 29. Ripley's L functions for the entire front-hemisphere sample points (every 15th laser return) as originally done in this study (with an artificial front-back edge) and with the front-hemisphere points mirrored to eliminate the artificial front-back boundary. The x-axis is the search radii as a proportion of crown length, the y-axis is the Ripley's L value.

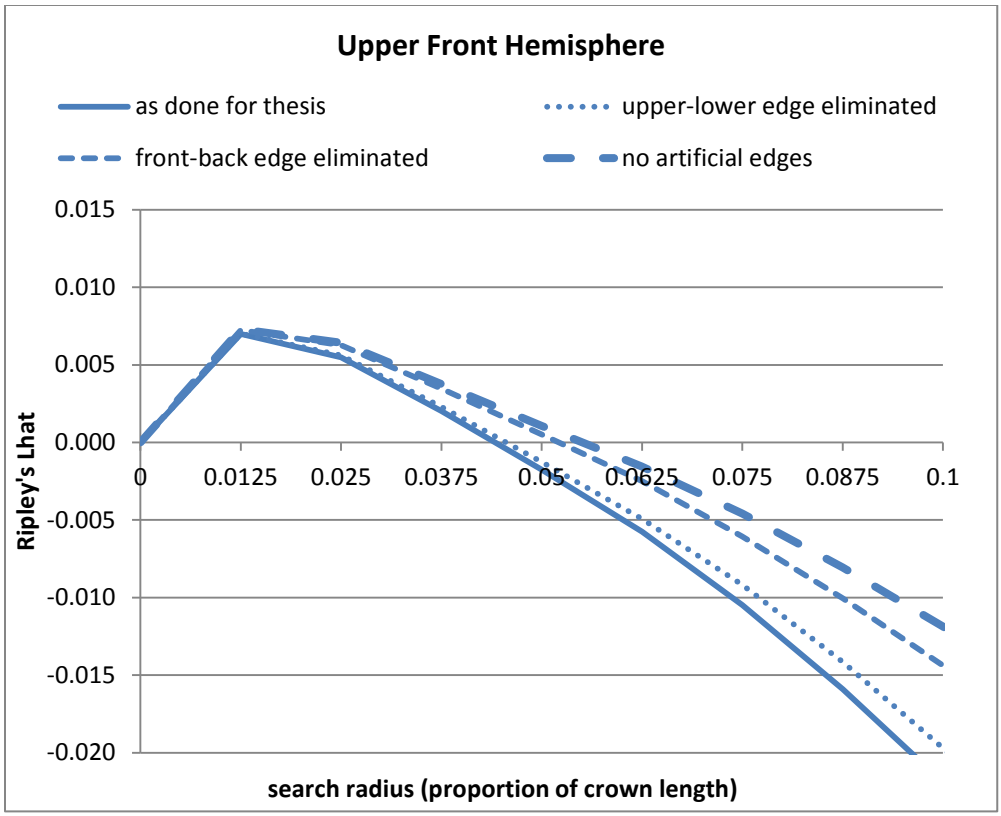

Figure 30. Ripley's L functions for the front-hemisphere, upper sample points (every 15th laser return) as originally done in this study (with artificial edges) and under three scenarios that remove one or both of the upper-lower and front-back artificial edges. The x-axis is the search radii as a proportion of crown length, the y-axis is the Ripley's L value.

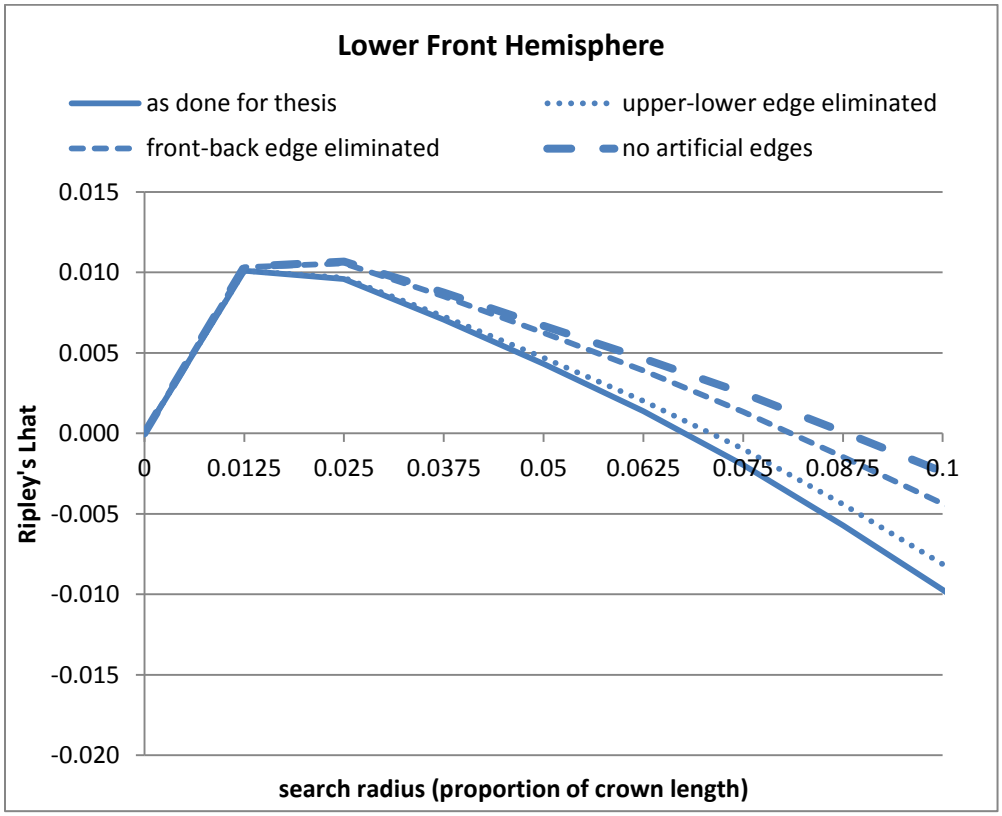

Figure 31. Ripley's L functions for the front-hemisphere, lower sample points (every 15th laser return) as originally done in this study (with artificial edges) and under three scenarios that remove one or both of the upper-lower and front-back artificial edges. The x-axis is the search radii as a proportion of crown length, the y-axis is the Ripley's L value.

Actual edges:

Unlike the effect from artificial edges that could be removed, the effect of the actual edge of the crown extent is difficult to quantify. One approach was to use multiple crown slices that maintained a consistent surface area to volume ratio. First, seven segments from different heights within the crown were analyzed using Ripley's L (Figure 32). The segments from the lower areas of the crown consistently demonstrate a greater degree of clustering (larger Ripley's L values), peak clustering occurring at larger search radii (~20cm), and clustering occurring across a larger range of sizes (up to and greater than 50cm). Segments from the upper areas of the crown show a lesser degree of clustering (smaller Ripley's L values), peak clustering occurring at smaller search radii (~10cm), and clustering occurring across a smaller range of sizes (up to ~30-40cm). The one Ripley's L function that displays a different pattern is that for the top section of the crown (15-19m in a 19.4m crown, the red line in Figure 32). Although the surface area to volume ratio for this segment is consistent with the others, this segment is much taller and thinner than the other segments, whose frustums are more cylindrical than conical.

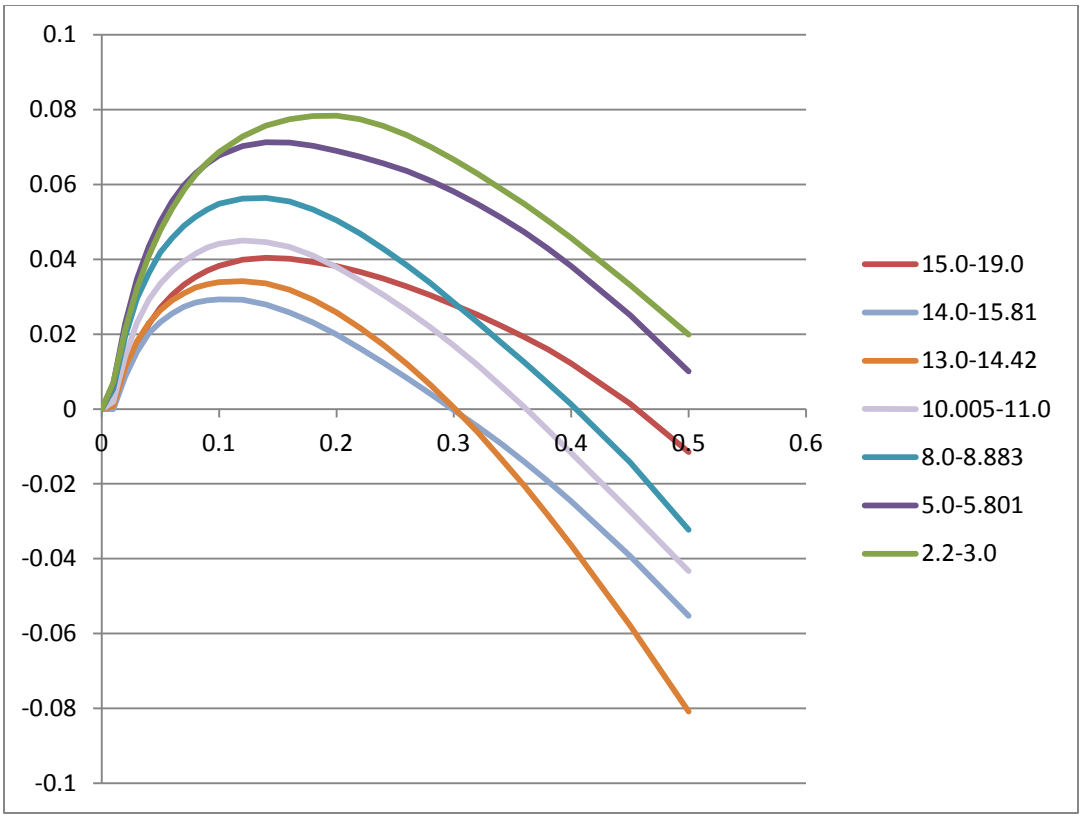

Figure 32. Ripley's L functions for a series of height increments within one tree's crown. The segments were height adjusted so that the frustums formed using the predicted Weibull curve value at each height had consistent surface area to volume ratios. The x-axis is the search radii in meters; the y-axis is the Ripley's L value. Heights are given from the base of the crown (i.e. the 2.2-3.0 segment is below the 5.0-5.801 segment).

Next, a crown of a short tree was sectioned so that its surface area to volume ratio was consistent with the long tree crown sections. That tree's crown length was 5.5m; the section of the crown used here was from 0.5-5.25m – a conical shape more similar to that of the uppermost long crown section than the lower segments. The Ripley's L function for the small tree is shown in Figure 33 (thicker dashed line), overlaid onto the functions from the long crown segments. The small tree function is more similar to the functions from the upper than lower portions of the long crown, and echoes the shape of the function from the uppermost segment of the long crown (shown as the thin red line).

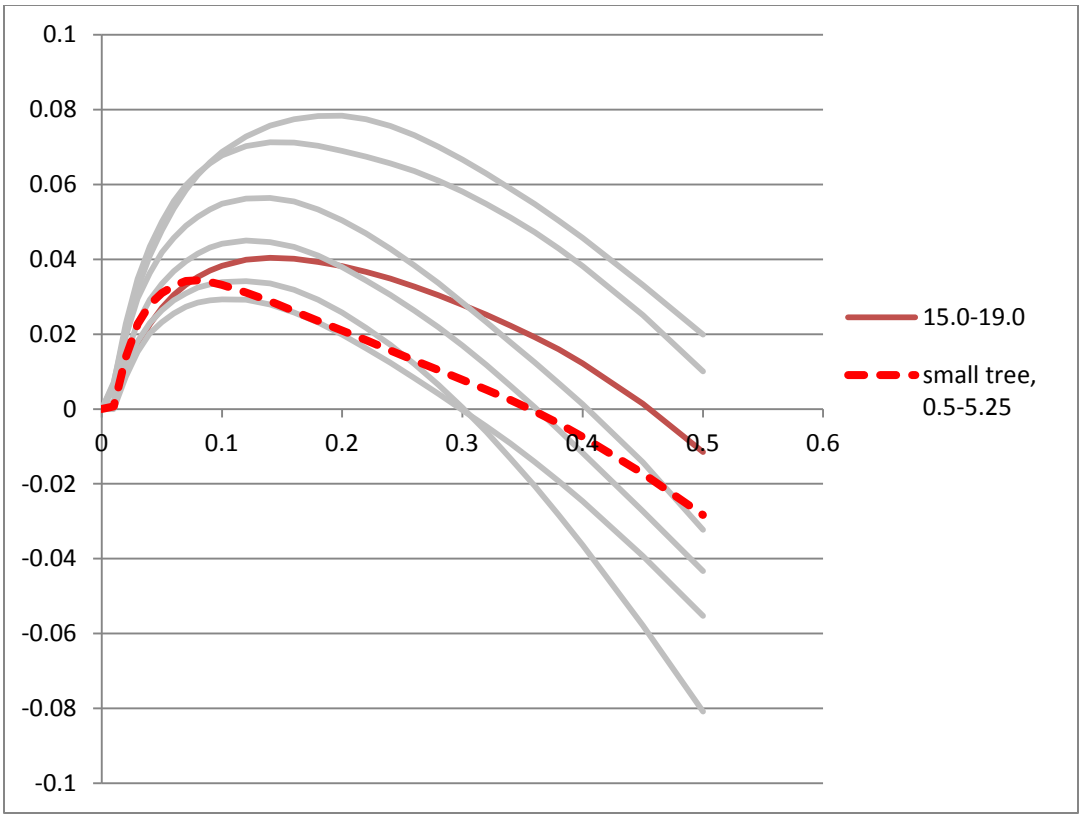

Figure 33. The Ripley's L function for the small tree crown segment (thick, dashed, red line) overlaid onto the functions from the long crown segments. The thin red line is the Ripley's L function for the uppermost section of the long crown. Although all the segments had consistent surface area to volume ratios, the short crown and uppermost segment of the long crown were more similar in shape to each other than to the long crown other segments.

(this page intentionally left blank)

Chapter 4. Discussion

This study examined two aspects of tree crown structure that are important to fire behavior modeling – the total crown volume as calculated from a defined outer profile, and the distribution of material within that volume. When combined with crown biomass measures, this work takes an important step toward the culminating goal of developing parameters to populate a stand inventory list with realistic information about where crown fuel is located in three-dimensional space.

For the three species sampled here (*Pseudotsuga menziesii, Pinus ponderosa, and Abies lasiocarpa*), crown profiles were found to be species-specific, and best modeled using a compressed Weibull curve. However, it is important to note that compared to simple geometries, curvilinear shapes increase model complexity, which does not always produce better results (e.g. *Abies lasiocarpa* was better modeled using a cone than a beta curve). Importantly, the crown profile was modeled as a function of vertical position within the crown, and requires only crown length for implementation.

Differences in within-crown clustering were also seen among species, and between the upper and lower portions of the crown. Across all species, the observed clustering in the lower portion of the crown occurred across coarser scales and to a greater degree than that observed in the upper portion of the crown. *Pinus ponderosa* and *Pseudotsuga menziesii* exhibited stronger clustering at coarser scales than did *Abies lasiocarpa*. Under the rescaling approach used here, cluster size was predicted to increase with crown length. Additional analysis suggested that this is a valid premise, although further investigation is needed. Due to the relationship of the cluster search increment to crown length, the relatively coarse step applied to large crowns precluded analysis of fine scale clumping in actual (not rescaled) space (recall that the step size was proportional to crown length). Nevertheless, rudimentary exploration suggests that clustering within large crowns also occurs at finer scales, similar to those found in smaller trees.

What follows is a more thorough look at details of each finding, how the results of this fit with extant work, and some of the limitations associated with each component of this thesis.

Crown Profiles

Traditionally, approaches to modeling tree crowns have used one of two methods – direct or indirect. The indirect method relies on modeling the interior branching architecture and requires detailed data collection of branch sizes, branch angles, branch heights from ground, etc… The more commonly used direct method calculates crown width as a function of various tree attributes in some model form. The ability of LiDAR to provide a detailed representation of the tree lends itself well to a direct calculation of crown profile. Roeh and Maguire (1997) chose to use indirect methods because of the "numerous logistical difficulties" associated with "direct measurement of crown diameters at different heights." This challenge is well addressed by the use of TLS. Previous studies employing direct measurements relied on limited samples of crown width, measured in the field on felled trees (Doruska and Mays 1998 [7 sampled widths], Hann 1999 [10 sampled widths], Marshall et al. 2003 [10 sampled widths]). I sampled profiles at 0.25m increments (18 – 146 measures per tree, dependent on crown length), from crowns measured *in situ* (i.e. as they are growing in place, not felled or simulated). Measuring standing trees minimizes the crown distortion incurred during felling (e.g. breakage). Photography also occurs *in situ*, but provides information only about the crown extent in the plane of the photo and can be limited by shadowing and distortion (e.g. Gill and Biging 2002, Remphrey et al. 1987). Conversely, the half-hemisphere LiDAR scans used here incorporate information from a full 180^{o} of the crown, and are not subject to photographic distortion.

Limitations

Field data collection

Tree selection:

Although trees were selected to represent multiple DBH classes, the middle sizes were more heavily represented than either extreme. One should also consider that the majority of trees were sampled from open and moderately open stands and results from this study may not apply across all stand conditions, particularly in fully closed environments. However, the research does represent a cross-section of trees from across the region.

Scans:

The unresolved conundrum of laser scanning is the attrition of laser reflections as they penetrate through dense material. This issue was partially addressed by utilizing only the half of the tree closest to the laser, but the occlusion of inner canopy on the front (scan) side of trees was not quantified. In short, areas in a scan not populated with laser returns may be empty because there was no material to return the energy, or may be empty because no pulses reached that area. Conventional wisdom suggests that biomass (particularly foliar biomass) is concentrated on the hull of the crown, and is supported by work such as Baldwin and Peterson (1997) and Kershaw and Maguire (1995), so the possibility of an occlusion effect is real. With this said, because material is concentrated on the outer crown, the laser may actually see most of the material important to fire behavior modelers.

In sampling trees for crown profiles, both photography and TLS require a clear view of the crown. For some trees, vegetation removal was quite prolonged (taking hours per tree in denser stands or those with heavy underbrush). Once clear, laser scanning is a more time consuming process (up to 40 minutes for large trees) than photography. The current trade-offs for detailed

crown capture in three dimensions are time expenditures (both data capture and processing) and monetary costs for instrumentation.

Although laser scanning is faster than destructive sampling, the total time needed for set up, scanning and data processing is substantial, and TLS is not well suited to be employed as a timesaver on typical field data collection projects. In some regards, TLS is like destructive sampling- time consuming enough that it may best be used to develop species-level or stand-level models for use in other studies rather than as a common field sampling tool. Studies like this one can be used to exploit the capabilities of laser scanning, inform models and simulations, and preclude the need to scan for every project. Due to the time constraints of sampling and processing laser data, the sample sizes in this study still may have been smaller than ideal for making regional, species-level generalizations about tree characteristics. Although the numbers of trees per species analyzed here were 27 – 30, that sample size was unlikely to capture the full variability of a species across an entire region. Even utilizing a modified scanning technique to facilitate relatively efficient sampling, I was time-limited, largely due in the field to the necessary clearing of surrounding vegetation and in the office due to data processing requirements.

Crown profile generation

Width percentiles:

Due to the previously noted possibility of occlusion of inner canopy material, width percentiles may be artificially skewed toward the outside of the tree (i.e. width percentiles may show a void near the bole due to poor laser penetration into dense material, not absence of material). Conversely, the exterior of the canopy, used for the crown profile generation, is reliably sampled.

Crown delineation:

Although field measures of crown base were available for trees sampled in 2012, and could have been reasonably estimated for other trees using photos and 3D visualization software, I desired a crown base metric that was based purely on the LiDAR data, independent of field measures and objectively repeatable. That the LiDAR-derived metric (LBH) is consistently lower than the CBH is not unexpected, as the branching pattern required to meet the CBH definition is strict. The HLC for each tree was also either at or below the corresponding CBH, which is also reasonable considering that the HLC considers *any* live branch, regardless of a specific branching pattern. The discrepancy between HLC and the LBH is most often due to dead branches attached to the bole. Because the LCB is based solely on width relationships, dead branches will meet the width criteria as well as live. The trees with the largest discrepancies between LCB and HLC (e.g. more than 3m difference - i001lgdf [9.0m], i003lgdf [4.2m], i004lgdf [3.2m], m001bysaf [4.2m]) all had many dead branches below their live crowns. The trees with the largest overestimation of HLC (e.g. more than 3m difference – i011tmdf [3.1m], i004asdf [3.7m], i004shdf [3.7m], i002lrpipo [3.7m], i012nmpipo [3.3m]) had live branches that were too short to meet the LCB metric.

Although it is possible to create a correction factor based on the field measurements, I proceeded using the LBH due to its objectivity and independence from field estimates. Additionally, for applications such as fire behavior modeling, it may actually be desirable to include all vegetative material (live or dead), as it can all act as fuel. Ignoring dead material at the base of a live crown artificially raises the distance between the surface and aerial fuels, potentially affecting predicted fire behavior.

Crown profile modeling:

To represent the outer crown profile, the 95th percentile was chosen instead of the 100th for several reasons. First, use of the extreme values carries the potential to include erroneous returns

not truly representing the crown. Additionally, because the laser point cloud was folded into 2D space, the 100th percentile captures the most extreme width for each height increment, which could reflect a single extra-long branch or erroneously included material from adjacent trees. Use of the 95th percentile reflects a "typical" crown extent from the 180^{o} point cloud. However, use of the 95th percentile as the outer crown was arbitrary, thus the effects of using the 91st or 99th width percentiles on crown shape and resultant volume were also explored. Based on these comparisons, the 95th percentile was reasonable, but there is no compelling evidence to suggest it is better or worse than the 91st or 99th percentile.

In a larger context, folding the crown from 3D to 2D as was done in this study space is a novel technique to integrate crown shape from 180 degrees of tree crown. Whether this approach provides the best approximation of crown envelope is uncertain. An alternative approach would be to sample the 3D point cloud with a series of vertical "slices" which could be averaged together to describe the mean crown extent at any given height.

Crown volumes:

The effect on crown volume from using differing width percentiles in *Pseudotsuga menziesii* and *Pinus ponderosa* was much smaller than the differences obtained using simple geometries instead of curves, although this difference was not seen in *Abies lasiocarpa*. This result implies that a simple geometry might be more suitable for *Abies lasiocarpa* than the other species, but the geometry of the cones and cylinders used could be adjusted (by varying the dimensions) for the other species to match the curve-derived volumes more closely. Here, although a rational process for determining the geometries was used, no optimization was employed. Thus, one can conclude that the particular simple geometry used in this study greatly overestimated crown volume for two species as compared to their modeled curves, but not that *all* simplified geometries might do this.

Goodness-of-fit analysis:

Ultimately, regardless of how shapes compare to each other, their accuracy relative to the width percentile points is the most important consideration. Recall that all crowns were vertically rescaled between zero and one, and horizontally scaled relative to crown length. Additionally, the error metric used was the mean absolute error (MAE), meaning that the calculated error values are meaningful both relatively among differing combinations and in absolute terms as a percentage of crown length. For instance, The DF beta curve had a MAE of 0.043. In a one-meter crown, this means an average horizontal error of 4.3cm; in a 10m crown the horizontal error scales up to 43cm, and to 86cm for a 20m crown. For all three species, the Weibull curve produced the least total error, and was a significantly better fit than the beta curve. However, an additional term was introduced into the Weibull function to increase its flexibility; I anticipate that introduction of an equivalent term to the beta would also increase flexibility, potentially lowering its resultant error. Under those conditions, the beta curve might outperform the Weibull.

Lower error values were obtained from when comparing crown curves of *Pseudotsuga menziesii* and *Pinus ponderosa* with each other than when either species was compared with *Abies lasiocarpa.* Intuitively, this agrees with field observations that *Pseudotsuga menziesii* and *Pinus ponderosa* crowns are shaped more similarly to each other than to *Abies lasiocarpa*. Perhaps because the Weibull curves were more accurate for each species, they were better able to discern the more subtle differences between not-starkly-different crown shapes such as *Pseudotsuga menziesii* and *Pinus ponderosa*. The gross differences between either of those and *Abies lasiocarpa* were apparent regardless of which modeled curve was used.

These findings and relationships can be used to guide crown shape modeling for these species, as well as for others not covered in this study. If a new species is to be modeled and the crown is known to be similar to that of one of the species in this study, it may prove better to use the curve from the known similar species than to use a simple geometry (e.g. using *Pseudotsuga*

menziesii for *Pinus ponderosa*, or *Abies lasiocarpa* for *Abies grandis*). However, if the new species does not have a similar crown to a known species, use of a simple geometry may produce less error than the curve from a markedly different species and simplify the analysis (e.g. using a cylinder for *Pinus ponderosa* instead of the *Abies lasiocarpa* curve).

These results also highlight that a more complex solution (i.e. a modeled curve) is not always better than a simple approach (i.e. standard geometric shapes). The beta curve for *Abies lasiocarpa* actually produced higher errors than the modeled cone, and statistically equivalent errors to those from the cylinder. In fact, although there are significantly different errors between most of the combinations, the acceptability of absolute error values for any modeled shape depends on the needs of the modeler.

Within-crown Heterogeneity

Very little work, as related to fire behavior modeling, has examined the structural heterogeneity of single crowns, although this variability has been acknowledged as important and incorporated into stand-level models of canopy structure (Mitsopoulos and Dimitrakopoulos 2007, Reinhardt et al. 2006). However, as ecological models become more sophisticated, there is a greater need for data at the individual tree level (Mell 2006, Mell 2009, Parsons et al. 2011). This work is a first step toward characterizing the internal distribution of biomass on an individual crown scale.

Studies in the radiative transfer modeling field examined 3-dimensional variation in vegetative structure most closely. That work has focused on a very fine scale, looking at the influence of changing within-shoot leaf or needle arrangement on light interception, and is based on statistical distributions of photosynthetically active material (Kim et al. 2011, Therezien et al. 2007, and others). Some studies have attempted to estimate the larger 3D structure within the crown by revising allocation of material until modeled light parameters approximate those obtained through

field measures (Kubo et al. 2008 and Parveaud et al. 2008), but with limited success. Giuliani et al. (2005), simulated point-intercept sampling on one walnut tree using a dataset created by digitizing 1558 leaves – a task with limited applicability to large sample sizes. They state that "unfortunately, direct techniques to acquire tree canopy geometrical features cannot be exploited … because of the massive number of elements to be monitored and/or impracticable foliage access."

TLS is well suited to sample large numbers of elements, and does not require direct contact with a canopy. Unlike previous work, this thesis focused on capturing and measuring the arrangement of vegetation *in situ* (i.e. not from destructively sampled or simulated trees), not relying on reconstructed models that conform to some limited number of parameters. Although Ripley's K does not explicitly locate material within a crown, it does provide information about the *actual* spatial patterning of detected crown elements, not simulated positions. This thesis demonstrates that the approach of utilizing TLS to characterize the vegetative patterning at an individual crown level using directly measured locations is promising.

Field data collection

Scans:

Analysis was performed on the laser returns, which are assumed to capture the crown material. However, it is possible, particularly in a very dense canopy such as *Abies lasiocarpa*, that the inner vegetation remains unsampled. Thus, although the observed clustering is still valid for the dataset, the dataset may underrepresent the true canopy. Undersampling is usually addressed by scanning from multiple angles, but this would confound cluster analysis based on the number of events in any given area or volume by "double-counting" material that is scanned from multiple directions. In this study, when a tree required two scans to capture its entire extent, the doubling effect of the overlap area was removed by first aligning using the entire overlap, but merging scans

above and below a horizontal plane that excluded returns extending past that plane into the other scan.

Global clustering

Time in the field, looking at trees, suggests that material is not uniformly distributed throughout a tree crown, and this observation is conceptually supported by theories of light utilization (Kim et al. 2011, King and Maindonald 1999, Cohen et al. 1995, Oker-blom and Kellomaki 1983, Whitehead et al. 1990). One goal of this study was to explore characterization of material arrangement within an identified crown envelope (generated from a profile). An initial, global characterization of clustering within the crown was calculated using Ripley's K (and its normalized variant, Ripley's L) in 3D, comparing the observed proximity of points to what is expected under a spatially random distribution. Although the strength of Ripley's K is that, unlike other nearest-neighbor spatial analysis methods that rely on highly local information, it considers departure from CSR over a range of scales. The main drawback to implementing Ripley's K in this setting is the lack of spatially explicit results. In short, Ripley's K can be used to identify departure from spatial randomness (clustering), but not where the clusters are located.

Pinus ponderosa exhibited the greatest clustering of the three species, which is consistent with the characteristic *Pinus ponderosa* shape of heavy, gnarled limbs reaching out from the trunk in isolation from one another, each possessing broom-like clusters of foliage. Although this is an extreme expression of the form, as a whole, *Pinus ponderosa* did show a greater departure from random at all scales and clustering occurring through larger scales than the other two species.

Conversely, *Abies lasiocarpa* showed the least clustering overall (both smallest magnitude and smallest scale) which may reflect the density of vegetation within the crown (e.g. branches that are contiguous both vertically and horizontally). As anyone who has had to measure DBH on an

Abies lasiocarpa will tell you, there is very little open space in the crown. Because so much space is filled, discrete clusters from branching patterns may not be apparent.

Clustering by height partition:

I also hypothesized that there would be a difference in clustering from the top to the bottom of the tree. Personal observations argue that within the crown envelope, material is distributed differently as a function of height. At the top of the tree, there are needles and fine branches occupying much of the entire crown volume, while at the base of the tree there is often a void near the bole, with needles and fine branches only being present toward the outer portion of the crown envelope. Testing a division of the sample set of *Pseudotsuga menziesii* trees into upper and lower crown did show a difference with the lower portion of the crown showing clustering across a larger range of scales and to a greater degree than the upper portion of the crown. These differences led to analyzing the entire dataset by upper vs. lower crown.

In this study, I vertically divided the crowns at the halfway mark, an arbitrary delineation. Thus, clustering differences between the "upper" and "lower" portions may differ depending on where that partitioning occurs.

Clustering by intensity:

Fire behavior modelers are most concerned with fine fuels, but the laser records any material it encounters, without discrimination. An attempt was made to separate laser points based on range-corrected intensity, but without true reference data, quantifying the accuracy of such separation was not possible. However, it was the sense of this author that although subjective, a visually determined intensity threshold did produce a reasonable differentiation between coarse and fine fuels – a rough estimate, but perhaps better than nothing. If one accepts that a somewhat reasonable separation was achieved, then the clustering results from comparing all the points to

just the "fine fuel" points suggests little difference from separating out diffuse returns. It is possible that, as the sample trees do mostly show a very slight increased degree of clustering from just the diffuse returns that there is a difference, but one that is too small to capture with a coarse visual separation. That the Ripley's L results show little difference between foliage-only and full crown point clouds perhaps reflects a similar arrangement of branchwood and fine fuels within the crown (i.e. fine fuel locations are closely tied to branching pattern).

Although laser return intensity was distance normalized, the threshold values varied between trees (which were all *Pseudotsuga menziesii*) and all were quite different from the thresholds determined by Seielstad et al. (2011) for individual *Pseudotsuga menziesii* branches. There is some work (Dr. Carl Seielstad, personal communication, 15 March 2013) suggesting that intensity increases as material depth increases. This is consistent with the values seen when comparing whole trees to the *Pseudotsuga menziesii* branches from the study above. However, this is quite preliminary and requires more investigation.

Post facto exploratory analysis:

Several exploratory analyses were undertaken *post facto* to address some of the assumptions and limitations associated with this work. What follows is a discussion of the findings of each analysis, and how they may affect the interpretation of the original study results.

Rescaling

Because peak clustering for a species was observed at a consistent search radius on the rescaled crowns, it followed that the actual size of the unnormalized clustering within the unscaled crown would increase with crown length. A small test set did confirm this, but a larger sample is needed to be confident it was characteristic of differences between large and small trees. Another way to approach departure from CSR would be to apply Ripley's K to unscaled tree crowns and identify the scales over which clustering occurs and peaks. Then, to aggregate information from

multiple trees, the size of peak clustering could be related to some other factor. Tree size metrics would be likely variables, but other factors such as stand density or canopy position might also be worth investigation.

The second issued tied to scaling of search radii by crown length was that cluster detection limits were inherently coarser in large crowns. Fine-grain clustering was not captured for large trees because the minimum search increment (proportionate to crown length) was already larger than the cluster. The test set demonstrates that greater resolution is needed, particularly for large trees. Thus, although this work offers evidence that the maximum scale of clustering in small trees is smaller than that of large trees, it cannot be used to make conclusions about minimum scales of clustering between large and small trees.

Subsample methodology

In the longer crown (*Pseudotsuga menziesii*, 16.5m crown length), there was no discernible effect on detected clustering from how the crown returns were subsampled. At the scale of search radii used here, for this tree the smallest search radius (0.0125 as a proportion of crown length) scales up to 20cm. With a spot spacing of 4mm, every 15^{th} point results in a minimum spacing of 6cm; it is probably that the Ripley's L values were not affected because the search radii were sufficiently larger than the spacing between points.

For the shortest crown (*Abies lasiocarpa*, 4.5m crown length), the smallest search radius (0.0125 as a proportion of crown length) scales to 5.6cm, smaller than the predicted spacing of 6cm after taking $1/15^{th}$ of the original data. The differences in Ripley's L values at that scale are likely due to that disparity. Although the effects of different subsampling methods are apparent at the smallest scales, these differences did not change the overall trend of the Ripley's L function.

Edge effects

Two separate analyses were conducted to investigate the impact of artificial and actual edges on the clustering results. The artificial upper-lower and front-back edges were removed through mirroring the front hemisphere of laser returns, and allowing points in the sample area (e.g., the upper or lower crown) to consider the points from the entire mirrored crown for calculation of the Ripley's K and L values. Cluster analyses after removing each artificial edge (upper-lower or front-back) separately and then together (no artificial edges) showed that the front-back boundary had the greatest impact on the Ripley's L value. This is probably because that edge was larger than the upper-lower boundary, thus affecting a greater number of points. Although the Ripley's L values increased when the artificial edges were removed, the relationships between clustering in the upper and lower crowns remained consistent with earlier findings – clustering in the lower crown occurs to a greater magnitude and across greater scales than in the upper crown.

Although the artificial edges could be compensated for, the tree crowns in this study also had actual edges – the extent of the crown. This edge was expected to influence the Ripley's L values in a similar to the artificial edges, by producing smaller values than would exist if the patterning within the tree crown were analyzed as if it were part of a continuous field of the same pattern. These smaller Ripley's K values would then indicate less clustering than may be actually occurring, as well as clustering occurring over smaller scales (because the Ripley's K values that are negative or close to zero may in fact be positive without the edge effect). In the case of the artificial edges, both those effects are artifacts of the artificial study area bounds. However, because the crown extent is an actual edge, the impacts are more nuanced. In smaller trees, or the upper regions of larger trees, there are a greater proportion of points that are close to the boundary, and thus subject to edge effect. Although the suppression of the magnitude of clustering is a valid concern (and is addressed below), the impact on cluster size is real. If a crown is small, there is a

physical limit to the cluster size that can be detected – a 3m sphere does not fit within a 2m wide crown. Thus, the edge effect on cluster size is legitimate, and should not be corrected for.

However, the calculated degree to which material is clustered within the crown is also affected by the crown extent edge. Trees of different sizes and shapes, as well as different regions within a crown (e.g., the upper and lower crown partitions used here) have varying amounts of crown extent edge, and the resulting clustering will reflect those differences, potentially overshadowing the actual within-crown patterning. Unlike addressing the front-back boundary, mirroring the crown's outer extent was not done here because it would artificially inflate the cluster size, which, as described above, is truly limited by the crown extent edge. Instead, multiple sections of a tree crown were delineated so that their surface area to volume ratio was constant. However, it should be noted that there was still some potential for variation among segments due to the non-uniform nature of the outer crown extent, which was not controlled for. The results showed that clustering in the lower segments of the crown occurred at a greater magnitude than in the upper crown segments (larger Ripley's L values), that peak clustering occurred at larger sizes in the lower crown segments, and that clustering was found across a greater range of sizes in the lower crown segments than in the upper segments. These results are consistent with what was found in the original study. In this series of comparisons, although the surface area/volume ratio was consistent, the absolute volumes did vary among segments, as did the shape of segments. There is still a possibility that the observed differences in patterning are an artifact of sample area characteristics. Understanding the effect of the actual crown extent edge on detected clustering warrants further investigation, but was not within the scope of this work.

Conclusions and Future Work

Conclusions

Overall, TLS demonstrates potential to be more than a novel way to make the "same old" fuels measurements and instead provides a new suite of techniques that can provide new types of information, including *in situ* measures of external crown architecture and detailed 3D measures of internal crown structure.

When combined with biomass allometry, crown profile and internal structural information could be used to populate a tree list with reasonable parameters about how much biomass to expect, and where to locate that biomass. The results of this work have provided species-specific equations to delineate crown profiles (and thus volumes), but are not yet sufficient to distribute biomass within that crown. This work indicates that non-homogeneous distributions are needed, but does not provide spatially explicit clustering information.

Specifically, this work finds that:

- An objective, repeatable canopy base metric is derivable solely from TLS data. This metric is consistently lower than field-measures of canopy base height as measured by USFS guidelines (USDA Forest Service 2009), likely due to its consideration of all branches, live or dead.
- The 95th width percentile was found to be an adequate descriptor of the "outer" limits of the crown, and little variation in profile shape was seen using alternate width percentiles. The volumetric changes associated with using different width percentiles were smaller than those from using simple shapes (i.e. cones or cylinders), with one exception.
- For all species, a modified Weibull curve gave the most accurate fit to the aggregated 95th width percentile points, as measured using the MAE and cross-validation where appropriate. The Weibull curve produced statistically significant smaller errors than did the beta curve, cone or cylinders.

- Curves are species-specific, and interchanging curves among different species produced poorer fits (statistically significant increased error).
- Ripley's K analysis of crown laser returns indicates departure from spatial randomness, with peak clustering occurring at a scale of 1.25 – 2.5% of crown length.
- Clustering in the lower canopy was detected across larger scales and to a greater extent than that in the upper canopy (as divided at the midpoint), although this may be an artifact of sample area characteristics (size and shape).
- Observed canopy clustering does not seem to be affected by inclusion or exclusion of branchwood from the crown point cloud, although the differentiation of fine fuels from branchwood employed in this study was subjective.
- There is preliminary evidence that argues for cluster analysis performed at finer scales than implemented in this study.

Future work

The first type of work that builds on this thesis can be considered improvements to the approaches presented here, utilizing the lessons learned in this study. The intensity stratification implemented here relied primarily on subjective interpretation of the visual display. Additional experimental data to guide fuel size class separation based on laser return intensity values could make the process more objective. However, collecting field data to act as the ground truth in an accuracy assessment would be logistically difficult. A second improvement could be implementing cluster analysis in fine increments on unscaled crowns, and producing confidence envelopes for the distribution under CSR. Implementing either of these would be quite time intensive, but possible. Further analysis of edge effect (particularly addressing the actual edge of the crown extent) is needed to understand the observed differences due to vertical partitioning of the tree crown. The question of obscuration could be partly addressed by scanning trees from multiple angles, and

merging the scans using vertical planar boundaries to eliminate the over-sampling of areas covered by multiple scans. However, this still does not address the larger issue of occlusion within the interior of the canopy. Ultimately, it may be necessary to quantify the horizontal distribution of biomass in tree crowns by field sampling.

The more interesting type of work that builds on this thesis is thinking about how to actually apply these findings within a fire behavior modeling framework. Currently, the bar for arranging biomass in tree crowns is quite low. Modelers simply adjust biomass amount and move it around in the crown until they obtain model output similar to laboratory observation of fires in small trees. Although my work does not explicitly locate material in space, there are a few possibilities of how to overcome this limitation. First, for a hypothetical tree, one could predict the expected biomass and crown volume (from the crown profile). Then, because the outer profile is fixed but some literature (e.g., Baldwin and Peterson 1997, Kershaw and Maguire 1995) (and personal experience) suggests that the interior of a crown is often mostly void (, the volume could be constrained ("hollowed out") until a realistic bulk density is reached. Although this approach would not provide detailed information about biomass location (i.e. is it vertically uniform within the shell?), it may be an improvement over no existing methods to estimate how biomass is distributed. An approach to locating clusters within the defined crown volume would be to calculate the number of clusters of some size to total biomass (from allometry) at a given bulk density. Then, that number of clusters could be distributed within the crown volume defined by the profile. A second option would be to partition the crown volume into voxels dimensioned to match the scale at which the greatest clustering occurs, and fill voxels until, given a realistic bulk density, the predicted biomass is reached.

LITERATURE CITED

Affleck, D.L.R. &Turnquist, B.R. 2012, "Assessing the accuracy of crown biomass equations for the major commercial species of the interior northwest: study plans and preliminary results", in: McWilliams, W., Roesch, F.A., eds. *Monitoring Across Borders: 2010 Joint Meeting of the Forest Inventory and Analysis (FIA) Symposium and the Southern Mensurationists*. E-General Technical Report SRS-157. Asheville, NC: U.S. Department of Agriculture, Forest Service, Southern Research Station. pp. 247-252.

Baldwin, V.C. Jr. & Peterson, K.D. 1996, "Predicting the crown shape of loblolly pine", *Canadian Journal of Forest Research*, vol. 27, pp. 102-107.

Beil, M., Fleischer, F., Paschke, S. & Schmidt, V. 2005, "Statistical analysis of the three-dimensional structure of centromeric heterochromatin in interphase nuclei", *Journal of Microscopy*, vol 217, pp. 60-68.

Beland, M., Widlowski, J.-L., Fournier, R.A., Cote, J.-F., & Verstraete, M.M. 2011, "Estimating leaf area distribution in savanna trees from terrestrial LiDAR measurements", *Agricultural and Forest Meteorology*, vol. 151, no. 9, pp. 1252-1266.

Biging, G.S. & Wensel, L.C. 1990, "Estimation of Crown Form for 6 Conifer Species of Northern California", *Canadian Journal of Forest Research-Revue Canadienne De Recherché Forestiere,* vol. 20, no. 8, pp. 1137-1142.

Brown, J.K. 1978, Weight and density of crowns of Rocky Mountain conifers. Research Paper INT-RP-197. Ogden, UT: U.S. Department of Agriculture, Forest Service, Intermountain Forest and Range Experiment Station. 56pp.

Canham, C.D., Coates, K.D., Bartemucci, P. & Quaglia, S. "Measurement and modeling of spatially explicit variation in light transmission through interior cedar-hemlock forests of British Columbia", *Canadian Journal of Forest Research-Revue Canadienne De Recherché Forestiere*, vol. 29, no. 11, pp. 1775-1783.

Clark, M.L., Roberts, D.A., Ewel, J.J. & Clark, D.B. 2011, "Estimation of tropical rain forest aboveground biomass with small-footprint lidar and hyperspectral sensors", *Remote Sensing of Environment*, vol. 115, no. 11, pp. 2931-2942.

Cluzeau, C., Legoff, N. & Ottorini, J.M. 1994, "Development of Primary Branches and Crown Profile of Fraxinus-Excelsior", *Canadian Journal of Forest Research-Revue Canadienne De Recherché Forestiere,* vol. 24, no. 12, pp. 2315-2323.

Cochran, P.H., Geist, J.M., Clemens, D.L., Clausnitzer, R.R. & Powell, D.C. 1994, Suggested Stocking Levels for Forest Stands in Northeastern Oregon and Southeastern Washington. Research Note PNW-RM-513. Portland, OR: U.S. Department of Agriculture, Forest Service, Pacific Northwest Research Station. 21pp.

Cohen, S., Mosoni, P., & Meron, M. 1995, "Canopy clumpiness and radiation penetration in a young hedgerow apple orchard", *Agricultural and Forest Meteorology*, vol. 76, no. 3-4, pp. 185-200.

Cote, J., Widlowski, J., Fournier, R.A. & Verstraete, M.M. 2009, "The structural and radiative consistency of three-dimensional tree reconstructions from terrestrial LiDAR", *Remote Sensing of Environment,* vol. 113, no. 5, pp. 1067-1081.

Crecente-Campo, F., Marshall, P., LeMay, V. & Dieguez-Aranda, U. 2009, "A crown profile model for Pinus radiata D. Don in northwestern Spain", *Forest Ecology and Management,* vol. 257, no. 12, pp. 2370-2379.

Crookston, N. & G. Dixon. 2005, “The Forest Vegetation Simulator: A review of its structure, content and applications”, *Computers and Electronics in Agriculture,* vol.49, pp. 60-80.

Danson, F.M., Hetherington, D., Morsdorf, F., Koetz, B. & Allgoewer, B. 2007, “Forest canopy gap fraction from terrestrial laser scanning”, *IEEE Geoscience and Remote Sensing Letters*, vol. 4, no. 1, pp. 157-160.

Da Silva, D., Boudon, F., Godin, C. & Sinoquet, H. 2008, “Multiscale framework for modeling and analyzing light interception by trees”, *Multiscale Modeling and Simulation*, vol. 7, no. 2, pp. 910-933.

da Silva, E.C., Silva, A.C., de Paiva, A.C., Nunes, R.A. & Gattass, M. 2008, “Diagnosis of solitary lung nodules using the local form of Ripley’s K function applied to three-dimensional CT data”, *Computer methods and Programs in Biomedicine*, vol. 90, pp. 230-239.

Dassot, M., Colin, A., Santenoise, P., Fournier, M., & Constant, T. 2012, “Terrestrial laser scanning for measuring the solid wood volume, including branches, of adult standing trees in the forest environment”, *Computers and Electronics in Agriculture*, vol. 89, pp. 86-93.

Delagrange, S. & Rochon, P. 2011, "Reconstruction and analysis of a deciduous sapling using digital photographs or terrestrial-LiDAR technology", *Annals of Botany,* vol. 108, no. 6, pp. 991-1000.

Deleuze, C., Herve, J.C., Colin, F. & Ribeyrolles, L. 1996, "Modeling crown shape of Picea abies: Spacing effects", *Canadian Journal of Forest Research-Revue Canadienne De Recherché Forestiere,* vol. 26, no. 11, pp. 1957-1966.

Dixon, G. 2002a, Essential FVS: A user’s guide to the Forest Vegetation Simulator, USDA Forest Service, Internal Report, Forest Management Service Center, Fort Collins, CO. 189pp.

Dixon, P. 2002b, “Nearest neighbor methods”, in: El-Shaarawi, A.H. & Piegorsch, W.W., eds. *Encyclopedia of Environmentrics*, *Vol. 3*. John Wiley & Sons, new York, NY, USA, pp. 1370-1383.

Doruska, P.F. & Mays, J.E. 1998, “Crown profile modeling of loblolly pine by nonparametric regression analysis”, *Forest Science*, vol. 44, no. 3, pp. 445-453.

Duursma, R.A. & Makela, A. 2007, “Summary models for light interception and light-use efficiency of non-homogeneous canopies”, *Tree Physiology*, vol. 27, no. 6, pp. 859-870.

Edminster, C.B. 1987, “Growth and yield of subalpine conifer stands in the central Rocky Mountains”, in: Troendle, C.A., Kaufmann, M.R., Hamre, R.H., & Winokur, R.P., tech. coords. *Management of Subalpine Forests: Building on 50 Years of Research.* General Technical Report RM-GTR-149. Fort Collins, CO: U.S. Department of Agriculture, Forest Service, Rocky Mountain Forest and Range Experiment Station. pp. 33-40.

Erdody, T.L. & Moskal, L.M. 2010, "Fusion of LiDAR and imagery for estimating forest canopy fuels", *Remote Sensing of Environment,* vol. 114, no. 4, pp. 725-737.

ESRI. 2010. Arc GIS Desktop: Release 10. Redlands, CA: Environmental Systems Research Institute.

Exelis Visual Information Solutions. 2007. Interactive Data Language (IDL): version 8.0. Boulder, CO.

Fernandez-Sarria, A., Velaquez-Marti, B., Sajdak. M., Martinez, L., & Estornell, J. 2013, “Residual biomass calculation from individual tree architecture using terrestrial laser scanner and ground-level measurements”, *Computers and Electronics in Agriculture*, vol. 93, pp. 90-97.

Finney, M. 1998, FARSITE: Fire Area Simulator - Model development and evaluation. Research Paper RMRS-RP-4. Ogden, UT: U.S. Department of Agriculture, Forest Service, Rocky Mountain Research Station. 47 pp.

Garcia, M., Popescu, S., Riano, D., Zhao, K., Neuenschwander, A., Agca, M. & Chuvieco, E. 2012, "Characterization of canopy fuels using ICESat/GLAS data", *Remote Sensing of Environment*, vol. 123, pp. 81-89.

Gill, S. & Biging, G. 2002, "Autoregressive moving average models of conifer crown profiles", *Journal of Agricultural Biological and Environmental Statistics,* vol. 7, no. 4, pp. 558-573.

Giuliani, R., Magnanini, E., Muzzi, E., & Sinoquet, H. 2005, "Canopy probabilistic reconstruction inferred from Monte Carlo point-intercept leaf sampling", *Agricultural and Forest Meteorology*, vol. 128, no. 1-2, pp. 17-32.

Graham, J. 2 May 2012, "Class lecture notes: Ripley's K-function." STAT 544 Spatial Statistics Spring 2012. Umiversity of Montana, Missoula, MT. pp. 215-220.

Hann, D.W. 1999, "An adjustable predictor of crown profile for stand-grown Douglas-Fir trees", *Forest Science,* vol. 45, no. 2, pp. 217-225.

Henning, J.G. & Radtke, P.J. 2006, "Ground-based laser imaging for assessing three-dimensional forest canopy structure", *Photogrammetric Engineering and Remote Sensing*, vol. 72, no. 12, pp. 1349-1358.

Hiers, J.K., O'Obrien, J.J., Mitchell, R.J., Grego, J.M, & Loudermilk, E.L. 2009, "The wildland fuel cell concept: an approach to characterize fine-scale variation in fuels and fire in frequently burned longleaf pine forests", *International Journal of Wildland Fire*, vol. 18, no. 3, pp. 315-325.

Hoffman, C., Morgan, P., Mell, W., Parsons, R., Strand, E. & Cook, S. 2012, "Numerical simulation of crown fire hazard immediately after bark beetle-caused mortality in lodgepole pine forests", *Forest Science*, vol. 58, no. 2, pp. 178-188.

Hosoi, F. & Omasa, K. 2006, "Voxel-based 3-D modeling of individual trees for estimating leaf area density using high-resolution portable scanning lidar", *IEEE Transactions on Geoscience and Remote Sensing*, vol. 44, no. 12, pp. 3610-3618.

InnovMetric. 2009. Polyworks: version 11.0.1. Quebec, Canada.

Jafari-Mamaghani, M., Andersson, M., & Krieger, P. 2010, "Spatial point pattern analysis of neurons using Ripley's K-function in 3D", *Frontiers in Neuroinformatics*, vol. 4, 9pp. DOI: 10.3389/fninf.2010.00009

Keane, R.E., Reinhardt, E.D., Scott, J., Gray, K. & Reardon, J. 2005, "Estimating forest canopy bulk density using six indirect methods", *Canadian Journal of Forest Research*, vol. 35, no. 3, pp. 724-739.

Kershaw, J.A. & Maguire, D.A. 1996, "Crown structure in western hemlock, Douglas-fir, and grand fir in western Washington: horizontal distribution of foliage within branches", *Canadian Journal of Forest Research*, vol. 26, pp. 128-142.

King, D.A. & Maindonald, J.H. 1999, "Tree architecture in relation to leaf dimensions and tree stature in temperate and tropical rain forests", *Journal of Ecology*, vol. 87, no. 6, pp. 1012-1024.

Kim, H.-S., Palmroth, S., Therezien, M., Stenberg, P., & Oren, R. 2011, "Analysis of the sensitivity of absorbed light and incident light profile to various canopy architecture and stand conditions", *Tree Physiology*, vol. 31, no. 1, pp.30-47.

Kubo, T., Kobayashi, T., Kato, K., Nishimura, S., Uemura, S., Ono, K., Sumida, A., & Hara, T. 2008, "Estimating the three-dimensional structure of canopy foliage based on the light measurements in a *Betula ermanii* stand", *Agricultural and Forest Meteorology*, vol. 148, no. 8-9, pp. 1293-1304.

Lancaster, J. & Downes, B.J. 2004, "Spatial point pattern analysis of available and exploited resources", *Ecography*, vol. 27, pp. 64-102.

Lesak, A.A., Radeloff, V.C., Hawbaker, T.J., Pidgeon, A.M., Gobakken, T. & Contrucci, K. 2011, "Modeling forest songbird species richness using LiDAR-derived measures of forest structure", *Remote Sensing of Environment*, vol. 115, pp. 2823-2835.

Linn, R., Reisner, J., Colman, J.J. & Winterkamp, J. 2002, "Studying wildfire behavior using FIRETEC", *International Journal of Wildland Fire*, vol. 11, no. 4, pp. 233-246.

Lovell, J., Jupp, D., Culvenor, D. & Coops, N. 2003, "Using airborne and ground-based ranging LiDAR to measure canopy structure in Australian forests RID B-1326-2012", *Canadian Journal of Remote Sensing,* vol. 29, no. 5, pp. 607-622.

Maguire, D.A. & Bennett, W.S. 1996, "Patterns in vertical distribution of foliage in young coastal Douglas-fir", *Canadian Journal of Forest Research*, vol. 26, pp. 1191-2005.

Marshall, D., Johnson, G. & Hann, D. 2003, "Crown profile equations for stand-grown western hemlock trees in northwestern Oregon", *Canadian Journal of Forest Research,* vol. 33, no. 11, pp. 2059-2066.

Mawson, J.C., Thomas, J.W. & DeGraaf, R.M. 1976, Program HTVOL: The determination of tree crown volume by layers. Research Paper NE-354. Upper Darby, PA: U.S. Department of Agriculture, Forest Service, Northeastern Forest Experiment Station. 9pp.

Mell, W., Manzello, S. & Maranghides, A. 2006. "Numerical modeling of fire spread through trees and shrubs", V International Conference of Forest Fire Research. Viegas (Ed.)

Mell, W., Maranghides, A., McDermott, R. & Manzello, S.L. 2009, "Numerical simulation and experiments of burning Douglas fir trees", *Combustion and Flame,* vol. 156, no. 10, pp. 2023-2041.

Mitsopoulos, I.D. & Dimitrakopoulos, A.P. 2007, "Canopy fuel characteristics and potential crown fire behavior in Aleppo pine (*Pinus halepensis* Mill.) forests", *Annals of Forest Science*, vol. 64, pp.287-299.

Moore, J.A., Mike, P.G. & Vander Ploeg, J.L. 1991, "Nitrogen fertilizer response of Rocky Mountain Douglas-fir by geographic area across the Inland Northwest", *Western Journal of Applies Forestry*, vol. 6, no. 4, pp. 94-98.

Moorthy, I., Miller, J.R., Jimenez Berni, J.A., Zarco-Tejada, P., Hu, B. & Chen, J. 2011, "Field characterization of olive (*Olea europaea* L.) tree crown architecture using terrestrial laser scanning data", *Agricultural and Forest Meteorology,* vol. 151, no. 2, pp. 204-214.

Mori, S. & Hagihara, A. 1991, "Crown profile of foliage area characterized with the Weibull distribution in a hinoki (*Chamaecyparis obtusa*) stand", *Trees*, vol. 5, pp. 149-152.

Oker-blom, P. & Kellomaki, S. 1983, "Effect of grouping of foliage on the within-stand and within-crown light regime – comparison of random and grouping canopy models", *Agricultural Meteorology*, vol. 28, no. 2, pp. 143-155.

Ottmar, R.D., Blake, J.I., & Crolly, W.T. 2012, "Using fine-scale fuel measurements to assess wildland fuels, potential fire behavior and hazard mitigation treatments in the southeastern USA", *Forest Ecology and Management*, vol. 273, pp.1-3.

Palminteri, S., Powell, G.V.N., Asner, G.P., & Peres, C.A. 2012, "LiDAR measurements of canopy structure predict spatial distribution of a tropical mature forest primate", *Remote Sensing of Environment*, vol. 127, pp. 98-105.

Parsons, R.A., Mell, W.E. & McCauley, P. 2011, "Linking 3D spatial models of fuels and fire: Effects of spatial heterogeneity on fire behavior", *Ecological Modeling,* vol. 222, no. 3, pp. 679-691.

Parveaud, C.-E., Chopard, J., Dauzat, J., Courbaud, B., & Auclair, D. 2008, "Modelling foliage characteristics in 3D tree crowns: influence on light interception and leaf irradiance", *Trees- Structure and Function*, vol. 22, no. 1, pp. 87-104.

R Development Core Team (2008). R: A language and environment for statistical computing. R Foundation for Statistical Computing, Vienna, Austria. ISBN 3-900051-07-0.

Reinhardt, E. & Crookson, N.L. (tech. editors) 2003. The Fire and Fuels Extension to the Forest Vegetation Simulator. General Technical Report RMRS-GTR-116. Ogden, UT: U.S. Department of Agriculture, Forest Service, Rocky Mountain Research Station. 209 pp.

Reinhardt, E.D. & Ryan, K.C. 1988, Eight-year Tree Growth Following Prescribed Under-burning in a Western Montana Douglas-fir/Western Larch Stand. Research Note INT-387. Ogden, UT: U.S. Department of Agriculture, Forest Service, Intermountain Research Station. 6 pp.

Reinhardt, E., Scott, J., Gray, K. & Keane, R. 2006, "Estimating canopy fuel characteristics in five conifer stands in the western United States using tree and stand measurements", *Canadian Journal of Forest Research*, vol. 36, pp. 2803-2814.

Remphrey, W.R., Davidson, C.G., & Blouw, M.J. 1987, "A classification and analysis of crown form in green ash (*Fraxinus pennsylvanica*)", *Canadian Journal of Botany*, vol. 65, no. 11, pp.2188-2195.

Riano, D., Meier, E., Allgower, B., Chuvieco, E. & Ustin, S. 2003, "Modeling airborne laser scanning data for the spatial generation of critical forest parameters in fire behavior modeling", *Remote Sensing of Environment,* vol. 86, no. 2, pp. 177-186.

Riano, D., Chuvieco, E., Condes, S., Gonzalez-Matesanz, J. & Ustin, S. 2004, "Generation of crown bulk density for Pinus sylvestris L. from LiDAR", *Remote Sensing of Environment,* vol. 92, no. 3, pp. 345-352.

Ripley, B.D. 1977, "Modelling spatial patterns (with discussion)", *Journal of the Royal Statistical Society,* vol. 93, no. 2, pp. 172 – 212.

Roeh, R. & Maguire, D. 1997, "Crown profile models based on branch attributes in coastal Douglas-fir", *Forest Ecology and Management,* vol. 96, no. 1-2, pp. 77-100.

Rosell, J.R. & Sanz, R. 2012, "A review of methods and applications of the geometric characterization of tree crops in agricultural activities", *Computers and Electronics in Agriculture*, vol. 81, pp. 124-141.

Saito, S., Sato, T., Kominami, Y., Nagamatsu, D., Kuramoto, S., Kakai, T., Tabuchi, R., & Sakai, A. 2004, "Modeling the vertical foliage distribution of an individual *Castanopsis cuspidata* (Thunb.) Schottky, a dominant broad-leaved tree in Japanese warm-temperate forest", *Trees*, vol. 18, pp. 486-491.

Sanz-Cortiella, R., Llorens-Calveral, J., Escola, A., Arno-Satorra, J., Ribes-Dasi, M., Masip-Vialta, J., Camp, F., Gracia-Aquila, F., Solanelles-Battle, F., Planas-DeMarti, S., Palleja-Cabre, T., Palacin-Roca, J., Gregorio-Lopez, E., Del-Moral-Martinez, I., & Rosell-Polo, J.R. 2011, "Innovative LIDAR 3D dynamic measurement system to estimate fruit-tree leaf area", *Sensors*, vol. 11, no. 6, pp. 5769-5791.

Scott, J & E. Reinhardt. 2001, "Assessing crown fire potential by linking models of surface and crown fire behavior", USDA Forest Service, Research Paper RMRS-RP-29, Rocky Mountain Research Station, Fort Collins, CO. 59pp.

Seielstad, C., Stonesifer, C., Rowell, E., & Queen, L. 2011, "Deriving fuel mass by size class in Douglas-fir (*Pseudotsuga menziesii*) using terrestrial laser scanning", *Remote Sensing*, vol. 3, no. 8, pp. 1691-1709.

Sinoquet, H. & Rivet, P. 1997, "Measurement and visualization of the architecture of an adult tree based on a three-dimensional digitizing device", *Trees – Structure and Function*, vol. 11, no. 5, pp. 265-270.

Skowronski, N.S., Clark, K.L., Duveneck, M. & Hom, J. 2011, "Three-dimensional canopy fuel loading predicted using upward and downward sensing LiDAR systems", *Remote Sensing of Environment,* vol. 115, no. 2, pp. 703-714.

Sonohat, G., Sinquet, H., Kulandaivelu, V., Combes, D. & Lescourret, F. 2006, "Three-dimensional reconstruction of partially 3D-digitized peach tree canopies", *Tree Physiology*, vol. 26, no. 3, pp. 337-351.

Stage, A.R., Renner, D.L. & Chapman,R.C. 1988, Selected Yield Tables for Plantations and Natural Stands in Inland Northwest Forests. Research Paper INT-394. Ogden, UT: U.S. Department of Agriculture, Forest Service, Intermountain Research Station. 63pp.

Takeda, T., Oguma, H., Sano, T., Yone, Y. & Fujinuma, Y. 2008, "Estimating the plant area density of a Japanese larch (Larix kaempferi Sarg.) plantation using a ground-based laser scanner", *Agricultural and Forest Meteorology,* vol. 148, no. 3, pp. 428-438.

Therezien, M., Palmroth, S., Brady, R., & Oren, R. 2007, "Estimation of light interception properties of conifer shoots by an improved photographic method and a 3D model of shoot structure", *Tree Physiology*, vol. 27, no. 10, pp. 1375-1387.

U.S.D.A. Forest Service. 2009. Field Instructions, Stand Exam, Timber Management Data Handbook. FSH 2409.21h R-1 Chapter 400. Missoula, MT: U.S. Department of Agriculture, Forest Service Region One. Appendix Q.

VanderSchaaf, C.L. 2008, "Estimating understory vegetation response to multi-nutrient fertilization in Douglas-fir and ponderosa pine stands", *Journal of Forest Research*, vol. 13, pp. 43-51.

Westerling, A.L., Bryant, B.P., Preisler, H.K., Holmes, T.P., Hidalgo, H.G., Das, T. & Shrestha, S.R. 2011, "Climate change and growth scenarios for California wildfire", *Climatic Change,* vol. 109, pp. 445-463.

Whitehead, D., Grace, J.C., & Godfrey, M.J.S. 1990, "Architectural distribution of foliage in individual *Pinus radiata* D Don crown and the effects of clumping on radiation interception", *Tree Physiology*, vol. 7, no. 1-4, pp. 135-155.

Appendix A. Scan Details

Date	Site	Scan Name	Species	basal area	DBH (cm)	Ht (m)	CBH (m)	HLC (m)	Range (m)	Spot Spacing (mm)
6/13/2012	Ambrose Saddle	i001asdf	DF	60	49.4	22.7	4.8	4.4	23.5	3.80
6/11/2012	Lubrecht Garnet	i001lgdf	DF	60	39.2	22.1	14.1	12.7	30.5	3.70
6/25/2012	Morrell Creek	i001mcdf	DF	70	21.9	15.2	7.0	3.6	23.4	3.70
6/8/2012	Plant Creek	i001pcdf2	DF	30	37.2	22.5	7.7	6.6	40.6	4.10
6/11/2012	Lubrecht Garnet	i002lgdf	DF	40	33.8	20.0	10.0	5.1	24.7	4.00
6/25/2012	Morrell Creek	i002mcdf	DF	60	33.7	20.3	5.7	2.6	33.9	4.10
6/12/2012	Nine Mile	i002nmdf	DF	50	17.7	12.9	1.4	0.9	19.7	3.90
6/8/2012	Plant Creek	i002pcdf2	DF	30	44.6	20.7	3.0	3.0	31.7	3.80
6/11/2012	Lubrecht Garnet	i003lgdf	DF	40	50.9	23.3	10.4	7.7	41.3	4.10
6/25/2012	Morrell Creek	i003mcdf	DF	40	38.4	22.0	2.2	2.2	28.3	4.00
6/12/2012	Nine Mile	i003nmdf	DF	60	10.1	6.5	0.9	0.6	14.5	3.80
6/8/2012	Plant Creek	i003pcdf	DF	30	48.5	21.5	2.7	1.8	36.8	3.70
6/18/2012	Ambrose Saddle	i004asdf	DF	40	52.8	27.0	9.7	7.3	44.4	3.60
6/14/2012	Bandy	i004bydf	DF	150	41.4	19.7	2.7	1.2	30.9	3.70
8/22/2012	Kootenai	i004kndf2	DF	30	16.4	9.9	1.4	1.4	11.7	4.00
6/11/2012	Lubrecht Garnet	i004lgdf	DF	70	29.4	18.6	6.2	5.2	28.0	3.90
6/12/2012	Nine Mile	i004nmdf	DF	100	28.0	13.5	2.4	2.3	20.2	3.60
6/29/2012	Swan-hemlock	i004shdf	DF	100	45.1	22.6	10.5	7.8	31.8	3.80
6/18/2012	Ambrose Saddle	i005asdf	DF	70	60.0	26.9	8.4	3.3	52.2	4.20
6/12/2012	Nine Mile	i005nmdf	DF	40	16.2	10.7	3.2	3.2	21.1	3.80
8/22/2012	Kootenai	i006kndf	DF	70	30.2	12.1	2.7	0.8	12.3	3.90
6/25/2012	Morrell Creek	i006mcdf	DF	20	30.3	14.6	7.3	6.1	21.0	3.80
6/12/2012	Nine Mile	i006nmdf	DF	120	13.1	7.8	1.4	1.4	18.7	3.70
8/22/2012	Kootenai	i007kndf	DF	80	18.1	11.4	1.1	1.1	13.4	4.00
6/20/2012	Wellpinint - Tomine	i007tmdf	DF	40	40.0	21.2	8.7	7.7	42.4	4.20
6/20/2012	Wellpinint - Tomine	i008tmdf	DF	40	30.7	20.6	7.5	5.4	46.3	3.70
6/20/2012	Wellpinint - Tomine	i009tmdf	DF	30	62.9	31.9	11.0	7.9	42.5	4.30
6/20/2012	Wellpinint - Tomine	i011tmdf	DF	70	53.4	23.8	6.5	3.9	40.1	4.00
8/23/2012	Kootenai	i012kndf	DF	50	28.3	14.5	1.8	1.5	20.7	4.10
7/4/2012	Nine Mile	i013nmdf	DF	40	47.9	19.5	9.5	6.3	24.0	3.80
5/31/2012	Deer Creek	i001dcpipo	PIPO	30	47.7	25.9	15.3	13.7	38.0	3.80
8/22/2012	Kootenai	i001knpipo	PIPO	70	17.4	12.4	4.1	3.1	15.7	3.80
8/14/2012	Lubrecht Garnet Road	i001lrpipo	PIPO	40	59.5	21.1	7.0	4.7	26.1	3.70
6/12/2012	Nine Mile	i001nmpipo	PIPO	90	14.0	8.4	2.8	2.3	14.2	3.70

8/2/2011	Priest River	i001pr	PIPO		69.9				29.3	4.10
5/31/2012	Deer Creek	i002dcpipo	PIPO	60	39.0	23.4	12.7	10.0	28.0	3.90
8/14/2012	Lubrecht Garnet Road	i002lrpipo	PIPO	60	63.2	26.5	13.5	9.3	37.5	3.80
8/2/2011	Priest River	i002pr	PIPO		57.2				23.0	4.10
6/14/2012	Bandy	i003bypipo	PIPO	40	27.3	14.4	3.0	3.0	22.2	4.00
8/22/2012	Kootenai	i003knpipo	PIPO	70	24.7	14.4	3.7	0.2	17.3	3.80
6/25/2012	Morrell Creek	i004mcpipo	PIPO	20	42.7	15.6	3.8	3.2	19.3	3.90
6/7/2012	Deer Creek	i005dcpipo	PIPO	110	80.2	33.2	15.5	12.3	37.2	4.5
6/25/2012	Morrell Creek	i005mcpipo	PIPO	20	44.0	18.2	3.3	3.3	25.3	4.00
6/7/2012	Deer Creek	i006dcpipo	PIPO	90	65.4	35.7	18.3	15.1	51.5	4.1
6/25/2012	Morrell Creek	i007mcpipo2	PIPO	60	30.2	12.7	3.2	3.2	39.2	3.90
7/2/2012	Ambrose Saddle	i008aspipo	PIPO	10	63.6	22.3	2.7	2.7	54.9	4.40
8/23/2012	Kootenai	i008knpipo2	PIPO	160	62.9	35.5	21.9	20.7	29.6	4.10
6/25/2012	Morrell Creek	i008mcpipo	PIPO	40	34.4	19.7	7.0	5.6	34.0	4.10
6/25/2012	Morrell Creek	i009mcpipo	PIPO	10	16.8	6.4	1.0	0.5	19.8	4.00
10/1/2012	Deer Creek	i010dcpipo	PIPO	50	62.0	27.7	7.8	6.3	37.8	3.80
7/4/2012	Nine Mile	i010nmpipo	PIPO	40	40.0	25.4	15.3	13.7	34.2	4.10
8/23/2012	Kootenai	i011knpipo	PIPO	40	21.2	11.5	2.0	1.6	19.0	3.80
7/4/2012	Nine Mile	i011nmpipo	PIPO	60	46.0	28.1	9.2	9.2	31.3	3.80
10/1/2012	Deer Creek	i012dcpipo	PIPO	30	34.0	21.1	12.3	12.3	23.9	3.80
7/4/2012	Nine Mile	i012nmpipo	PIPO	70	44.0	26.9	15.0	8.2	25.0	4.00
10/1/2012	Deer Creek	i013dcpipo	PIPO	40	17.5	9.3	1.9	1.9	15.5	4.00
10/1/2012	Deer Creek	i014dcpipo	PIPO	30	28.5	12.5	4.0	3.3	17.0	3.70
7/4/2012	Nine Mile	i014nmpipo	PIPO	60	64.8	27.5	12.2	7.0	32.0	3.80
7/11/2012	Bonner's Ferry	i020bfpipo	PIPO	20	19.2	9.4	1.7	0.8	21.1	3.80
7/11/2012	Bonner's Ferry	m013bfsaf	SAF	180	5.8	4.5	0.7	0.7	8.2	3.90
7/26/2011	Granite Pass	i004gp	SAF		7.0				24.0	3.8
7/11/2012	Bonner's Ferry	i011bfsaf	SAF	120	7.2	5.5	0.2	0.2	8.4	4.00
7/11/2012	Bonner's Ferry	i012bfsaf	SAF	120	7.8	5.5	0.2	0.2	9.9	4.00
6/27/2012	Bonner's Ferry	i004bfsaf	SAF	50	10.8	7.1	1.7	1.0	17.1	3.80
10/2/2012	Ambrose Saddle	i014assaf	SAF	200	11.5	6.6	2.6	2.6	13.9	3.90
6/27/2012	Bonner's Ferry	i005bfsaf	SAF	50	11.8	8.4	2.4	1.4	21.7	3.90
7/26/2011	Granite Pass	i005gp	SAF		13				23.2	5.60
8/21/2012	Lubrecht Section 1	m003lssaf	SAF	40	14.2	9.8	0.1	0.1	14.0	3.90
10/2/2012	Ambrose Saddle	i013assaf	SAF	210	14.3	10.0	0.7	0.7	15.0	3.90
6/27/2012	Bonner's Ferry	m006bfsaf2	SAF	140	14.6	10.7	0.5	0.1	15.6	3.70
7/26/2011	Granite Pass	i003gp	SAF		15.0				16.0	3.80
6/27/2012	Bonner's Ferry	i002bfsaf	SAF	80	15.3	12.1	2.9	2.2	21.4	3.90
6/14/2012	Bandy	i002bysaf	SAF	80	18.3	10.8	0.0	0.0	20.1	4.00
10/2/2012	Ambrose Saddle	i010assaf	SAF	250	21.2	14.7	0.5	0.5	14.8	3.80
6/27/2012	Bonner's Ferry	i003bfsaf	SAF	130	21.8	15.5	3.8	1.4	27.9	3.90

6/14/2012	Bandy	m001bysaf	SAF		22.0	17.2	5.9	4.2	12.1	3.90
6/27/2012	Bonner's Ferry	m007bfsaf	SAF	140	22.2	12.5	0.3	0.0	22.2	4.00
7/26/2011	Granite Pass	m229gp	SAF		25				21.9	3.90
6/27/2012	Bonner's Ferry	m008bfsaf2	SAF	170	25.1	19.1	2.0	0.8	16.8	4.00
6/27/2012	Bonner's Ferry	i001bfsaf	SAF	80	27.7	16.4	1.0	0.4	24.5	3.90
10/2/2012	Ambrose Saddle	i012assaf	SAF	300	28.0	19.3	6.8	6.8	16.8	4.00
6/14/2012	Bandy	m002bysaf3	SAF	150	29.4	20.1	6.6	2.3	21.7	3.90
10/2/2012	Ambrose Saddle	i011assaf	SAF	290	31.1	18.6	8.4	1.6	18.1	4.00
6/21/2011	Lubrecht Stinkwater	i003lsaf	SAF		37				25.0	4.00
6/27/2012	Bonner's Ferry	i009bfsaf	SAF	80	42.2	18.7	0.9	0.9	14.9	3.90
7/2/2012	Ambrose Saddle	i007assaf	SAF	150	62.7	36.7	1.2	0.0	51.5	4.10

(this page intentionally left blank)

Appendix B. Individual Tree Ripley's L Functions

Blue is *Pseudotsuga menziesii* – the upper crown is the dashed line and the lower crown is the dotted line. In all cases, the y-axis ist he Ripley's Lhat value and the x-axis is the search radius on the scale of the data (the unitless, rescaled 0-1 crown length).

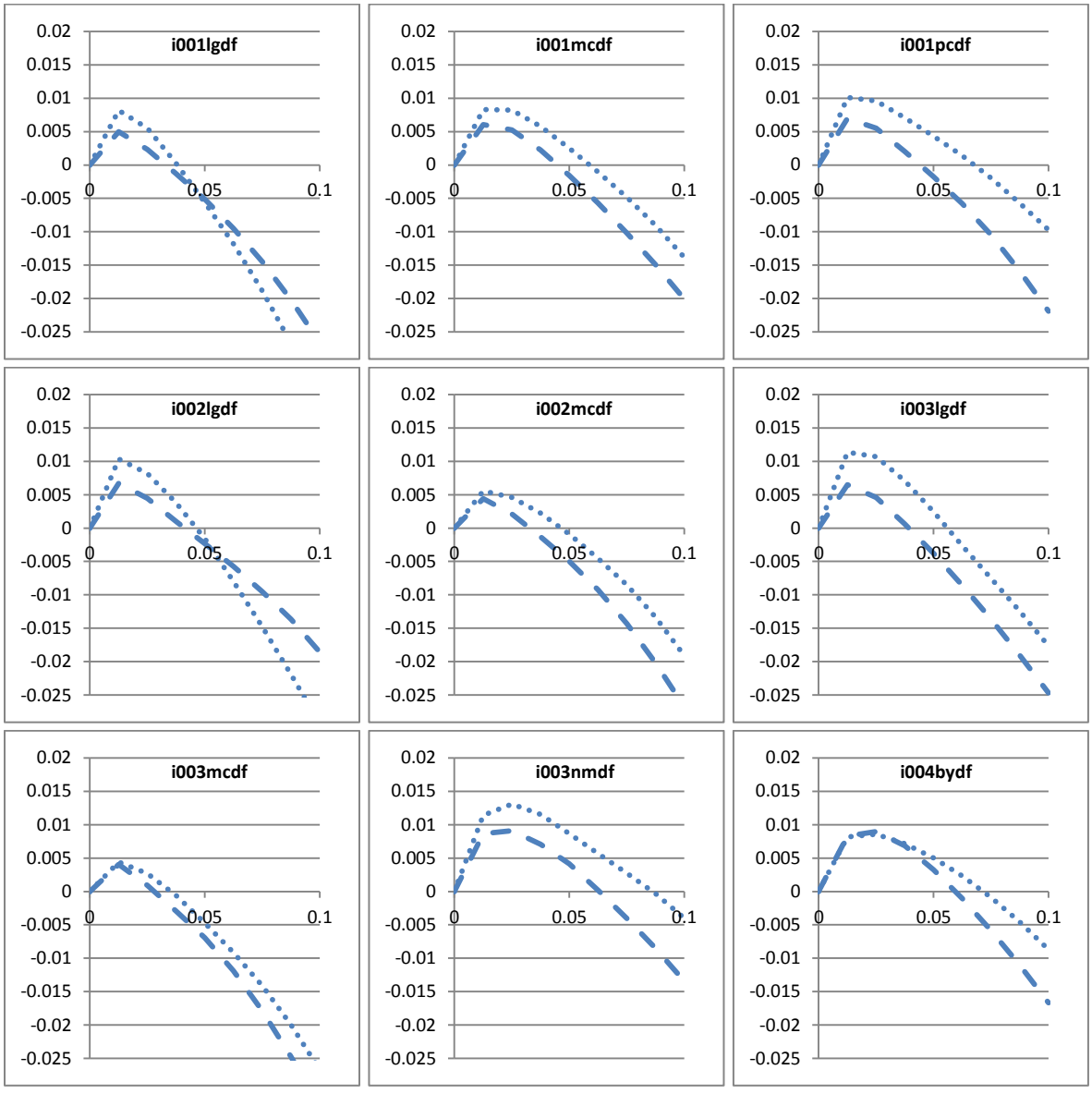

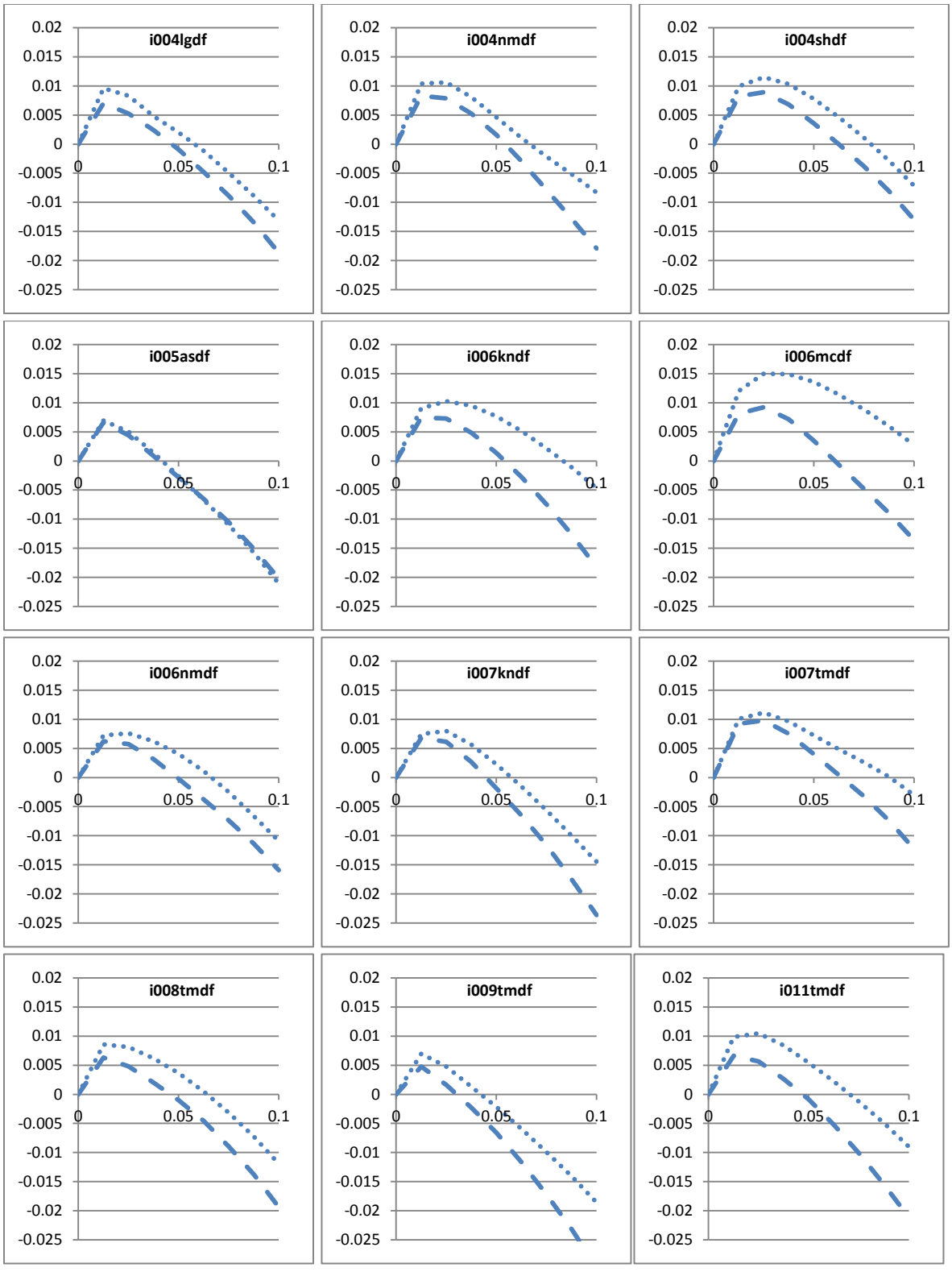
i004lgdf
i004nmdf
i004shdf
i005asdf
i006kndf
i006mcdf
i006nmdf
i007kndf
i007tmdf
i008tmdf
i009tmdf
i011tmdf
0.02
0.015
0.01
0.005
0
-0.005
-0.01
-0.015
-0.02
-0.025
0
0.05
0.1

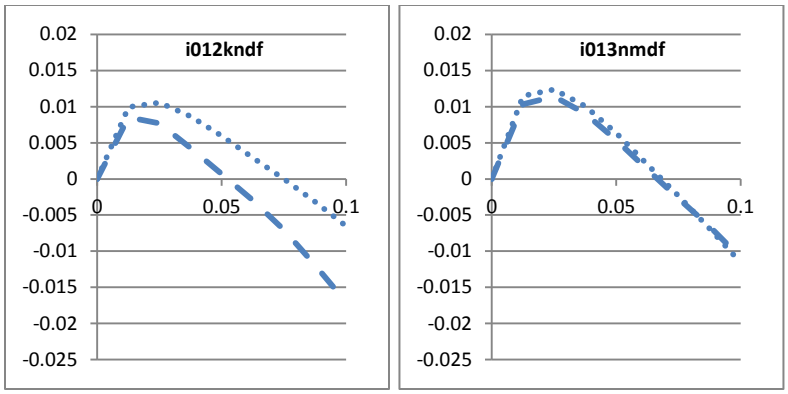
i012kndf
0.02
0.015
0.01
0.005
0
-0.005
-0.01
-0.015
-0.02
-0.025
0
0.05
0.1

i013nmdf
0.02
0.015
0.01
0.005
0
-0.005
-0.01
-0.015
-0.02
-0.025
0
0.05
0.1

Green is *Pinus ponderosa* – the upper crown is the dashed line and the lower crown is the dotted line. In all cases, the y-axis ist he Ripley's Lhat value and the x-axis is the search radius on the scale of the data (the unitless, rescaled 0-1 crown length).

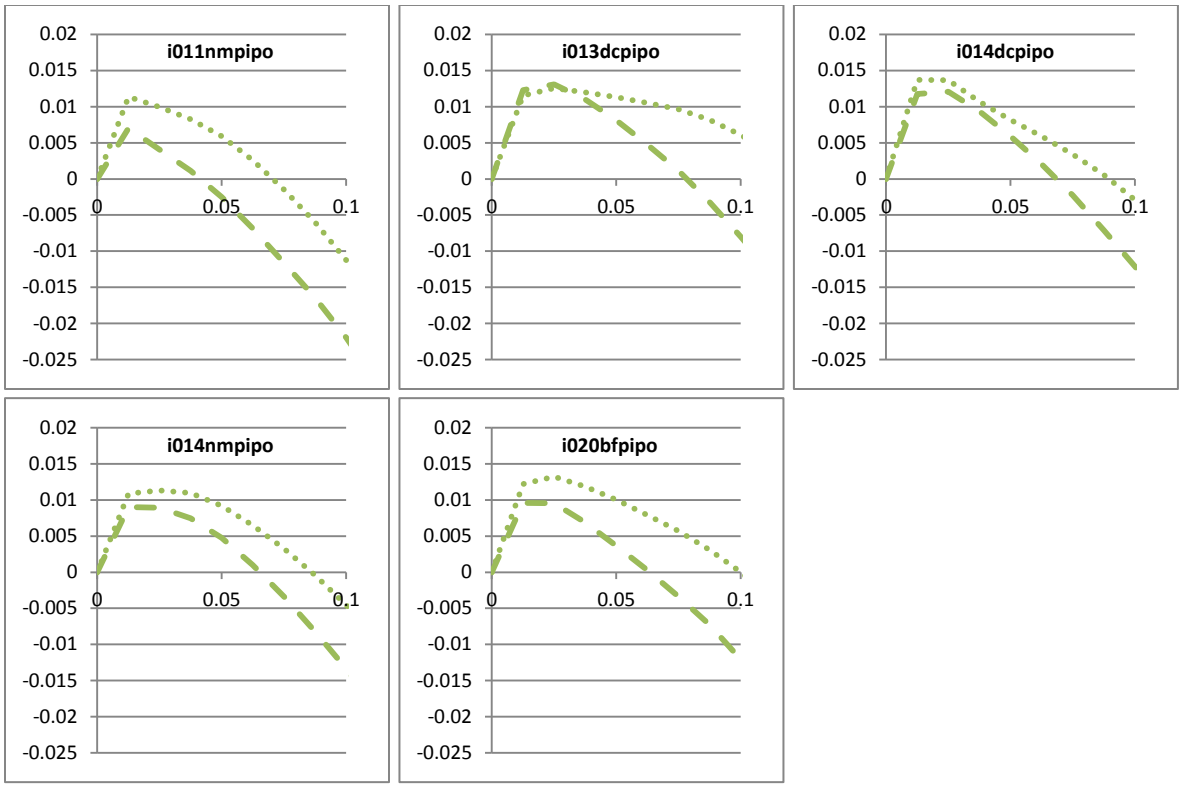
i011nmpipo
i013dcpipo
i014dcpipo
i014nmpipo
i020bfpipo
0.02
0.015
0.01
0.005
0
-0.005
-0.01
-0.015
-0.02
-0.025
0
0.05
0.1

Red is *Abies lasiocarpa* – the upper crown is the dashed line and the lower crown is the dotted line. In all cases, the y-axis ist he Ripley's Lhat value and the x-axis is the search radius on the scale of the data (the unitless, rescaled 0-1 crown length).

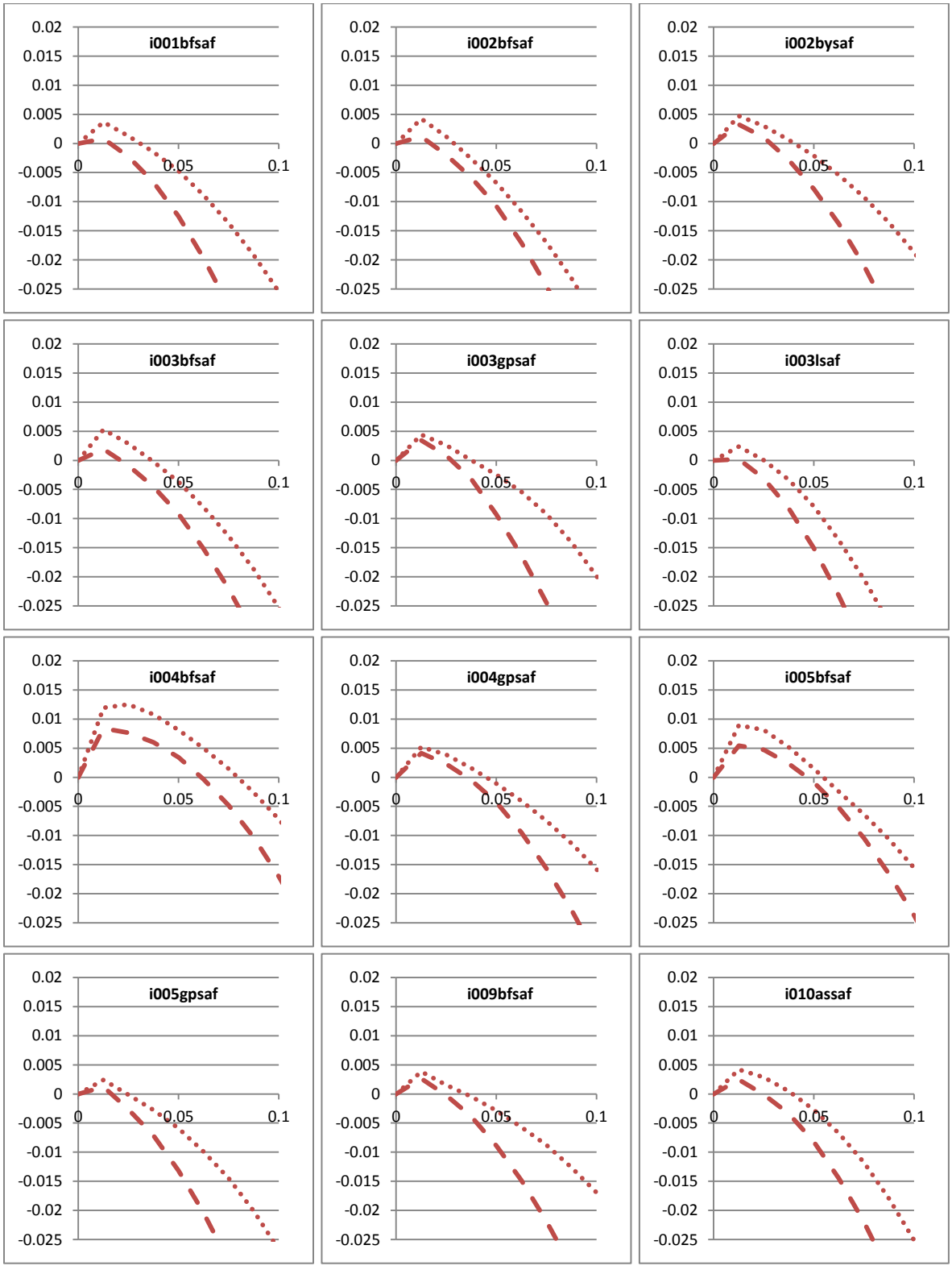

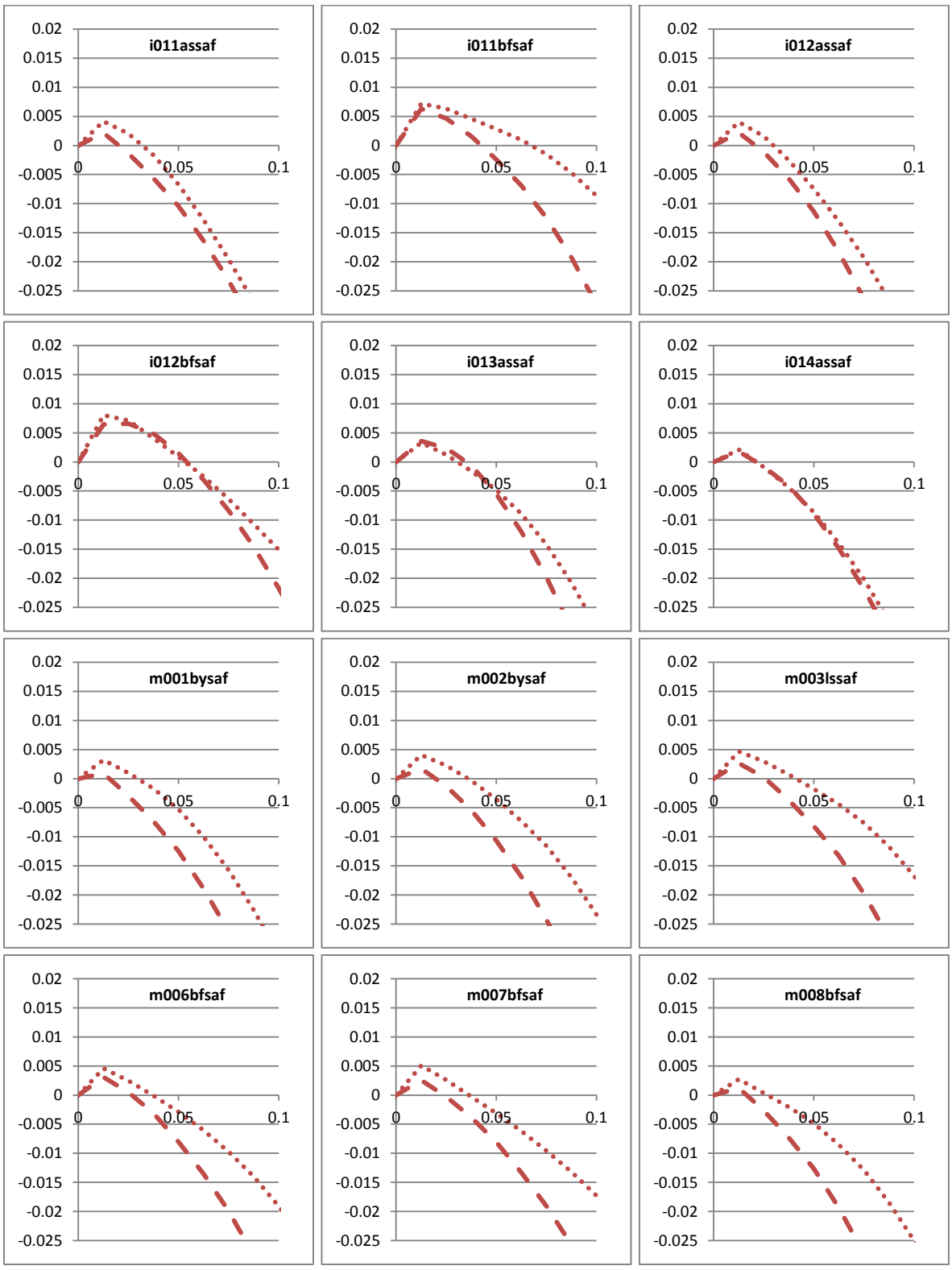
i011assaf
i011bfsaf
i012assaf
i012bfsaf
i013assaf
i014assaf
m001bysaf
m002bysaf
m003lssaf
m006bfsaf
m007bfsaf
m008bfsaf
0.02
0.015
0.01
0.005
0
-0.005
-0.01
-0.015
-0.02
-0.025
0
0.05
0.1

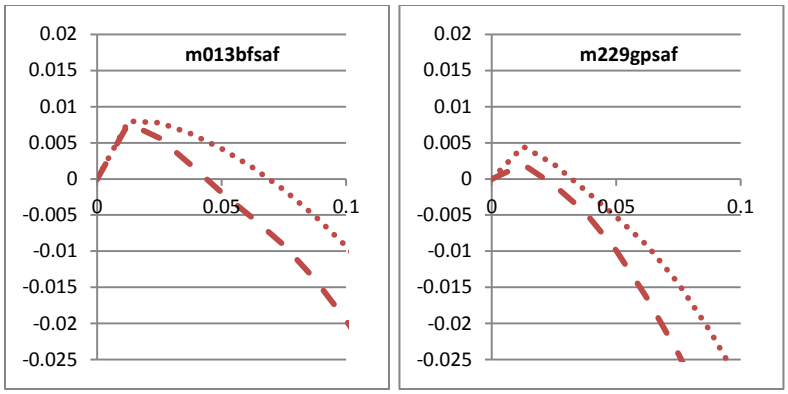
m013bfsaf
0.02
0.015
0.01
0.005
0
-0.005
-0.01
-0.015
-0.02
-0.025
0
0.05
0.1

m229gpsaf
0.02
0.015
0.01
0.005
0
-0.005
-0.01
-0.015
-0.02
-0.025
0
0.05
0.1

Appendix C. Supplemental Edge Effect Analysis

To explore the *post facto* edge effect analyses (described in the body of this thesis), I calculated Ripley's L for the seven consistent surface area to volume ratio segments, but dispersed the points randomly within each volume. For simplicity, each volume was defined as a cylinder with a radius equal to the mean of the top and bottom radii from the original frustum. The measurements for each volume segment are presented in Table 8. Although all the segments had constant surface area to volume ratios, the areas and volumes did vary. Figure 34 shows the Ripley's L functions for each segment. The functions are ordered on the plot by increasing volume and surface area, indicating that a consistent ratio is not enough to produce uniform edge effects. The departure of the functions from zero (where CSR should fall) may quantify the edge effect, although interpretation is uncertain. The shape of the Ripley's function is likely a reflection of the geometry of the study area, although this too is uncertain.

Table 8. Geometric parameters for consistent surface area to volume ratio segments with random point distributions.

height above crown base (m)	cylinder height (m)	cylinder radius (m)	total surface area (m2)	volume (m3)	surface area/ volume	number of points
15.0-19.0	4.0	0.655	19.167	5.396	3.552	10591
14.0-15.81	1.81	0.832	13.807	3.934	3.509	9193
13.0-14.42	1.42	0.955	14.245	4.066	3.503	10311
10.005-11.0	0.995	1.339	19.642	5.607	3.503	10858
8.0-8.883	0.883	1.610	25.227	7.193	3.507	11568
5.0-5.801	0.801	1.967	34.196	9.732	3.514	14163
2.211-3.0	0.789	2.040	36.257	10.314	3.515	13033

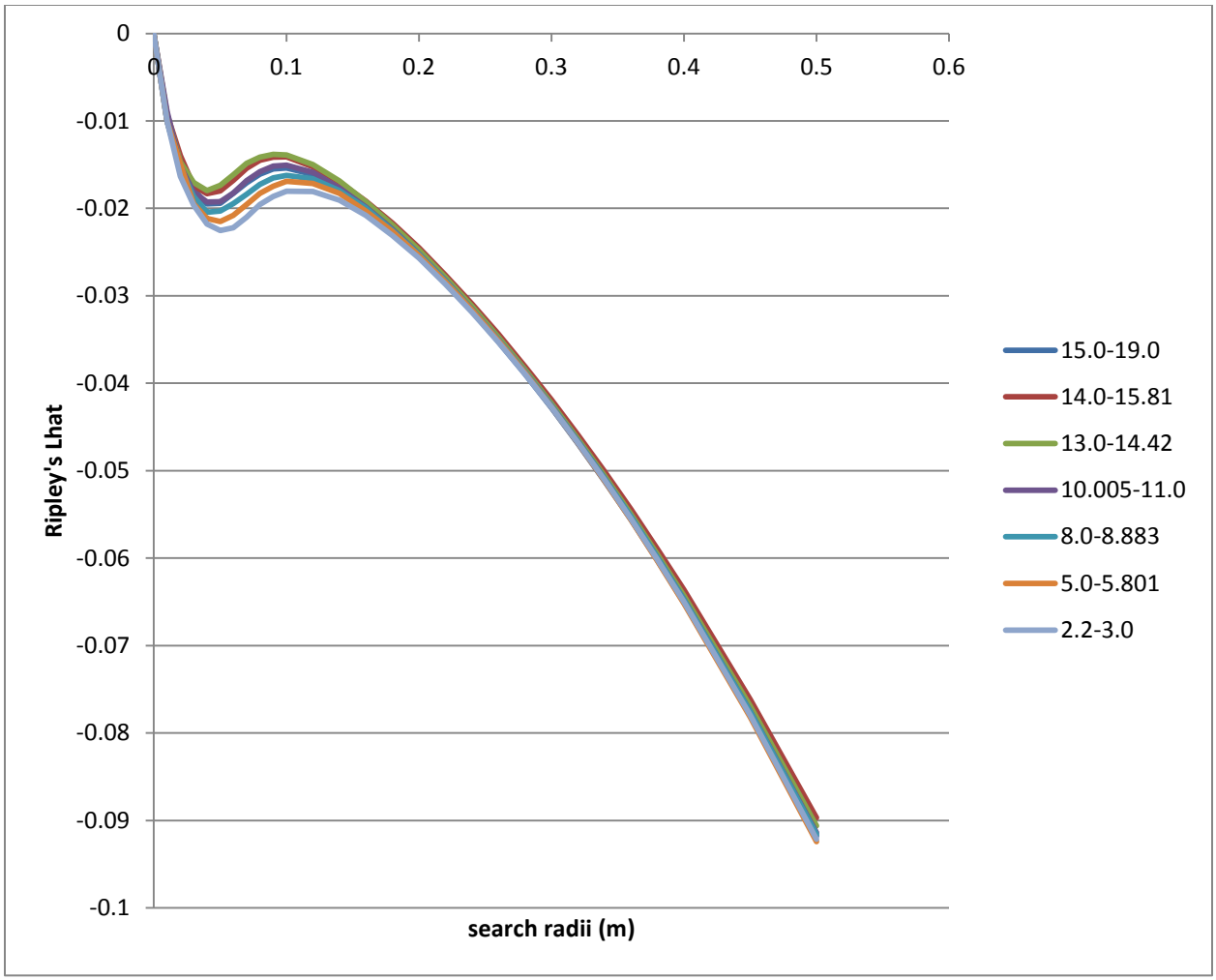

Figure 34. Ripley's L functions for random point distributions within search areas that have consistent surface area to volume ratios. Each function represents points from a segment of the sample tree at a given height interval above the crown base (e.g., 2.2-3.0 are the points and sample area geometry from 2.2-3.0m above the crown base). The order of the functions is consistent with increasing area and volume, not vertical position.